

INFORMATION TO USERS

This manuscript has been reproduced from the microfilm master. UMI films the text directly from the original or copy submitted. Thus, some thesis and dissertation copies are in typewriter face, while others may be from any type of computer printer.

The quality of this reproduction is dependent upon the quality of the copy submitted. Broken or indistinct print, colored or poor quality illustrations and photographs, print bleedthrough, substandard margins, and improper alignment can adversely affect reproduction.

In the unlikely event that the author did not send UMI a complete manuscript and there are missing pages, these will be noted. Also, if unauthorized copyright material had to be removed, a note will indicate the deletion.

Oversize materials (e.g., maps, drawings, charts) are reproduced by sectioning the original, beginning at the upper left-hand corner and continuing from left to right in equal sections with small overlaps.

Photographs included in the original manuscript have been reproduced xerographically in this copy. Higher quality 6" x 9" black and white photographic prints are available for any photographs or illustrations appearing in this copy for an additional charge. Contact UMI directly to order.

ProQuest Information and Learning
300 North Zeeb Road, Ann Arbor, MI 48106-1346 USA
800-521-0600

UMI[®]

UNIVERSITY OF ALBERTA
LABORATORY MEASUREMENT OF ELASTIC-WAVE VELOCITY, ASSOCIATED
DISPERSION, ATTENUATION AND PARTICLE RESONANCE

by

JOSEPH B. MOLYNEUX



A THESIS

SUBMITTED TO THE FACULTY OF GRADUATE STUDIES IN PARTIAL
FULFILLMENT OF THE REQUIREMENTS FOR THE DEGREE OF DOCTOR OF
PHILOSOPHY

IN

GEOPHYSICS

DEPARTMENT OF PHYSICS

EDMONTON, ALBERTA

SPRING 2000.



**National Library
of Canada**

**Acquisitions and
Bibliographic Services**

**395 Wellington Street
Ottawa ON K1A 0N4
Canada**

**Bibliothèque nationale
du Canada**

**Acquisitions et
services bibliographiques**

**395, rue Wellington
Ottawa ON K1A 0N4
Canada**

Your file Votre référence

Our file Notre référence

The author has granted a non-exclusive licence allowing the National Library of Canada to reproduce, loan, distribute or sell copies of this thesis in microform, paper or electronic formats.

The author retains ownership of the copyright in this thesis. Neither the thesis nor substantial extracts from it may be printed or otherwise reproduced without the author's permission.

L'auteur a accordé une licence non exclusive permettant à la Bibliothèque nationale du Canada de reproduire, prêter, distribuer ou vendre des copies de cette thèse sous la forme de microfiche/film, de reproduction sur papier ou sur format électronique.

L'auteur conserve la propriété du droit d'auteur qui protège cette thèse. Ni la thèse ni des extraits substantiels de celle-ci ne doivent être imprimés ou autrement reproduits sans son autorisation.

0-612-60005-X

Canada

UNIVERSITY OF ALBERTA

RELEASE FORM

NAME OF AUTHOR: Joseph Benedict Molyneux

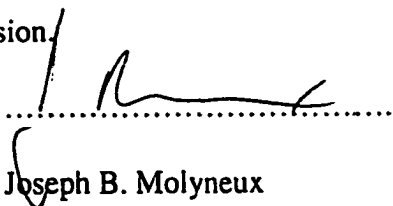
TITLE OF THESIS: Laboratory measurement of elastic-wave velocity, associated
dispersion, attenuation and particle resonance

DEGREE: Doctor of Philosophy in Geophysics

YEAR THIS DEGREE GRANTED: 2000

Permission is hereby granted to the University of Alberta to reproduce single copies of this thesis and to lend or sell copies for private, scholarly or scientific research purposes only.

The author reserves all other publication and other rights in association with the copyright in the thesis, and except as herein before provided neither the thesis nor any substantial portion thereof may be printed or otherwise reproduced in any material form whatever without the author's prior written permission.


.....
Joseph B. Molyneux

Permanent address

Brough Farm

Asmall Lane, Ormskirk,

Lancs., U.K., L40 8JL

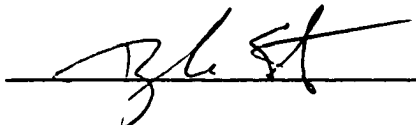
Date: January 4th 2000

“It is a vulgar error to suppose that America was ever discovered. It was merely detected.”

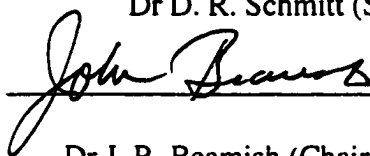
Oscar Wilde,

THE UNIVERSITY OF ALBERTA
FACULTY OF GRADUATE STUDIES AND RESEARCH

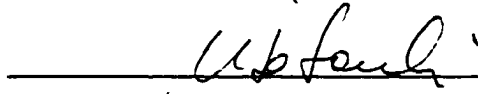
The undersigned certify that they have read and recommended to the Faculty of Graduate Studies and Research for acceptance, a thesis entitled **Laboratory measurement of elastic-wave velocity, associated dispersion, attenuation and particle resonance** submitted by Joseph B. Molyneux in partial fulfillment of the requirements for the degree of **Doctor of Philosophy** in Geophysics.



Dr D. R. Schmitt (Supervisor)



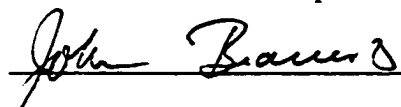
Dr J. R. Beamish (Chair Examiner)



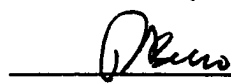
Dr M. D. Sacchi (Physics)



Dr T. J. T. Spanos (Physics)



Dr T. Chacko (Earth and Env. Sciences)



Dr R. Secco (External, Western Ontario)

Date: December 10th 1999

Abstract

Laboratory velocity measurements are an integral component of solid earth seismic investigations. Typically, ultrasonic measurements from centimeter scale plug samples are used to model large sections of the crust, core and mantle. By using the laboratory determined velocities, the seismic arrival time can more accurately calibrate spatial physical properties of the solid-earth. A semi-automated picking procedure is presented which determines the velocity measured from recorded ultrasonic pulses propagated through laboratory samples. This procedure is quicker and more consistent than the standard hand picking method, allowing larger data sets to be accurately investigated. Furthermore, a series of common velocity analyses are compared to the physical properties of phase and group velocity in an attenuating medium of glycerol saturated glass bead packs ($Q \sim 3$). It is found that the velocity determined from the first break of the waveform (signal velocity) is up to 13% different from group and phase velocities. This illustrates that signal velocity is unsuitable to determine rock properties in highly attenuating media. Also, greater than 81% velocity dispersion is observed when the dominant propagating wavelength is comparable to the bead size. More surprisingly, on propagation of the broad band input signal a bimodal amplitude spectrum becomes apparent. The low frequency peak is consistent with standard attenuation, whereas the high frequency peak is related to resonance of either the constituent beads or the inter-bead fluid cavity. Such resonance partitions energy of the main incoming signal. This phenomenon represents a new and fundamental attenuation mechanism that should be considered in many wave-propagation experiments.

Acknowledgements

My PhD has proved to be a whole lot of fun, including the writing up! A major reason for this enjoyment has been the fascinating topic and my enthusiastic academic environment. Doug Schmitt, my supervisor, rather than being a direct influence on my research allowed me to follow my own path and indeed make my own mistakes. For this I owe him a huge debt of gratitude. I hope he's had as much fun as I have. The lab was a great place to do research with such stars as Len Tober, Jay Havestock and a multitude of summer students. Meanwhile, back in the office many students have rolled through the doors. I extend special mention to Ahmed Kabali, and YongYi Lee, my intellectual elder brothers, providing many a guiding hand. In addition, some of my more recent colleagues include Mad Mike from Malta, Youcef Bouzidi, Adam Baig and Marko Mah... thanks a lot lads. Of course its not all play and I will always look back with fond memories to the lads and lasses in the department. Shaun Hendy and Jason Myatt where always there for a friendly jibe, a quick pint and any excuse to go off to the mountains... its all about pub stories. I leave the last thanks to my family, though far away are always in my thoughts: Mum, Dad, Steve, Kath (plus little Sara), and Adi.

TABLE OF CONTENTS

TITLE	PAGE
Chapter 1. Introduction	1
References	6
Chapter 2. Background	9
2.1 Introduction	9
2.2 Group and phase velocities	10
2.3 Linking static elastic parameter to wave phase and group velocity	11
2.4 An example of velocity dispersion	12
2.5 The link between the attenuation constant α and Q	14
2.6 The link between velocity dispersion and attenuation	17
2.7 Conclusion	22
References	23
Chapter 3. First break timing: arrival onset times by direct correlation	25
3.1 Introduction	25
3.2 Previous methods	28
3.2.1 Seismic travel time picking	28
3.2.2 Laboratory travel time measurement	32
3.3 Onset time determination	33

3.3.1 Direct correlation	33
3.3.2 Validity of the cross-plot technique	35
3.3.3 Evaluation on Synthetic Data	36
3.4 Laboratory tests	38
3.5 Results and discussion	40
3.6 Conclusions	42
References	43
Appendix: Derivation of coefficients	47
Chapter 4. Compressional-wave speeds in attenuating media: a laboratory study	56
4.1 Introduction	56
4.2 Background	58
4.2.1 Group and Phase Wave-Velocities	58
4.2.2 Dispersion and Attenuation	61
4.2.3 Conventional Time-Lag Picking	63
4.3 Experimental description	65
4.4 Results	67
4.5 Discussion	70
4.5.1 Character of the Attenuation	70
4.5.2 Wave-velocity Comparisons	71
4.5.3 Group and Phase Velocities	71

4.5.4 Conventional Time Picks	73
4.5.5 Signal Velocity	73
4.5.6 Consistency of Criteria	74
4.6 Conclusion	75
Appendix – Windowing the First Arrival	77
References	78
Chapter 5. Scale Dependent Velocity, Attenuation, and Internal Resonance in Unconsolidated Glass Bead	94
5.1 Introduction	94
5.2 Background	96
5.2.1 A simple example of scale dependent dispersion: propagation through layered media	96
5.2.2 Previous experiments of wave propagation through bead packs and unconsolidated materials	98
5.3 Experiments	105
5.3.1 Sample Preparation	105
5.3.2 Pulse Transmission Measurements	106
5.4 Results	107
5.5 Discussion	109
5.5.1 Bead Size Dependent Waveform Attributes	109
5.1.1.1 Low Frequency Regime: $k_{\text{eff}} < 1$.	110

5.5.1.2 Intermediate Frequency Regime: $k_f a \sim 1$.	111
5.5.1.3 High Frequency Regime: $k_f a$ bigger or equal to 1.	112
5.6 Velocity modeling	112
5.6.1 Simple mixture theories	112
5.6.2 Velocity Modeling Incorporating Frame Strength	115
5.6.3 Empirical base velocity modeling	116
5.6.4 Comparison of Experiment to Theory	118
5.6.5 Internal Resonances	118
5.7 Conclusion	124
References	127
Chapter 6. Conclusion	152
References	158

LIST OF TABLES

TITLE	PAGE
Chapter 4	
Table 1: Physical properties of the porous media constituents	83
Table 2: Comparison of measured and estimated wave speeds	84
Chapter 5	
Table 1: Constituent Physical properties	137
Table 2: Frequency and apparent attenuation of spectral peaks	138
Table 3: Summary of observations for the bead packs	139
Table 4: Normalized toroidal and poloidal frequencies	140

LIST OF FIGURES

TITLE	PAGE
Chapter 2	
Figure 1. Beat phenomena	24
Chapter 3	
Figure 1. Typical transmitted ultrasonic waveforms acquired over a range of confining pressures to 300 MPa through a rock cylinder.	49
Figure 2. Illustration of the direct correlation procedure.	50
Figure 3. Example of calculated Pearson's correlation coefficient $r(\tau)$ versus relative time shift τ for the 130 MPa and 290 MPa waveforms.	51
Figure 4. Microsecond and 100 ns scale segments of the synthetic test waveforms derived from the observed 290 MPa trace.	52
Figure 5. Mean transit time determination error and its standard deviation versus level of added noise.	53
Figure 6. Simplified experimental configuration.	54
Figure 7. Pressure and method dependent measures of transit time, velocity, and attenuation.	55
Chapter 4	
Figure 1. Illustration of Fourier method to calculate phase and group	85

delay.	
Figure 2. Illustration of the common time picking criteria employed.	86
Figure 3. Photomicrographs of sand and glass pack samples.	87
Figure 4. Experimental setup.	88
Figure 5. Directly observed and pulse-isolated traces for #3 sand, #7 glass beads, and #3 bead packs.	89
Figure 6. Relative distance ($x_2 - x_1$) versus relative group delay time ($t_2 - t_1$) for #7 glass beads @ 0.38 MHz.	90
Figure 7. Attenuation, Q, group and phase velocity variation with frequency.	91
Figure A1. Cartoon description describing the modulation of a primary arrival, $y(t)$, contaminated by secondary signal to an isolated primary arrival.	92
Figure A2. Two interfering Ricker wavelets.	93
Chapter 5	
Figure 1. Sample configuration.	141
Figure 2. Sample porosity versus bead pack length.	142
Figure 3. Experimental configuration.	143
Figure 4. Transmitted normalized amplitude versus time for differing pack lengths	144
Figure 5. Amplitude spectra of the observed traces of Figure 4 for the	145

differing lengths	
Figure 6. Peak spectral frequencies observed from Figure 5 versus pack length for the differing lengths	146
Figure 7. Natural log of the observed amplitude of the spectral peaks versus pack length for the differing lengths	147
Figure 8. Comparison of velocities	148
Figure 9. Peak frequency versus reciprocal bead diameter	149
Figure 10. Expected modal frequencies versus bead diameter	150
Figure 11. Concave triangular pore facet shape	151

CHAPTER 1

Introduction

This work focuses on the experimental determination of the speed of sound through materials in the laboratory with the pulse transmission method. This technique is perhaps the most basic: one simply measures the transit time of a pulse through a known distance. The velocity is then just the ratio of the distance to the time. This simplicity has made the pulse transmission method very popular in the rock physics and nondestructive testing communities. However, belying this simplicity is the problem of choosing the transit time. In particular, how should an observed waveform be interpreted in order to provide a useful transit time yielding a physically meaningful velocity? In this thesis, I explore this issue experimentally and go on to examine some problems of the relative scale between the material structure and the wavelength of the waves illuminating it. In the first part of the thesis, accurate travel time determination methods are applied to a find velocity through highly attenuative media and then contrasted with more fundamental group and phase determinations. In the second, the effects of scale on velocity measurement are examined through a range where the wavelength λ is approximately the same as the characteristic dimension of the material structure. The materials displayed unexpected internal resonances that may impact our ability to make attenuation measurements.

Chapter 2 introduces the concepts of velocity, attenuation and their correct application to physical property investigations. This chapter provides the background from which the rest of the thesis draws. More specifically, concepts of group and phase velocities are described, theoretically and conceptually with their relation to static elastic

rock properties. Further, phase velocity is seen to be intrinsically linked to wave attenuation. It is noted that all transforms from group and phase velocity to rock properties are based on a Fourier analysis of the waveform. Chapters 3 and 4 describe how common and simpler velocity estimates may differ in magnitude from these intrinsic properties in the presence of significant wave attenuation.

Chapter 3 describes a method to semi-automatically determine the time-of-flight velocities in ultrasonic pulse-transmission experiments [Molyneux and Schmitt, 1999a, Molyneux and Schmitt, 1997]. The general literature may be roughly divided into two types of time-picking methodologies. The first type relies on the maintenance of coherency between a reference waveform and those that follow and then exploiting this coherency to give a relative time shift between the two. The second employs some type of threshold or feature of an observed waveform. For example, the first break of the arriving wavelet is determined when the amplitude of the arriving wavelet exceeds a subjective threshold. Both methods suffer from deficiencies as will be discussed. The first method loses accuracy because waveforms change; attenuation and dispersion force a propagating pressure pulse to spread with propagation distance. The second method is intrinsically subjective especially in the presence of ambient noise. Here, a hybrid coherency method is employed which is minimally affected by dispersion. The time at which the pulse is first detected is identified by an objective maximum value of a time dependent accuracy-of-fit function.

The method is first evaluated on a series of model pulse transmission waveforms that contain increasing levels of noise. The procedure was then applied to a real metamorphic core sample whose porosity is characterized by low aperture microcracks. The overall

compressibility decreases nonlinearly with confining pressure with subsequent nonlinear increase of compressional wave speed due to the progressive closure of the microcracks. The open microcracks and subsequent attenuative properties at room pressure indicate that the rock has been distressed from its peak P-T (pressure-temperature) in its exhumation to the surface outcrop. The microcracks have a large effect on the velocity and attenuation. However, workers often require instead the value of the crack free, or intrinsic, velocity of the material as it is often assumed that no microcrack porosity exists at great depth in the earth. One great problem for workers in this area has been to judge at which pressure the microcrack porosity is sufficiently closed such that velocity measured provides a useful estimate of the in-situ value. Here, I propose a more quantitative measure of microcrack closure based on the attenuation of the sample. Specifically, I found that the attenuation and the velocity dispersion are essentially constant above a certain hydrostatic confining pressure. This indicates that most of the microcracks, which scatter the elastic waves, have closed and the nearly intrinsic mineral properties of the rock are being measured.

Chapter 4 contains a detailed analysis of the link between the velocity measured using a variety of conventional time-picking techniques and the more fundamental measures of phase and group velocity [Molyneux and Schmitt, 1999b]. The experiments were conducted on a highly attenuating medium composed of saturated packs of glass beads and quartz grains. Various lengths of the same media are required to determine group and phase velocities and for each sample different lengths to 50 mm were measured. The glycerol saturated sand and glass bead packs had large signal attenuation ($Q \sim 3$) and some velocity dispersion was seen. In the comparison, it was found that

many of the, common velocity picking methods reasonably estimate the group velocity to within 3%. This observation was much as expected. However, the time picking methods did not necessarily yield values of the phase velocity in the material especially in the case where the first arrival is used as a velocity measure. Such a discrepancy may be problematic if one wishes to test various models of wave propagation, all of which are developed using plane-wave phase velocity concepts.

Chapter 5 examines the relationship of velocity to both the dominant propagating wavelength and the structural dimension in saturated glass bead packs [Molyneux and Schmitt, in submission] similar to those used in Chapter 4. When the wavelength is less than the grain size (e.g., the high frequency regime), the ray theory limit is reached whereby the first arriving signals propagate through the relatively high velocity beads reducing the apparent travel-times through the sample. Conversely, where the wavelength is larger than the grain size the propagating wavefront does not interact singly with each incident grain, but rather in an effective sense with increased transit times across the bead pack. The travel times in this latter case are in relatively good agreement with the predictions of existing mixture models. Quantification of this transition is important to evaluate how, for example, relatively short wavelength ultrasonic experiments performed in the lab can be applied to the long wavelength seismic scales. It is also important to allow us to better understand wave propagation in the earth, which is arguably a structure whose scale dimensions are difficult to describe. Similar work has been carried out on layered media [e.g.; Marion et al, 1994], and on glass beads suspended in a solid epoxy matrix [Kinra & Anand, 1982; Yin et al, 1994]. The present experiments differ in that: 1) the beads are unconsolidated (i.e., the frame modulus of the bead pack does not

contribute significantly to the wave propagation); 2) the matrix has no rigidity and hence scattering is reduced to P-P or S-P from the beads to the fluid; and 3) the relative impedance between the glycerol and the glass beads is substantially larger than that between the beads and epoxy employed in the previous studies. Apart from the dramatic 81% velocity dispersion observed, new phenomena are observed when the dominant wavelength is comparable to the length scale of beads in the bead pack. The properties of such media are somewhat contradictory. The apparent attenuation of the signal as deduced from relative measures is reduced; but the overall signal amplitude is substantially smaller. Further, a high mono-frequency, bead size dependent component is introduced to the received signal. This high frequency component represents a resonance condition related to the dimensions of the individual grains and may indicate the existence of a previously undiscovered wave resonant scattering propagation mechanism. Such problems may further complicate the study of wave propagation in heterogeneous earth materials.

During my tenure as a graduate student a number of other projects, not included here in order to maintain a consistent theme, were carried out. Additional research included; 1) a VSP (Vertical Seismic Profiling) method to identify multiples in a reflection seismic section and 2) a statistical/physical property investigation of a metamorphic shear zone in Flin-Flon Saskatchewan to help delineate deep crustal reflectors. The former exploits the downgoing separated section of the VSP waveform, which when auto-convolved yields seismic traces with readily identifiable primary and multiple events as would be recorded at surface [Molyneux, Jones and Schmitt, 1996]. This work was carried out extensively during one summer of research consultancy at Schlumberger of Canada. The latter work

involves a comprehensive suite of physical property measurements from 106 core plugs. Measurements included bulk density, ultrasonic velocity @ 300 MPa confining pressure, velocity anisotropy, mineralogy, chemistry, preferred orientation of crystals, grain size distribution, and garnet-biotite identification of temperature of crystallization. This work has been presented in part in several meetings, the most complete and recent of which at the Canadian Geophysical conference in Banff [Molyneux and Schmitt, 1999c], and is being compiled for publication. However, both works are somewhat removed from my main thesis topic and are therefore omitted from the main body of work.

The conclusion summarizes the body of work and suggests avenues of further research. Of special note is the application of this research to parameterize experimental procedures to ensure velocity measurements performed at one frequency scale relate to velocity measurements on the same rock body at a frequency scale orders of magnitude different.

It is noted that this thesis is organized in a paper-based format. Each chapter is a 'stand-alone' entity with separate introduction, conclusion and references.

References

Kinra, V.K., and A. Anand, Wave propagation in a random particulate composite at long and short wavelengths, *Int. J. Solids Structures*, 18, 367-380, 1982.

Marion, D., Mukerji, T., and Mavko, G., 1994, Scale effects on velocity dispersion: From ray to effective medium theories in stratified media: *Geophysics*, 59, 1613-1619.

J.B. Molyneux, D. R. Schmitt, 1999a, Compressional wave speeds in attenuating media: a laboratory study. *Geophysics*, in press.

J.B. Molyneux, D. R. Schmitt, 1999b, Scale dependant velocity, attenuation and internal resonances in unconsolidated glass bead media. *Journal of Geophysical Research*, in submission.

J.B. Molyneux, D. R. Schmitt, 1999c, First Break Timing: Arrival onset times by direct correlation. *Geophysics*, in Press.

J.B. Molyneux and D.R. Schmitt, 1997, Semi-automatic determination of transit times in ultrasonic laboratory experiments. *Lithoprobe annual report*.

J.B. Molyneux, D. R. Schmitt, 1999, Statistical evaluation of rock properties from a metamorphic shear zone. Flin-Flon Saskatchewan. *CGU annual meeting*, 1999.

J.B. Molyneux, M. Jones and D.R. Schmitt, 1996, Identification of multiples contaminating surface seismic data using a VSP analysis technique. *Experiments*, 66th Annual Internat. Mtg., Soc. Expl. Geophys., Expanded Abstracts, Vol 1, pp 206-209.

Yin, H., G. Mavko, T. Mukerji, and A. Nur, Scale-dependent dynamic wave propagation in heterogenous media: I. Experiments, 64th Annual Internat. Mtg., Soc. Expl. Geophys., Expanded Abstracts, 1147-1150, 1994.

CHAPTER 2

Background

2.1 Introduction

Speed has been studied since the human awareness of distance and time. Even since the advent of a mathematical framework for elastic and anelastic wave propagation many misconceptions of wave propagation exist. For example, many scientists are surprised that in certain extreme conditions commonly used models are inadequate and experiments have displayed group velocities exceeding the speed of light [eg., Bolda et al., 1994]. Here, it is noted that relativity is not violated as the wave front propagates at up to the speed of light but the mathematical concepts of group and phase velocity are not so constrained [e.g, Brillouin, 1960, Stenius and York, 1995, Stratton, 1941]. This background is based in the research and understanding of over thirty years past. Indeed, Stenius and York's [1995] paper quotes "... I never learn anything anymore at the [annual] conferences. It seems like every paper covers some topic that my colleagues and I investigated thirty to forty years ago!" The following paragraphs will elaborate this history discussing the physical interpretation of group and phase speed, the relationship of static elastic parameters to phase velocity and the link of velocity dispersion (frequency dependent propagation velocity) to attenuation.

2.2 Group and phase velocities

Two fundamental measures of the rate of propagation are group and phase speeds. In short, it is often conceptualized that phase speed is that at which a monochromatic plane wave travels. The group speed is commonly associated with the rate of movement of a superposed packet of two or more such plane waves. It is useful to illustrate these concepts by investigating the classic example of two superposed waves in 1-dimension.

A propagating plane wave with a maximum amplitude A of angular frequency ω and wavelength λ ($k = \text{wavenumber} = 2\pi/\lambda$) can be characterized by the following equation:

$$\varphi = A \cos(kx - \omega t). \tag{1}$$

Using,

$$V_p = f\lambda, \tag{2}$$

where V_p is the phase velocity of the signal with frequency f , it is shown from equation (2) that the propagation rate is ω/k . The superposition of two such waves with slightly different angular frequency ($\Delta\omega$) and wave number (Δk) results in the following,

$$\begin{aligned} \varphi &= A \cos((k + \Delta k)x - (\omega + \Delta\omega)t) + A \cos((k - \Delta k)x - (\omega - \Delta\omega)t) = \\ &= 2A \cos[\Delta kx + \Delta\omega t] \cos[kx + \omega t] \end{aligned} \quad (3)$$

The first part of the solution to equation (3) has a wavenumber Δk and angular frequency $\Delta\omega$, which via equation (1) and (2) has an associated speed of $\Delta\omega/\Delta k$. This perturbation superposes on the last part of the solution to equation (3) with associated speed ω/k . Graphically this is seen in Figure 1 as a low frequency amplitude envelope propagating at a speed $\Delta\omega/\Delta k$ – the group speed, with the high frequency information within this packet propagating at a speed ω/k – the phase speed.

2.3 Linking static elastic parameter to wave phase and group velocity

The static elastic properties of Poisson's ratio, ν , Young's modulus, E , bulk density, ρ , and the Lamé parameters Λ and μ are related to phase velocity in either of the following manners. Firstly compressional wave speed,

$$\begin{aligned} V_{\text{compressional}} &= \sqrt{\frac{\Lambda + 2\mu}{\rho}} \\ V_{\text{compressional}} &= \sqrt{\frac{E(1-\nu)}{(1+\nu)(1-2\nu)}} \end{aligned} \quad (4)$$

and also shear wave speed,

$$\begin{aligned}
 V_{shear} &= \sqrt{\frac{\mu}{\rho}} \\
 V_{shear} &= \sqrt{\frac{E}{2(1+\nu)}}
 \end{aligned}
 \tag{5}$$

By a simple transformation the group velocity V_g is derived from the above calculated phase velocity V_p ,

$$V_g(\omega) = k \frac{dV_p(\omega)}{dk} + V_p(\omega)
 \tag{6}$$

Here, equation (6) evidences that group velocity only differs from phase velocity if the propagating medium is dispersive. $|dV_p/d\omega| > 0$.

2.4 An example of velocity dispersion

A classic example of dispersion and differences between group and phase velocities can be drawn from the analysis of surface water waves [Rayleigh, 1929, Brillouin, 1960]

$$V_p^2 = \left(\frac{g}{k} + \frac{Tk}{\rho} \right) \tanh(kl),$$

(7)

where g is the acceleration due to gravity, T the surface tension and l the water depth. For the simplified case of relatively deep water, equation (7) becomes,

$$V_p^2 = \frac{g}{k} + \frac{Tk}{\rho}.$$

(8)

To relate to our final example I will concentrate on only the small wavelength approximation ($k^2 \gg g\rho/T$),

$$V_p = \sqrt{\frac{Tk}{\rho}}$$

(9)

which is valid for ripples on a pond as opposed to a long wavelength approximation more suitable to ocean waves,

Applying equation (6) to (9) results in,

$$V_g = \frac{3}{2}V_p. \tag{10}$$

Such a disparity between group and phase velocities can be seen when throwing a stone into a pond. The produced rings are comprised of a small number of ripples. As the rings (velocity V_g) propagate, the internal ripples (velocity V_p) lag behind and eventually disappear on the inside of the rings.

2.5 The link between the attenuation constant α and Q

Q is a dimensionless property of intrinsic attenuation of a medium (thermodynamic energy loss, internal friction etc...), defined by the fractional amount of energy loss in each cycle of a mono-frequency wave [e.g., Aki and Richards, 1980],

$$\frac{1}{Q(\omega)} = -\frac{\Delta E}{2\pi E} \tag{11}$$

where E and ΔE are the peak strain energy and energy loss per cycle respectively. As most arrivals from elastic waves are recorded as amplitudes, for small attenuation ($Q \gg$

1) the differential of the energy-amplitude relationship ($E \sim A^2$) yields $\Delta E \sim 2A\Delta A$, where A is the maximum amplitude of a recorded mono-frequency wave,

$$\frac{1}{Q(\omega)} = -\frac{\Delta A}{\pi A}.$$
(12)

Thus for each cycle, the wave amplitude is decreased by a factor of π/Q such that,

$$A(t) = A_0 \exp(1 - \pi / Q)^n$$
(13)

where equation (13) is valid for integer periods. n ,

$$t = 2n\pi / \omega$$
(14)

and it follows,

$$A(t) = A_0 \exp[1 - \omega t / 2Qn]^n$$
(15)

and for large n ,

$$A(t) = A_0 \exp[-\omega t / 2Q]$$

(16)

It is difficult to monitor the time evolution of an infinite sinusoid amplitude decay. Experimentally, it is easier to monitor the evolution of amplitude with distance. Transforming equation (16) from time to distance via $t = x/V_p$, the following distance dependant attenuation equation becomes apparent,

$$A(x) = A_0 \exp \frac{-\omega x}{2V_p Q}$$

(17)

Which is commonly written as,

$$A(x) = A_0 e^{-\alpha(x)}$$

(18)

defining how the attenuation coefficient α relates to angular frequency phase velocity and Q .

$$\alpha(\omega) = \omega / 2V_p Q$$

(19)

2.6 The link between velocity dispersion and attenuation

Drawing from the work of O'Donnell et al. [1981], in the following description it is assumed that an elastic wave satisfies Hooke's elasticity law,

$$s(t) = \int_{-\infty}^{\infty} R(t-t')p(t')dt' \quad (20)$$

where s is the strain at a given time t , R the adiabatic compressibility and p the pressure of the elastic wave pulse at a stimulus time t' . The link of attenuation to dispersion is manifest by invoking causality i.e., the strain response $s(t)$ cannot be influenced by future stimuli $p(t')$ and the compressibility and propagating wavenumber can be complex.

A Fourier representation of the compressibility is given by,

$$R(t) = \int_{-\infty}^{\infty} \frac{d\omega}{2\pi} R(\omega)e^{-i\omega t} \quad (21)$$

and the reaction of strain to a pressure delta function results in

$$R(t) = \int_{-\infty}^{\infty} \frac{d\omega'}{2\pi} R(\omega') e^{-i\omega' t}$$

(22)

$R(\omega)$ is can be represented by a complex function $R(\omega) = R_1(\omega) + iR_2(\omega)$, the real and imaginary parts respectively. However, $R(\omega)$ is a real and measurable quantity and so $R(-\omega) = R^*(\omega)$, that is the real part of compressibility must be symmetric and the imaginary antisymmetric such that

$$s(t) = \frac{1}{\pi} \left(\int_0^{\infty} d\omega' R_1(\omega') \cos \omega' t + \int_0^{\infty} d\omega' R_2(\omega') \sin \omega' t \right)$$

(23)

Further, causality imposes

$$\int_0^{\infty} d\omega' R_1(\omega') \cos \omega' t + \int_0^{\infty} d\omega' R_2(\omega') \sin \omega' t = 0 \quad t < 0$$

(24)

or equivalently,

$$\int_0^{\infty} d\omega' R_1(\omega') \cos \omega' t - \int_0^{\infty} d\omega' R_2(\omega') \sin \omega' t = 0, \quad t > 0. \quad (25)$$

Transforming (25) by multiplying through by $\exp(-\eta t)$ in which $\eta = \varepsilon + i\omega$, and integrating over positive times yields,

$$\int_0^{\infty} \frac{\eta R_1(\omega') - \omega' R_2(\omega')}{\omega'^2 + \eta^2} d\omega' = 0 \quad \varepsilon > 0 \quad (26)$$

as ε tends to zero, the denominator of equation (26) becomes,

$$\begin{aligned} (\omega'^2 + \eta^2) &\longrightarrow P(\omega'^2 - \omega^2) - i\pi\delta(\omega'^2 + \omega^2) \\ &= P(\omega'^2 - \omega^2) - \frac{i\pi\delta}{2\omega} (\delta(\omega' - \omega) + (\omega' + \omega)) \end{aligned} \quad (27)$$

where P represents the Cauchy Principal component. Substituting equation (27) back into equation (26) results in a separation between real and imaginary components such that,

$$R_1(\omega) = \frac{2}{\pi} P \int_0^{\infty} \frac{\omega' R_2(\omega')}{\omega'^2 - \omega^2} d\omega' \quad (28)$$

and,

$$R_2(\omega) = \frac{2}{\pi} P \int_0^{\infty} \frac{\omega' R_1(\omega')}{\omega'^2 - \omega^2} d\omega' \quad (29)$$

Equations (28) and (29) represent the Kramers-Kronig relationship [Kronig and Kramers, 1928] most commonly applied in electromagnetic problems. The compressibility so discovered also needs to satisfy the dispersion relation for acoustic wave propagation.

$$k^2 = \omega^2 \rho R(\omega) \quad (30)$$

in which it follows that k must be complex,

$$k = \frac{\omega}{V_p} + i\alpha(\omega) \quad (31)$$

such that a plane wave ϕ is represented by,

$$\phi(x, t) = e^{i(kx - \omega t)} = e^{-\alpha x} e^{i(\omega x / v_p - \omega t)} \quad (32)$$

Upon substitution of (30) into (31)

$$\frac{\omega^2}{V_p^2(\omega)} - \alpha^2(\omega) + \frac{2i\omega\alpha(\omega)}{V_p(\omega)} = \omega^2 \rho [R_1(\omega) + iR_2(\omega)],$$

(33)

and upon separation of real and imaginary components,

$$\begin{aligned} \frac{\omega^2}{V_p^2(\omega)} - \alpha^2(\omega) &= \omega^2 \rho R_1(\omega), \\ \frac{2\omega\alpha(\omega)}{V_p(\omega)} &= \omega \rho R_2(\omega). \end{aligned}$$

(34)

Generally, the imaginary part of the wavenumber is less than the real part ($\alpha(\omega)V_p(\omega)/\omega \ll 1$), which decouples the equations,

$$V_p(\omega) = \frac{1}{(\rho R_1(\omega))^{1/2}}$$

(35)

and,

$$\alpha(\omega) = (\rho V_p(\omega) / 2) \omega R_2(\omega).$$

(36)

Equations (28) (29) (35) and (36) allow the phase response of the system to be calculated if attenuation is known at all frequencies and vice versa. Here it is noted that equations (28) and (29) are considered solvable at high frequencies as inertia ensures that the compressibility terms fall off rapidly enough for the integrals to converge. O'Donnell et al [1981] illustrates further simplifications for experimentally useful bandlimited problems. However, the present description is sufficient to demonstrate how attenuation and dispersion are mathematically linked.

2.7 Conclusion

In this discussion it is seen that the mathematical framework for non-invasive investigations of the static elastic properties of a medium via wave velocity and attenuation characteristics is centered on the correct measurement of group and/or phase velocity. We shall see in subsequent chapters that not all analyses of the received signal return these fundamental velocities, misrepresenting the material properties.

References

Aki, K. and Richards, P. G., Quantitative seismology theory and methods, W. H. Freeman and Company.

Bolda, E. L., Garrison, J. C. and Chiao, R. Y., 1994, Optical propagation at negative group velocities due to a nearby gain line: Physical Review A, v 49, 2938-2947.

Brillouin, L., 1960, Wave propagation and group velocity: New York, Academic Press.

Kronig, R. and Kramers, H. A., 1928, Absorption and dispersion in X-ray spectra. Z. Phys., v 48, 174.

O'Donnell, M., Jaynes, E. T. and Miller, J. G., 1981, Kramers-Kronig relationship between ultrasonic attenuation and phase velocity: J. Acoust. Soc. Am., v 69, 696-701.

Rayleigh, Theory of sound. The Macmillan Company, 1929.

Stratton, J. A., 1941, Electromagnetic Theory: New York, McGraw-Hill.

Stenius, P., and York, B., 1995, On the propagation of transients in waveguides: IEEE Antennas and Propagation Magazine, v 37, 39-44.

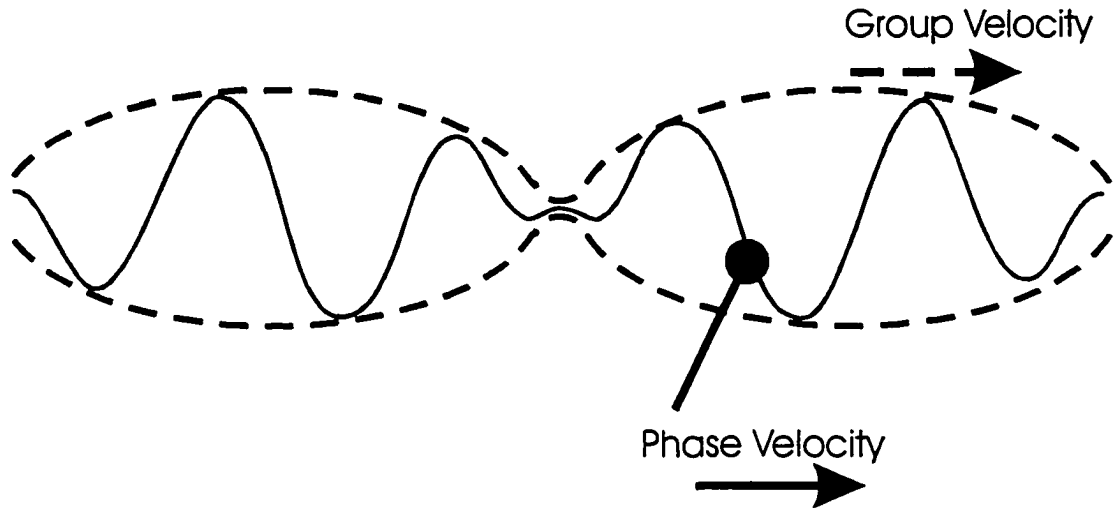


Figure 1. Beat phenomena. Two superposed cosine waves propagating through a media with slightly different wavenumber and angular frequency produce an envelope, which propagates at the group speed, and high frequency internal carrier information which propagates at the phase speed.

CHAPTER 3

First Break Timing: Arrival Onset Times by Direct Correlation¹

3.1 Introduction

The time of the *first break* is employed in velocity measurements ranging from elementary refraction profiling to the most sophisticated tomographic inversions. The term *first break* is not precisely defined, and it is relevant to ask which feature of the arriving waveform provides the best measure of the time-of-flight. Is the initial time of onset or a more readily identifiable characteristic, such as the first peak, more important? If the propagating wavelet is stationary the determination of interval velocities from either of these criteria yields identical results. However, in the real world both intrinsic absorption and scattering contribute to the signal attenuation, manifest as a broadening in time of a propagating wavelet. In some measurements the onset times differ by several percent from those determined with a first peak. In such situations, this discrepancy ceases to be of only academic interest. Unfortunately, it is not immediately obvious which waveform feature provides the most representative measure of material properties or physical structure.

For any propagation mode (i.e. compressional, shear, Rayleigh, etc.) the wave speed is the quotient of propagation distance with time-of-flight. In real media, these wave speeds depend on frequency. This dispersion results from a combination of intrinsic absorption and scattering effects (e.g. Brillouin, 1960, Futterman (1962)) and requires development of the concepts of phase V_p , group V_g , energy V_e , and signal V_s velocities.

¹ A version of this chapter has been accepted for publication. Molyneux and Schmitt, in press, Geophysics

Both phase and group velocities depend on frequency. Because of this, a band-limited disturbance changes form as it propagates. The phase delay time

$$t_p(\omega) = \frac{\phi(\omega)}{\omega}, \quad (1)$$

where ϕ is the change in the phase of the signal component of frequency ω is used to calculate the phase velocity across a distance l .

$$V_p(\omega) = \frac{l}{t_p(\omega)} = \frac{\omega}{\phi(\omega)}. \quad (2)$$

One way to provide the phase ϕ is from the difference of the unwrapped phases between two observations of a propagating pulse. This phase is also required to determine the group delay

$$t_g(\omega) = \frac{d\phi(\omega)}{d\omega} \quad (3)$$

describing propagation of a wave packet (i.e. the envelope of a number of frequencies). In a band limited signal centered on a ω , the signal's peak amplitude travels at V_g . Here Claerbout (1992) observes it is often said: "what you see is the group velocity".

It is also useful to define the energy-transport, or ray, velocity (Federov, 1968) which is the velocity at which energy is transmitted. V_e is equal to the ratio of the intensity to the energy density of the wave (White, 1983; Bourbie et al., 1987) and in non-

attenuating materials is the same magnitude as V_g . In the special case of isotropic and purely viscoelastic attenuating media, this energy-transport velocity and the phase velocity are the same (White, 1983). In attenuating media, the frequency content of the wave packet evolves and group velocity is no longer meaningful, whereas the energy transport velocity has a real physical interpretation. This is a particular concern when the attenuation of the sample under study changes with varying states of saturation (Bourbie et al., 1987) or confining pressures as in the present investigation.

Signal velocity is another important measure. Sommerfeld (see Brillouin, 1960) defined the signal onset time, used in calculating the signal velocity, to be the time at which the energy of the signal is first detectable. One advantage of using the onset time is that it is less influenced by dispersion dependent waveform modification. A possible explanation for this is that in media displaying inverse dispersion (i.e. those in which phase velocity increases with frequency) the earliest arriving portions of the signal are preferentially composed of the fastest frequency components. Onset travel times may then be more consistent than those which rely on the picking of some later waveform feature likely to be influenced by dispersion.

The overall question of which velocity definition is most useful will not be answered in this chapter, which instead focuses on the technical issue of accurately determining the onset arrival time in high fidelity waveforms acquired in laboratory experiments. Sommerfeld's definition is adopted here and a method to accurately pick the onset time in high fidelity laboratory waveforms devised. Below, earlier first break picking schemes are reviewed. A strategy to measure the onset times is described and implemented with a suite of pressure-dependent ultrasonic waveforms (Figure 1) acquired

in the laboratory. The results illustrate how critical the definition of the first break is in attenuating media. Finally, the absorptive and transit time characteristics of a candidate rock are compared; these reveal additional criteria with which to judge the quality of intrinsic velocity determinations in materials containing micro-crack porosity.

3.2 Previous methods

3.2.1 Seismic travel time picking

Modern seismic studies require that large data volumes be analyzed. Manual travel time picking is both too slow and subject to inconsistent operator bias and error. To attempt to circumvent these shortcomings several automated picking schemes have been developed and these may be classified as either 'running window' or 'coherency' methods.

In the former, certain characteristics are repeatedly calculated within successive sections of the time series producing a time dependent function. The onset time is usually identified by an obvious change in the behavior of this function. Such 'running window' methods proficiently identify changing waveform character. The averaging inherent to these techniques smoothes the calculated response and complicates travel time determination. In one example, Boschetti et al. (1996) calculate the fractal dimension of time windows along a seismic signal. This method relies on the empirical observation that the fractal dimension of coherent signal differs substantially from that of pre-arrival noise. The first onset time is indicated by a decline in the magnitude of the fractal dimension, and such a change in character is visible in even the noisiest data. However,

this measure does not abruptly change and as such there remain potential timing ambiguities.

A second method relies on employing the coherence characteristics between traces. Coherency based methods rely on a quantitative comparison of object and a shifting reference waveform. The relative first break time is taken to be that when the measure of the quality of match is maximum. Such correlation or convolution methods presumably yield group velocities as the properties of the waveform as a whole are compared. In a refraction seismic study, Peraldi and Clement (1972) cross-correlate the reference waveform, with an ostensibly known arrival time to other traces in the data set. This method assumes the waveforms in each trace are reasonably similar to the reference; the respective maxima of this cross-correlation indicate the shifts of their travel times with respect to the reference waveform time.

Numerous additional coherency based methods may be found in the literature. Ervin et al (1983) convolve a boxcar whose time width equals the dominant period of the seismic data; the maximum of the resulting function occurs near the first onset of signal. Ramanantoandro and Beritsas (1987) further adapt this approach by employing a series of different width boxcar functions. They found that the time of the successive maxima of the convolution of the boxcar and the model arrival were all the same for box-car widths exceeding half the period of the signal. Consequently, the signal onset time was then given by subtracting half-width time of the shortest boxcar sharing these identical times. This method obviates the need to evaluate the dominant period, and is to some degree prescient of modern wavelet transform methods employing the Haar wavelet.

The following travel time determined methods employ a blend of both the running window method and the comparison technique. Coppens (1985) identifies the first break with a running window energy function after reducing the influence of uncorrelated noise by coherency filtering. Spagnolini (1991) applies a two step picking scheme to refraction data. First, the running window is split into two sections about the center position. A substantial change in the ratio of the powers between these two sections approximately indicates the signal onset. Secondly, the first arrivals are converted to stationary zero-phase wavelets by an adaptive filter, and this final stationary wavelet data set is compared to a reference to evaluate the relative travel times.

Gelchinsky and Shtivelman (1986) use statistical techniques to estimate the signal onset time and then cross-correlate adjacent traces to further correct the time of refracted arrivals. Hatherly (1982) determines the first break by applying a set of empirical pass-fail tests. After approximate identification of the onset, the first arrival is modeled by a quadratic interpolation method from which the first inflection point on the rising portion of the waveform is determined. This assumes the inflection point is a more consistent feature than the manually picked onset of signal. The average difference between these two picked times in the data set is subtracted from the times to the first inflection points to reveal smoothly trending first arrival travel times. Again, this method assumes the wavelet is stationary.

Murat and Rudman (1992), use various trace attributes to determine the first arrival in their neural net approach. These attributes include the peak amplitude of a half cycle, the amplitude difference between the peak value of the half cycle to those half

cycles surrounding it, the RMS amplitude ratio of a running window, and the RMS amplitude ratio for adjacent traces.

In application to whole earth geophysics, Su and Dziewonski, (1992) employ a cross-correlation technique to evaluate the timing of teleseismic arrivals. In a comparison of a variety of picking methods, Gudmundsson (1996) applies such a correlation technique to modeled teleseismic waveforms which incorporate scattering. He found that the spatial resolution of tomographic studies which used these correlation travel-times was improved with the onset times.

Development of a truly causal first arrival in theoretical studies is often hindered by the deficiencies intrinsic to the modeling itself. For example, filtering of a trace causes the signal to become non-causal in the sense that a small amount of energy leaks into times prior to the first arrival; this effect was noted by Ricker (1953) who in a predigital age suggested that one can never find a portion of the signal with a zero amplitude such that the *arrival first kick* can be defined. As a practical result, Schmidt and Muller (1986) and Gudmundsson (1996) define the onset of calculated model signals to occur when the amplitudes exceed an arbitrary level which they choose as the time to 1/100 and 1/8, respectively, of the maximum amplitude.

Recently, Boschetti et al. (1996) quantitatively compared a number of the above techniques. However, in most of the above studies the automatic first break times are compared only to those determined manually. No objective measure of the picking accuracy was presented.

3.2.2 Laboratory travel time measurement

The primary differences between waveforms acquired in laboratory settings and those acquired in the field are that the laboratory data are usually considerably less contaminated with noise. Despite this, the picking of accurate transit times in laboratory samples is particularly critical given the high velocities (1-8 km/s) and short transit times (a few microseconds). In the earth sciences, the pulse overlap method described by Birch (1960) is traditionally used to find velocity in rock samples. (e.g., Christansen, 1965, Fountain et al., 1990). Ultrasonic pulses propagate simultaneously through a sample and a delay-line column of mercury. Both transmitted signals are displayed on an oscilloscope, and the length of the mercury delay line is varied until the two signals overlap. As the velocity of the mercury column is presumed known, the transit time through the sample is easily derived. In a similar manner, pulse echo overlap methods (e.g. Papadakis, 1990) involve finding the time delay between the first arrival of a pulse and its multiple reflections. Here, the oscilloscope time base is altered until a multiply reflected arrival overlaps the earlier arrival. The time sweep then provides a measure of the travel time. In many respects both of these methods are similar to the digital correlation techniques.

Alternatively, the first peak time of an input pulse as it propagates through a cored rock sample is often measured (Kern and Richter, 1981, King, 1966). The transit time through the recording apparatus is corrected by measuring the difference in the timing of the first peak amplitude when the rock core lies between the transducers relative to when the transducers are placed directly in contact. Such a measurement is predicated on the observation that the waveform is stationary at elevated pressures and as such consistently monitors travel time differences with increasing pressure. However, as indicated in Figure

1. waveforms acquired at lower pressures can significantly differ from those at high pressure. This can result in substantial differences between the travel time measured from signal onset and first peak.

Although the essential concepts of velocity determination apply to both seismic and ultrasonic laboratory applications, in practice one important difference is that the latter is usually less contaminated with noise. Further, such signals are also recorded at high sampling rates such that the Nyquist frequency is large relative to their frequency bandwidth. Such high-fidelity signals are advantageous in that they allow greater accuracy in the determination of the signal onset. In this context the running window approaches, although useful in coarsely sampled and noisy seismic data, are inappropriate due to their inherent smoothing. The waveform comparison methods unambiguously identify a transit time but suffer in that they assume stationary waveforms. Here, we present an alternative onset time determination that employs a correlation of the shape of the waveform but only in the vicinity of the signal onset.

3.3 Onset time determination

3.3.1 Direct correlation

In this section, the direct correlation travel time determination technique is described and then tested on synthetic data. The method relies on the comparison of waveform shapes near the signal onset, examples of which are shown in Figure 1b. The method is analogous to hodogram analyses (cross-plot of the amplitudes of two associated traces) usually employed, for example, to azimuth orient and rotate downhole

3-component geophone seismic data (e.g. Kebaili and Schmitt, 1996). The cross-plot of two well-correlated waveform segments is linear.

A simple example illustrates the picking methodology. A reference template X (Figure 2a) includes the signal onset whose time is presumably known. The signal onset time of the object waveform Y relative to that of the reference waveform X is to be found. Three separate waveform segments of the object trace Y are shown in Figure 2b. Cross-plots of these object segments with the reference (Figure 2c) display various behavior but only the cross-plot with the centermost window $Y2$ is linear. The non-linear cross-plots of $Y1$ and $Y3$, which are advanced or retarded with respect to X , simply indicates that their shapes differ from the template X . In contrast, the linearity of the middle cross-plot for $Y2$ suggests its shape is most similar to the template; consequently the time shift of window $Y2$ relative to template X yields the difference in their onset travel times.

A means to objectively provide a measure of the linearity in the cross-plots is required. The simplest and best known measure of linearity in this context is the Pearson's co-efficient of correlation (Taylor, 1982) here given as $r(\tau)$.

$$r(\tau) = \frac{N \sum XY(\tau) - (\sum X)(\sum Y(\tau))}{\sqrt{[N \sum X^2 - (\sum X)^2][N \sum Y(\tau)^2 - (\sum Y(\tau))^2]}}$$

(4)

where $X = \{X_0, X_1, \dots, X_N\}$ is the vector of amplitudes of the N sample length reference template waveform and $Y(\tau) = \{Y_0, Y_1, \dots, Y_N\}$ is a trial segment of the object waveform of the same length. The Pearson correlation coefficient, $r(\tau)$, is calculated for $Y(\tau)$ shifted

along the length of the object waveform a series of time shifts τ . As is well known, a value of $r = 1$ indicates perfect positive linear correlation between X and $Y(\tau)$ meaning both share the same shape. A value of $r = 0$ indicates no correlation meaning in this context that the shapes of the curves differ, $r = -1$ indicates an anti-regression: two curves of the same shape but with opposite polarity. Proximity of $r(\tau)$ to unity suggests a good correlation of shapes between the waveforms X and $Y(\tau)$; with the τ value at which $r(\tau)$ is maximum indicating the most appropriate time shift. An example of a calculated $r(\tau)$ versus τ for two real waveforms taken from Figure 1 is given in Figure 3. The shift which best matches the reference template occurs at 61 ns.

3.3.2 Validity of the cross-plot technique

Our picking method is based on the assumption that two similarly shaped waveform segments with the same onset times have a linear cross-plot. This will be tested by examining a simple model in which the signal onset is assumed to take a quadratic form:

$$X(t) = a_0 + a_1 t + a_2 t^2 \tag{5}$$

for the template where $t = 0$ is the time of the signal onset and a_0 , a_1 , and a_2 are polynomial coefficients. For purposes of this model, the object signal $Y(t - \tau)$ is similarly described with the coefficients b_0 , b_1 , and b_2 . The validity of this assumption is based on direct observation of waveform shapes; a least square regression analysis of observed waveform amplitudes (Figure 1) immediately following the manually picked onset time within a trace, are quadratic with a correlation coefficient better than 0.999.

Rigorously, even when their onset times are identical the cross-plot of the two quadratics X and Y take a non-linear form:

$$Y(t) = \alpha + \beta t + \delta X(t) \tag{6}$$

where the coefficients α , β , and δ are derived in the Appendix. However, for all practical purposes Equation (6) is nearly linear over a wide range of coefficients. For the real data examined, the non-linear term $\delta X(t)$ typically contributes less than 20 % to the final value of $Y(t)$ in equation (6), yet only deteriorates the linear correlation coefficients to an acceptable worst fit of 0.98. The most important point is that the reference, $X(t)$, need not exactly replicate the shape of the object $Y(t)$ near the onset. This observation allows substantial latitude in the selection of the reference $X(t)$.

3.3.3 Evaluation on Synthetic Data

It is difficult to calculate model waveforms that retain the causal nature of real arrivals with a distinct signal onset. Here, to evaluate the accuracy of the time determination procedure a synthetic data set was derived from the real traces of Figure 1. To provide a meaningful test, these synthetics have known arrival times, known noise levels, and a character similar to the real data. To this end, the synthetic waveforms were produced by a spline fit to the real waveforms of Figure 1. All amplitudes prior to the manually picked first arrival position were set to zero. The noise levels, as characterized from the real data over a 300 ns long pre-onset time window, were approximately -60 dB lower than the amplitude of the first amplitude minimum. The amplitudes of this noise were normally distributed. Similarly described random noise was then added to each

noise-free spline fit trace to produce the synthetic data sets (Figure 4). The advantage of this procedure is that the resulting traces are similar in form and noise level to the real data but have onset arrival times which are known *a priori*. The onset of energy time was 4727 ns for the 290 MPa synthetic reference waveform.

A variety of tests was carried out to optimize the method. First, the waveform recorded at 290 MPa confining pressure, which exhibited the lowest level of pre-onset noise, was used as the template. It was found that the best results were obtained if the template commenced 20 ns before the signal onset. Further, windows whose lengths were approximately one-seventh the dominant period of the signal provided the most accurate picking results. The template with the optimal length of 160 ns yielded a mean of negative 2 ns and a standard deviation of 6 ns between the actual onset arrival times and those picked with the Pearson correlation. This travel time error determination (i.e., total of the mean and standard deviation) represents less than 0.2% of the roughly 4800 ns propagation travel time. Elevated noise levels moderately increase this picking error (Figure 5).

One interesting observation is that the mean transit times so determined all tended to be slightly late as indicated by the systematic negative mean in Figure 5. This bias disappears for the perfect noise free data and is due to the leveraging effect of the higher amplitudes of Y3 on the cross-plot.

3.4 Laboratory tests

Real laboratory waveforms (Figure 1) have already been presented for illustrative purposes in the error estimation. The experimental acquisition of these waveforms is now described.

The travel time determination procedure was developed to aid P-wave velocity measurements in metamorphic rocks studied as part of the LITHOPROBE TransHudson Transect (Hajnal et al., 1996). The velocities of metamorphic and well-consolidated sedimentary rocks are notoriously nonlinear with pressure, due to the existence of high aspect ratio, crack-like, pressure-dependent porosity. As a result, velocities are often measured at high pressure when much of this porosity is closed in order to provide an estimate of the crack free in situ properties (Birch, 1961). This micro-crack problem is particularly severe in metamorphic rock samples and thus each sample measurement is carried out to pressures of 300 MPa (~ 45 000 psi). The travel time picking method was applied to over 150 different samples each with over 60 waveforms.

The experimental configuration employed is shown in Figure 6. Two 1 MHz resonant frequency piezoelectric ceramics (BaTiO_3) are attached directly to the parallel flattened ends (± 0.02 mm) of 2.54 cm diameter cylindrical core plugs. The example core plug used here is 31.70 mm in length. The transmitting transducer is activated by a square wave pulse and the received output is digitized by a high speed digital oscilloscope (at 1 ns sampling interval) and stored to disc. The core plug is dried under vacuum then hermetically sealed in flexible urethane before being placed in the fluid-filled pressure vessel. The plug is then subject to increasing pressure from standard conditions to 300 MPa in steps of 10 MPa. The P-waveform is acquired at each step

producing a suite of pressure dependent waveforms such as shown in Figure 1. Bandpass filtering was not applied to the data as removal of even low amplitude frequency components smoothes the relatively abrupt onset. The progressive decrease of the onset travel times with change in pressure is ubiquitous in metamorphic velocity studies. Also, the waveforms recorded at low confining pressure are much broader in shape than those recorded at greater pressures.

Apparent quality factor, Q , measurements were carried out using spectral ratios (e.g. Toksoz et al., 1979) over the entire pressure range to 300 MPa. In this method the ratio of the Fourier amplitude spectra $A_1(f)$ and $A_2(f)$ of the pulse transmitted through a standard and the rock sample, respectively, is used. The standard was an aluminum cylinder whose dimensions were identical to those of the rock sample and the *apparent* Q was determined from the slope in

$$\ln \frac{A_2(F)}{A_1(F)} = \frac{-\pi(t_2 - t_1)}{Q} f \quad (7)$$

where f is the frequency (in Hz) and t_1 and t_2 the propagation times through the aluminum standard and the rock core, respectively. The aluminum cylinder is assumed to have negligible attenuation at ultrasonic frequencies with $Q > 120,000$ for frequencies > 100 kHz (Zemanek and Rudnick, 1961). This spectral ratio method inherently assumes Q is constant over the (0.5 MHz to 1.5 MHz) bandwidth of the ultrasonic wave packet (Ganley and Kanasewich, 1980).

3.5 Results and discussion

The onset times of the real ultrasonic data of Figure 1 were determined both manually and with Pearson correlation. The 170 ns long template, X, was taken from the trace acquired at 290 MPa because of its low pre-event noise level. The manually determined transit times display significantly more scatter than those eventually determined with the direct correlation, relative to a presumably smooth trend of velocity with pressure (Figure 7a). Although this attribute does not in itself prove that the computer picked times are correct, it does suggest that the method is less error prone due to consistency than more subjective manual determinations. The times given by the Pearson correlation method are also compared to those provided by other automatic techniques (Figure 7b) of first amplitude extremum time (crosses), of cross-correlation of entire waveforms (open squares) and of the amplitude envelopes (x's) In all cases the 290 MPa waveform was used as the reference. The amplitude envelopes are calculated using the well known Hilbert transform (Taner et al. 1978). All results are displayed with respect to the differential time of onset, (i.e. relative to that of the 290 MPa template waveform). An absolute measure of the total travel time is given by adding the manually picked onset time (± 5 ns) of the 290 MPa waveform. As such, the systematic error introduced in this manual determination propagates through all subsequent velocity calculations, and is calculated to be 0.3%.

At the lowest hydrostatic confining pressures, below 100 MPa, the methods give dissimilar travel times. These differences transfer directly into the calculation of the material velocity when the sample length is divided by the travel times, (Figure 7c). It is further interesting to note that the difference between the travel times remains essentially

unchanged aside from random noise above 100 MPa of confining pressure. This is demonstrated by the nearly constant and small percentage difference between the signal and cross-correlation velocities above 150 MPa (Figure 7d). These observations show that the waveforms remain nearly stationary above this pressure suggesting that attenuation and dispersion change little.

The apparent Q increases from ~ 6 at room pressure to nearly 40 at 300 MPa (Figure 7e). These observations agree with those of Meglis et al. (1996) to 150 MPa who attributed the attenuation to scattering from the micro-crack porosity (Yamakawa, 1962, Mason and McSkimin, 1947). These pressure dependent variations of the apparent Q further illustrate the non-stationarity of the waveforms. Indeed, only above pressures of 150 MPa does Q exhibit a nearly constant value with pressure. Consequently, at low confining pressure, picking non-stationary features of the waveforms such as a first peak can yield ambiguous results and the travel times so measured have no clear, consistent meaning. Similarly, cross-correlation between reference and such non-stationary sample waveforms introduces additional travel time errors which directly propagate into the determination of velocity.

One valid criticism of rock core measurements is that they can never provide the "true intrinsic" velocity of the multiphase material due to the existence of micro-crack porosity. This is particularly true in more brittle igneous and metamorphic rocks (e.g., Meglis et al, 1996) or in highly consolidated calcareous rock (e.g., Schmitt and Li, 1995). It is difficult or impossible to gauge at which point the micro-crack porosity in such rocks is closed. Workers have usually assumed that the velocity versus pressure graph becomes linear once the majority of the cracks are closed. Further pressure dependent velocity

increases result primarily from the smaller changes in the elastic moduli. The results of Figure 7d and 7e suggest that leveling of the time difference between the signal onset and first peak times and the Q value versus pressure provide additional criteria towards the evaluation of "intrinsic" velocity measurements. Leveling of these measures indicates stationarity of the waveforms which in turn suggest that the general state of the material remains unaltered to the highest pressures in the experiment.

3.6 Conclusions

The travel times of the onset arrival of ultrasonic pulses transmitted through core samples were determined to within 0.3% by a direct correlation method. This time uncertainty compares well with the 2% error commonly quoted in laboratory pulse transmission methods. Essentially, the onset segment of the time series is correlated with a suitable reference which can either be a similar waveform or an appropriate quadratic function. Substantial differences of up to 4% in the velocities determined using the onset and other criteria were found in the laboratory data set a low confining pressure ($Q \sim 6$). At elevated confining pressures, the attenuation becomes less severe ($Q \sim 40$) and all the velocity measures have the same magnitude which may be indicative of microcrack closure.

The method described requires a template wavelet, with a manually picked first break, to compare to all other first breaks. An automated procedure, without the need for a manual pick, could be employed by running a series of slightly different quadratic templates in the Pearson picking scheme. The templates yielding the best correlation would provide an absolute travel time.

The direct correlation method was developed for use in highly time-resolved, low noise signals acquired in the laboratory. However, there is no reason why it would not successfully be used to determine onset travel-times in full-waveform sonic logging, high-frequency cross-hole tomography, VSP, and seismic refraction studies.

Finally, there are relatively large discrepancies observed between velocities determined using the onset and other, travel-time determination criteria. This suggests that care should be taken by experimentalists in the laboratory and the field in describing how travel time delays, and hence velocities, are measured. This is particularly critical when conditions such as confining stress, pore pressure, and saturation state influence the attenuation characteristics of the material. Experimental work in progress seeks to better understand the linkage between velocity measurement and attenuation.

References

- Birch F., 1960, The velocity of compressional waves in rocks to 10 kilobars, Part 1: *Journal of Geophysical Research*, **65**, 1083-1102.
- Birch F., 1961, The velocity of compressional waves in rocks to 10 kilobars, Part 2: *Journal of Geophysical Research*, **66**, 2199-2224.
- Boschetti F. Denitith, M. D., List R. D., 1996. A fractal-based algorithm for detecting first arrivals on seismic traces: *Geophysics*, **61**, 1095-1102.
- Bourbie T. and Zinszner B., 1987, Hydraulic and acoustic properties as a function of porosity in Fountainbleau sandstone: *Journal of Geophysical Research*, **90**, 11524-11542.
- Brillouin L., 1960, *Wave propagation and group velocity*: Academic Press, New York.

- Christansen N.I., 1965, Compressional wave velocities in metamorphic rocks at pressure to 10 kilobars: *Journal of Geophysical Research*, **70**, 6147-6164.
- Claerbout J. F., 1992, *Earth sounding analysis*: Blackwell Scientific Publications
- Coppens F., 1985, First arrival picking on common-offset trace collections for automatic estimation of static corrections: *Geophysical Prospecting*, **33**, 1212-1231.
- Ervin C., McGinnis L. D., Otis R. M., Hall M. L., 1983, Automated analysis of marine refraction data: *Geophysics*, **48**, 582-589.
- Fedorov F. I., 1968, *Theory of elastic waves in crystals*: Plenum Press, New York
- Fountain D., et al., 1990, Seismic structure of the continental crust based on rock velocity measurements from the Kapuskasing uplift: *Journal of Geophysical Research*, **95**, 1164-1186.
- Futterman W., 1962, Dispersive body waves: *Journal of Geophysical Research*, **67**, 5279-5291.
- Ganley D. C. and Kanasewich E. R., 1980. Measurement of absorption and dispersion from check shot surveys: *Geophysics*, **85**, 5219-5226.
- Gelchinsky B. and Shtivelman V., 1986, Automatic picking of first arrivals and parameterization of travel time curves: *Geophysical Prospecting*, **31**, 915-928.
- Gudmudsson O., 1996, On the effect of diffraction on travel time measurements: *Geophys. J. Int.*, **124**, 304-314.
- Hajnal, Z., Lucas S., White D., Lewry J., Besdan S., Stauffer M. R., and Thomas M. D., 1996, Seismic reflection images of high-angle faults and linked detachments in the Trans-Hudson Orogen: *Tectonics*, **15**, 427-439.
- Hatherly P.J., 1982, A computer method for determining seismic first arrival times:

- Geophysics, **47**, 1431-1436.
- Kebaili A. and Schmitt D.R., 1996, Velocity anisotropy observed in wellbore seismic arrivals: Geophysics, **61**, 12-20.
- Kern H. and Richter A., 1981, Temperature derivatives of compressional and shear wave velocities in crustal and mantle rocks at 6Kbar confining pressure: Journal of Geophysical Research, **49**, 47-56.
- King M.S., 1966, Wave velocities in rocks as a function of changes in overburden pressure and pore fluid saturation: Geophysics, **31**, 50-73.
- Mason W. P. and McSkimin H. J., 1947, Attenuation and scattering of high frequency sound waves in metals and glasses: Journal of the Acoustic Society of America, **19**, 454-473.
- Meglis I. L., et al., 1996, Pressure dependence of velocity and attenuation and its relationship to crack closure in crystalline rocks: Journal of Geophysical Research, **101**, 17523-17533.
- Murat M. and Rudman A., 1992, Automated 1st arrival picking: a neural network approach. Geophysical prospecting: **40**, 587-604.
- Papadakis E.P., 1990, The measurement of ultrasonic velocity: Physical Acoustics, **19**, 81-105.
- Peraldi R. and Clement A., 1972, Digital processing of refraction data study of first arrivals: Geophysical Prospecting, **20**, 529-548.
- Ramanantoandro R. and Beritsas N., 1987, A computer algorithm for automatic picking of refraction first-arrival time: Geoexploration, **34**, 147-151.
- Schmidt T. and Muller G., 1986, Seismic signal velocity in absorbing media: Journal of

- Geophysics, **60**, 199-203.
- Schmitt, D.R., and Y.Y. Li, 1995, A high pressure technique for determining the microcrack porosities of damaged brittle materials, *Can. J. Phys.*, **73**, 330-337.
- Spagnolini U., 1991, Adaptive picking of refracted first arrivals, *Geophysical Prospecting*: **39**, 293-312.
- Su W. and Dziewonski A.M., 1992, On the scale of mantle heterogeneity: *Physics of the Earth and Planetary Interiors*, **74**, 29-54.
- Taner M. T., 1978, Complex seismic trace analysis: *Geophysics*, **44**, 1041-1063.
- Taylor J. R., 1982, *An introduction to error analysis*: University Science Books.
- Toksoz M. N., Johnston D. H., Timur A., 1979, Attenuation of seismic waves in dry and saturated rocks: I. Laboratory measurements: *Geophysics*, **44**, 681-690.
- Ricker N., 1953, The form and laws of propagation of seismic wavelets: *Geophysics*. **18**, 10-40.
- White J. E., 1983, *Underground sound: application of seismic waves*: Elsevier Science Publishing Company inc.
- Yamakawa N., 1962, *Scattering and attenuation of elastic waves*: *Geophysical Magazine*, Tokyo, **31**, 63-103.
- Zamanek J. Jr. and Rudnick, J., 1961, Attenuation and dispersion of elastic waves in a cylindrical bar: *J. Acoust. Soc. Am.*, **23**, 1283-1288.

Appendix: Derivation of coefficients

We seek an expression of one quadratic $Y(t)$ as a function a second quadratic $X(t)$ where

$$\left. \begin{aligned} X &= X(t) = a_0 + a_1 t + a_2 t^2 \\ Y &= Y(t) = b_0 + b_1 t + b_2 t^2 \end{aligned} \right\} t = 0, 1, 2, 3 \dots$$

(A-1)

Both are first differentiated with respect to time and rearranged to provide:

$$t = \frac{1}{2b_2} \left(\frac{dY(t)}{dt} - b_1 \right) = \frac{1}{2a_2} \left(\frac{dX(t)}{dt} - a_1 \right)$$

(A-2)

This expression is then integrated, producing

$$(Y(t) - b_1 t) \Big|_{t=0}^{t=t} = \frac{b_2}{a_2} (X(t) - a_1 t) \Big|_{t=0}^{t=t}$$

(A-3)

and by substituting values for Y and X in the limits gives the final expression

$$Y(t) = \alpha + \beta t + \delta X(t)$$

(A-4)

the coefficients

$$\alpha = b_0 - \frac{b_2 a_0}{a_2}, \quad \beta = b_1 - \frac{a_1 b_2}{a_2}, \quad \delta = \frac{b_2}{a_2}$$

(A-5)

Strictly, equation (A-4) is a nonlinear expression of $Y(t)$ with $X(t)$. However, $Y(t)$ is approximately a linear function of $X(t)$ if the term βt is a small (i.e. $\beta t \ll \alpha + \delta X(t)$).

This condition was empirically found to hold true for the synthetic data studied in Figure 4 where over the 170 ns window used βt was never more than 0.15% $Y(t)$ even in comparing the room pressure and 290 MPa waveforms.

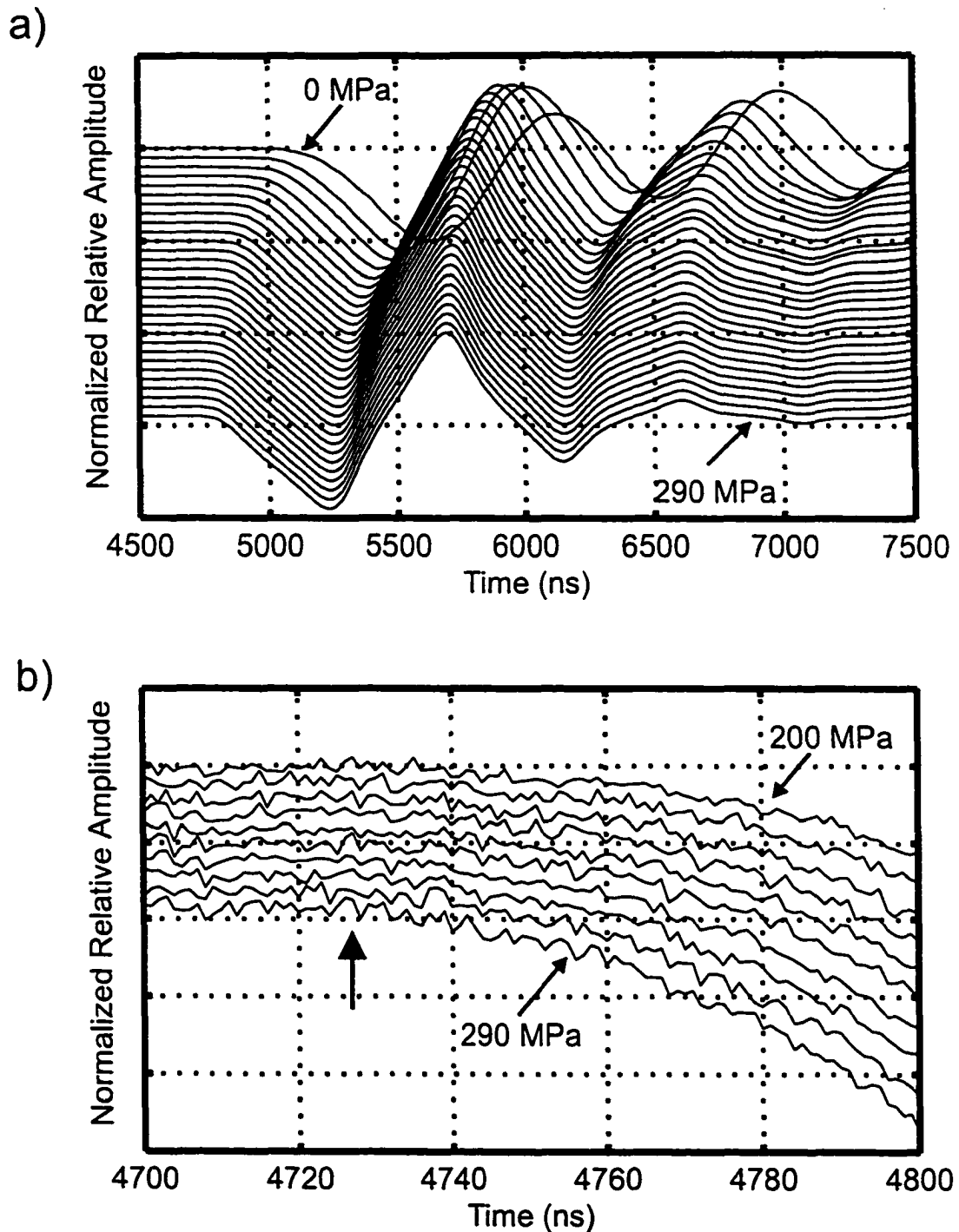


Figure 1. a) Typical transmitted ultrasonic waveforms acquired over a range of confining pressures to 300 MPa through a rock cylinder. Waveforms are vertically offset according to the pressure at which they were obtained for viewing convenience. b) Twenty times vertical exaggeration of a subset of the waveforms in a) with confining pressures from 190 MPa to 290 MPa. The arrow indicates the manually picked arrival onset time for the 290 MPa reference template waveform. Amplitudes are normalized with respect to each waveform's greatest amplitude.

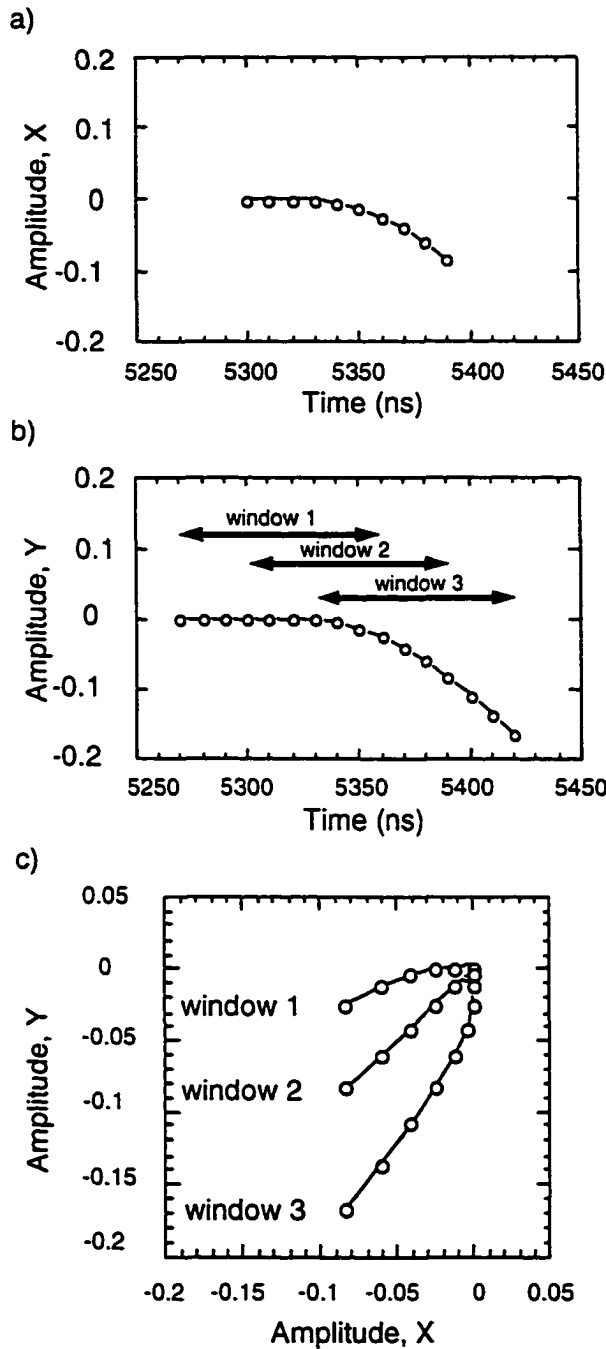


Figure 2. Illustration of the direct correlation procedure. a) reference segment X in the vicinity its known onset time. b) Positions of three time windows relative to the amplitudes of the object waveform Y . The windows are of the same length as X and their corresponding amplitudes denoted $Y1$, $Y2$, and $Y3$ in the text. c) hodograms of $Y1$, $Y2$, and $Y3$ versus reference template X .

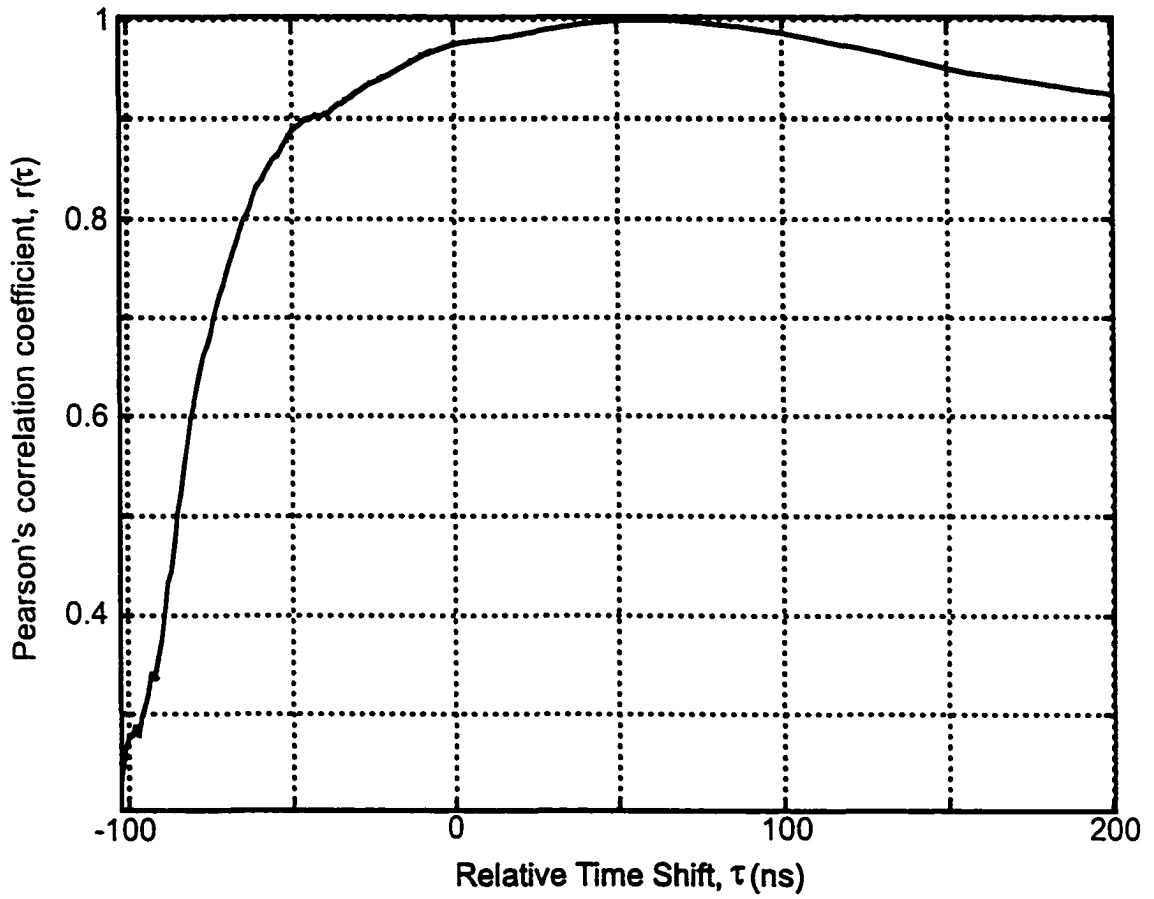


Figure 3. Example of calculated Pearson's correlation coefficient $r(\tau)$ versus relative time shift τ for the 130 MPa and 290 MPa waveforms.

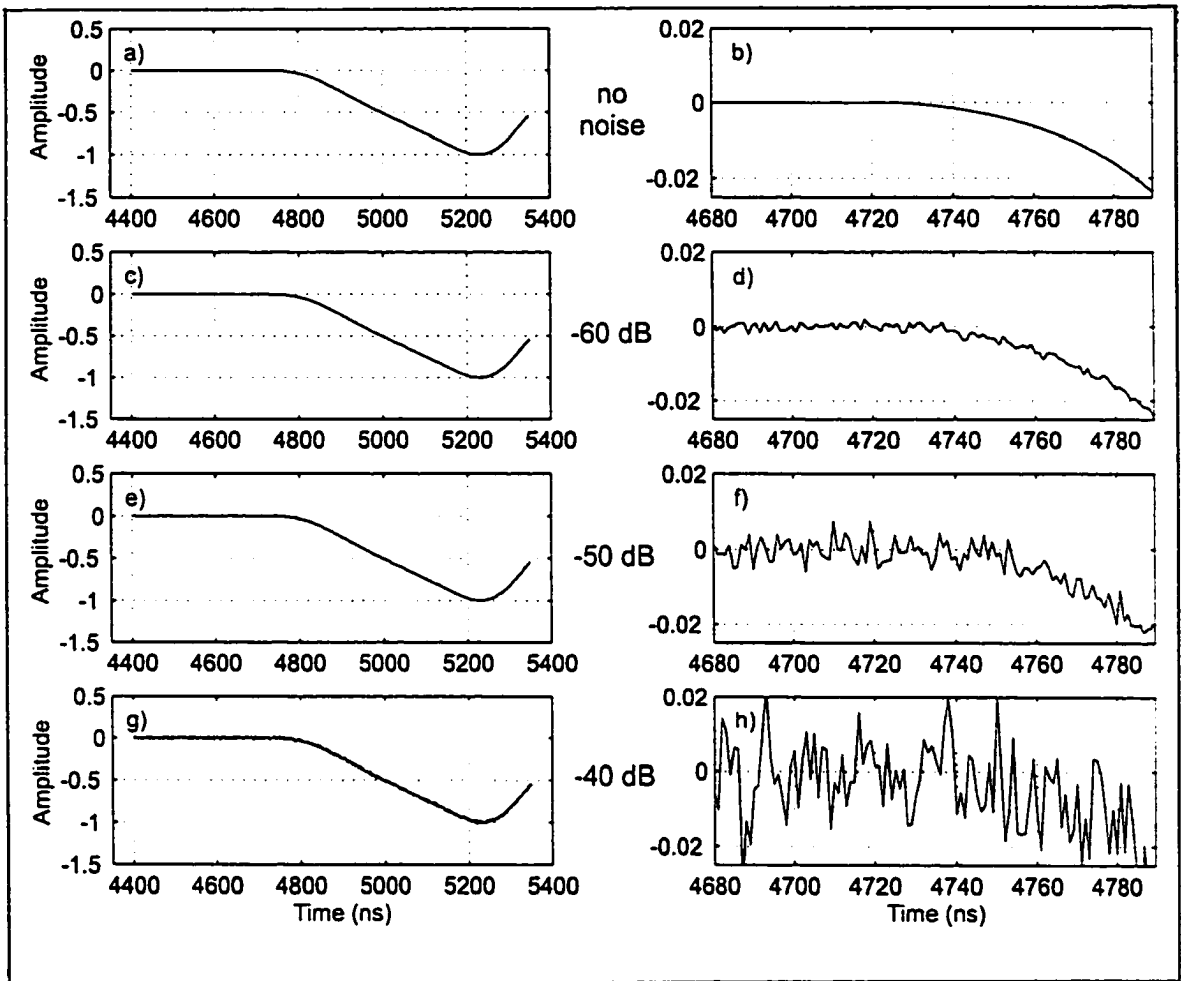


Figure 4. Microsecond and 100 ns scale segments of the synthetic test waveforms derived from the observed 290 MPa trace with a-b) no added noise, c-d) low noise (-60 dB), e-f) moderate noise (-50 dB), and high noise (-40 dB). Noise levels in decibels are calculated with the absolute value of the amplitude of the first minima.

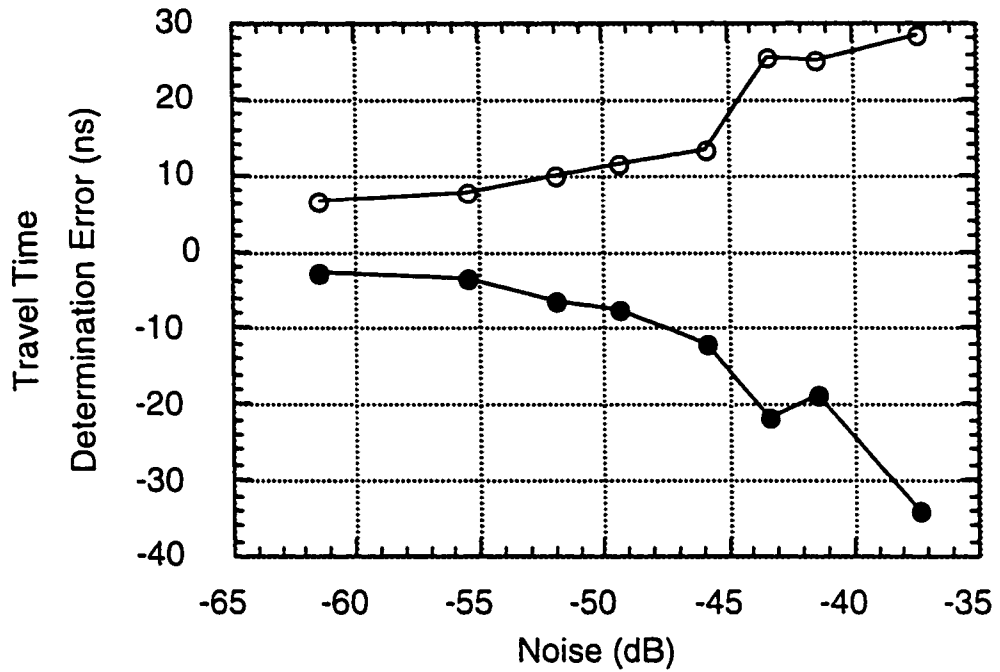


Figure 5. Mean transit time determination error (filled circles) and its standard deviation (open circles) versus level of added noise.

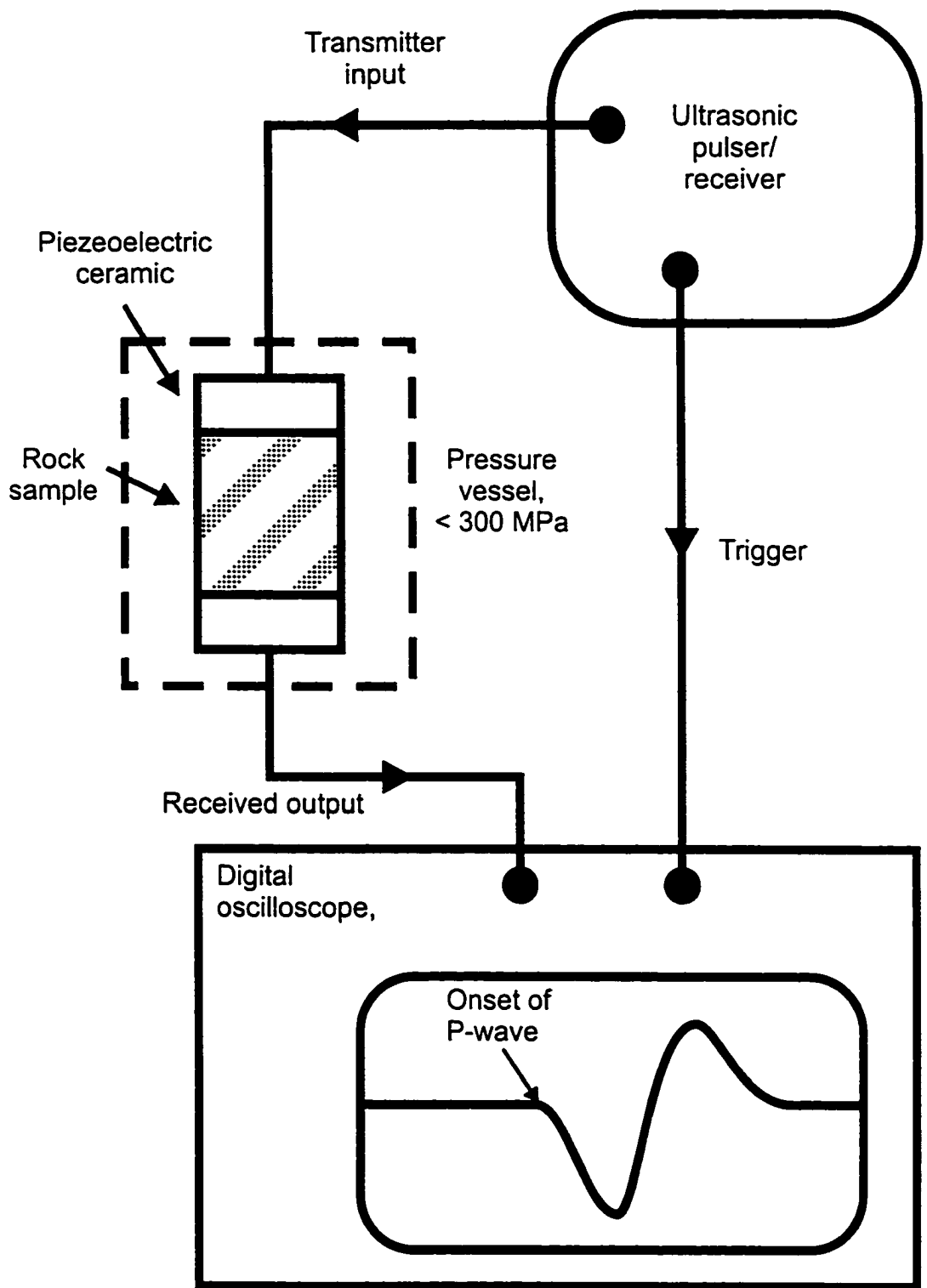


Figure 6. Simplified experimental configuration.

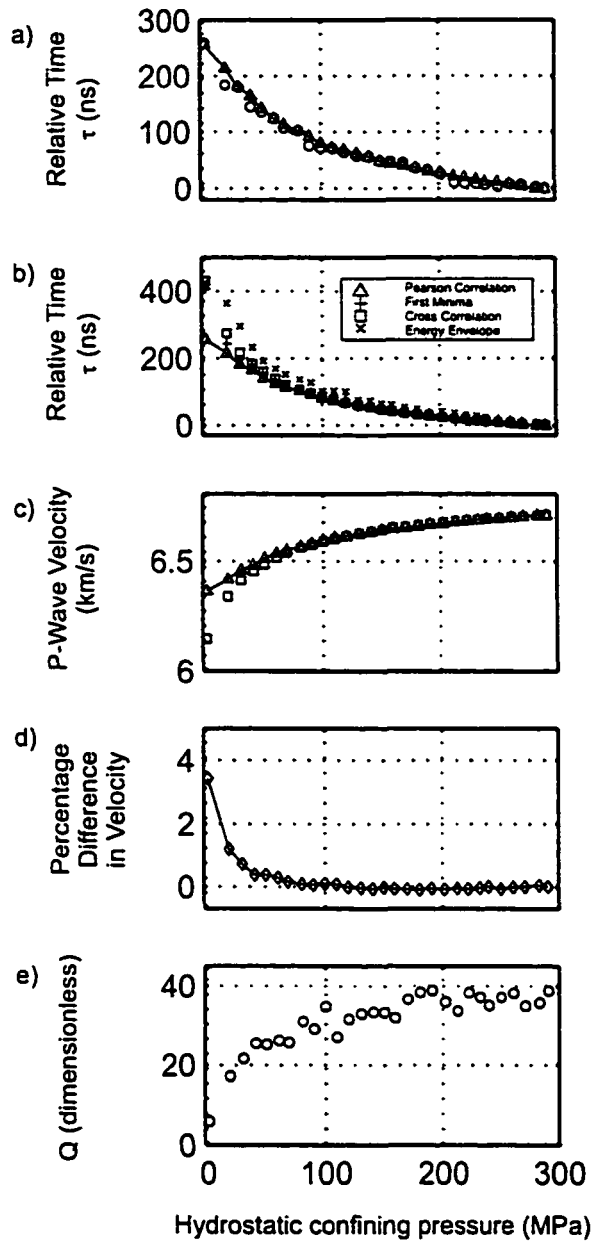


Figure 7. Pressure and method dependent measures of transit time, velocity, and attenuation. a) Manually picked (open circles) and Pearson regression relative time shift travel times (open triangles) to the 290 MPa reference versus confining pressure. b) Pearson regression onset (open triangles), first amplitude minima (crosses), waveform cross-correlation (open squares), and amplitude envelope cross-correlation (x's) transit times relative to the 290 MPa reference versus confining pressure. c) Velocities derived using Pearson regression onset (open triangles) and waveform cross-correlation (hollow squares) transit times versus confining pressure. d) Differences in the velocities in d) expressed as a percentage of the Pearson regression velocity versus confining pressure. e) Apparent quality factor Q versus confining pressure.

CHAPTER 4
Compressional -Wave Velocities in Attenuating Media:
A Laboratory Physical Model Study¹

4.1 INTRODUCTION

Although at first glance seemingly trivial, it is worthwhile to consider how the velocities of elastic waves propagating in real attenuating media should be determined experimentally from a recorded arriving signal. On one hand, theoretical analyses which link static elastic properties to wave propagation phenomena are almost exclusively based on the motion of monochromatic, elementary plane waves travelling at the frequency dependent phase-velocity. On the other hand, in many real laboratory and field situations wave-velocities are determined by charting the 'picked' transit times versus propagation distance of a band-limited wave-packet, the general assumption being that such methods yield group-velocity (e.g. Claerbout, 1992). However, phase-and group-velocities only coincide with certainty when there is no wave-velocity dispersion.

Attenuation is intrinsically linked to dispersion; phase- and group-velocities depend on frequency (see discussion in Aki and Richards, 1980). As a consequence, the evolution of a propagating wave-packet is related to the distance traveled and the attenuative properties of the medium. For example, in VSP analyses the higher frequency components of the downgoing wave are progressively diminished with increasing depth and in metamorphic rocks, pulse broadening is dependent on the extent of micro-fracture within a tested sample (e.g. Molyneux and Schmitt, in press). To determine a velocity in practice, one would plot the transit time of a certain feature of

the pulse, such as the first amplitude extremum, against propagation distance. However, if the shape of the pulse is continually evolving there is no reason to suspect, a priori, that the moveout of such a feature necessarily provides a good measure of the wave-velocity.

It is not immediately obvious what a more definitive measure of the wave velocity might be. Perhaps most fundamental are the phase- and group-velocities, the dispersion of which can provide important insight into mechanisms influencing attenuation and hence the petrophysical properties of the material (Winkler, 1983; Jones, 1986; Brown and Seifert, 1997). The determination of these wave velocities is non-trivial and requires the initial phase information of the outgoing pulse that is often absent in everyday field practice. Other problems, foremost of which is perhaps the generation of multiples in reflection profiling, are many. Similarly, even low levels of noise preclude the estimation of pulse onset transit times used in finding the signal-velocity. As a result, transit time determinations such as the picking of the first peak or zero crossing of amplitude are often used when calculating wave velocities.

Although a physical description of a material requires that the velocity-dispersion is determined, the picking of a single travel time in a pulse transit experiment will probably remain the common practice. To our knowledge there have been no studies in which the intrinsic measures of wave velocity have been compared to those commonly obtained using time picking; such a comparison is the objective of this study. An experimental physical model approach much along the lines of that first employed by Wuenschel (1965) is taken. The primary advantage of the physical model approach is that waves propagate through a real material whose attenuative character has not been predetermined by many of the simplifying assumptions brought to bear in the study of attenuation.

¹ A version of this paper has been accepted for publication. Molyneux and Schmitt, in press, *Geophysics*.

Theoretical modeling can be complicated by ambiguities associated with reproducing completely realistic and causal waveforms (e.g. Strick, 1970; Schmidt and Muller 1986; Gudmundsson, 1996). In this chapter, pulse-transit experiments designed for the determination of group- and phase-velocities through attenuating saturated quartz and glass grain packs are described. Both wave-velocity dispersion and attenuation of the packs are characterized. The determination of these wave velocities is assisted by an empirical windowing technique that objectively reduces the influence of spurious signal codas. Common time-picking procedures are then evaluated to see if any of these measures correspond to the intrinsic properties of the propagating media, group-and phase-velocities. The results have particular implications to the interpretation of laboratory physical property determinations, sonic-logging, cross-well tomography, and general seismology.

4.2 BACKGROUND

4.2.1 Group and Phase Wave-Velocities

In geophysical practice, wave velocities are often determined by measuring the transit time of a discrete pulse of wave energy. The amplitude $P(x, t)$ of this pulse, or wave-packet, can be described as the superposition of a number of mono-frequency plane waves, each of amplitude

$$A(x, t, \omega) = A_0(\omega) e^{i[Kx - \omega t + \phi_0(\omega)]} \quad (1)$$

such that

$$P(x, t) = \int_{\omega_1}^{\omega_2} A(x, t, \omega) d\omega,$$

(2)

where $P(x, t)$ contains band-limited angular frequencies between and including ω_1 and ω_2 . $A_0(\omega)$ and $\phi_0(\omega)$ are the initial, or reference, amplitude and phase of each planewave. $K(\omega) = k(\omega) + i\alpha(\omega)$ is the propagation constant consisting of a real wavenumber $k(\omega)$ (in rad/m) and the imaginary component $\alpha(\omega)$ which is the attenuation coefficient. This coefficient is here described in units of m^{-1} (often given the name neper, see Toksöz and Johnston, 1981). If attenuation exists, maintaining causality requires that both $k(\omega)$ and $\alpha(\omega)$ depend on frequency; the dispersion relation is the plot of $k(\omega)$ versus ω . In a nondispersive medium, the wave velocities are all the same and the dispersion curve is simply a straight line. The phase-velocity follows from the dispersion curve and is given by

$$V_p(\omega) = \omega/k(\omega)$$

(3)

The group-velocity can be interpreted as the propagation of a band-limited pulse of center frequency ω ,

$$V_g(\omega) = d\omega/dk(\omega)$$

(4)

Both $V_p(\omega)$ and $V_g(\omega)$ may be determined if $k(\omega)$ is known but this is rarely the case in a laboratory or a field experiment. However, the dispersion relation follows directly from

the phase spectrum of the pulse's Fourier transform. Such methods have long been used to obtain dispersion curves in studies of teleseismic surface waves (e.g., see Lay and Wallace, 1995), sediments (e.g., McDonal et al, 1958; Weunschel, 1965; Jacobsen, 1987), and complex materials in the laboratory (Weunschel, 1965; Winkler and Plona; 1982; Sachse and Pao; 1978; and Droin et al, 1998). A modified application is used here. Essentially, the phase $\phi_1(\omega)$ observed at position x_1 is

$$\phi_1(\omega) = \frac{\omega x_1}{V_p(\omega)} + \phi_0 \quad (5)$$

If the pulse is observed at two locations, x_1 and x_2 , then the difference in the phase is $\Delta\phi(\omega) = \phi_2(\omega) - \phi_1(\omega)$ and upon substituting and rearrangement

$$V_p(\omega) = \omega(x_2 - x_1) / \phi_1(\omega) \quad (6)$$

which has the advantage that the unknown initial phase $\phi_0(\omega)$ is eliminated.

In practice, we followed the description of group and phase lag times described by Claerbout (1992). The phase lag time between two observations is $\Delta t_p(\omega) = \Delta\phi(\omega)/\omega$ with the phase velocity equal to $(x_2 - x_1) / \Delta t_p(\omega)$. Similarly, the group delay times $\Delta t_g(\omega) = d(\Delta\phi(\omega))/d\omega$ leads to the group velocity $V_g(\omega) = (x_2 - x_1) / \Delta t_g(\omega)$.

Figure 1 illustrates the determination of group and phase delay times from observations of the same hypothetical propagating wave-packet at two different positions along its ray path, Figure 1a. The phase spectra of both are calculated and unwrapped (Figure 1b) and their difference $\Delta\phi(\omega)$ used to find $\Delta t_p(\omega)$ (Figure 1c). The group delays $\Delta t_g(\omega)$ are calculated at each frequency from the slope of the phase spectrum.

In the absence of attenuation, the propagation velocity of the amplitude-envelope maximum is equivalent to the group velocity as demonstrated by simple modeling (e.g., Hines, 1951; Sachse and Pao, 1978; Merkulova, 1967; and Raggiozino, 1981). However, the definition of the group velocity in attenuating media is less clear as the propagating wavepacket shape evolves with distance. Indeed, Hines (1951) noted that:

“ ‘group-velocity’ itself is largely a matter of mathematical definition. Whether or not it gives (approximately at least) the velocity of an experimental pulse through a medium is a more relevant question.”

4.2.2 Dispersion and Attenuation

Attenuation is intrinsically linked to wave-velocity dispersion by the requirement that a real pulse propagating in an attenuating medium must be causal (e.g. Aki and Richards, 1980; Futterman, 1962). Mathematically, $\alpha(\omega)$ and $k(\omega)$ are inter-related by the Kramer-Kronig relationship (e.g., see Landau and Lifshitz, 1958). Specifically, $\alpha(\omega)$ is determined from the Hilbert transform of the $k(\omega)$ (Sache and Pao, 1978; O’Donnell et al, 1981). As a consequence, although this study focuses on wave-velocity determination, it

is useful to characterize the corresponding attenuation, as this will be relevant to the evolution of the pulse. Attenuation coefficients are found by first noting that the absolute Fourier amplitude component of a pulse observed at position x follows from equation (1)

$$A_1(\omega, x_1) = A_0(\omega, 0)e^{-\alpha(\omega)x_1}$$

(7)

The amplitude ratio of two such observations of the same pulse but at two different locations x_1 and x_2 allows a direct determination of the attenuation coefficient $\alpha(\omega)$

$$\alpha(\omega) = \frac{\ln \left| \frac{A_2(\omega, x_2)}{A_1(\omega, x_1)} \right|}{(x_2 - x_1)}$$

(8)

It is worth noting that equation (8) holds for a plane wave in which there is no wavefront spreading. For realistic geometries, wave field divergence and diffraction effects need to be corrected by the appropriate modulation of the position dependent amplitudes (e.g. Winkler and Plona, 1982; Droin et al, 1998).

Although the frequency dependent attenuation $\alpha(\omega)$ may be considered as an intrinsic material property, attenuation is most often reported in the geophysical literature

by the quality factor $Q = -2\pi W/\Delta W$ where W is the maximum stored elastic energy and ΔW the energy loss per cycle. Q is most generally related to α by (Bourbie et al., 1987),

$$Q = \frac{\omega_0}{2\alpha V} \left[1 - \frac{\alpha^2 V^2}{\omega} \right] \quad (9)$$

and when $Q \gg 1$

$$Q \approx \frac{\omega_0}{2\alpha V} \quad (10)$$

4.2.3 Conventional Time-Lag Picking

It can be argued that V_p and V_k provide an intrinsic measure of the material properties. In practice, however, the pulse transit times used in determining wave-velocities are normally derived from simpler time picking criteria. Here, we compare the fundamental group and phase velocities to those derived by more common methods. These measures are the signal (V_s), the first extremum (V_m), the peak of the amplitude envelope (V_H) and the cross correlation (V_c), velocities. These standard measures of transit-time are illustrated in Fig. 2 and more specifically are:

- a) The signal onset time: This is the lag-time at which the first detectable amplitude is located (Molyneux and Schmitt, in press). This time is difficult to pick as even small levels of noise can critically mask the first onset. In deference to Brillouin (1952) we call the wave-velocity derived from this lag time the signal velocity V_s .

- b) The peak lag time of the amplitude envelope: This criterion, often used in the nondestructive testing community, the time lag of the peak of the amplitude envelope is employed. Such monitoring of the amplitude maximum in weakly attenuating media is commonly associated with group velocity. The amplitude envelope is calculated from the modulus (absolute value) of the complex analytic signal given by the Hilbert transform of the acquired trace (Young, 1962; Taner et al, 1979; Barnes, 1993). This velocity is referred to as V_H .
- c) The first amplitude extremum time: This is simply the lag-time of the first peak or trough. This is a criteria very commonly used in practice (e.g. Gudmunsson, 1996; King, 1966) as one may easily track the same peak coherently through a number of traces. Other similar criteria that could be employed are the lag time of the first zero amplitude crossing. We term this wave-velocity V_m .
- d) The lag time in the cross-correlation between two traces: This method is often used digitally with relative travel time delay measurements in the laboratory (e.g. Lu et al., 1990) or manually by visual comparison of the signals through a standard and the test sample (e.g. Birch, (1960). By adjusting the length of the standard to a point where the two signals visually correlate on the oscilloscope, the length of the calibrated standard is converted to a velocity. We refer to the resulting wave-velocity in subsequent discussions as V_x .

4.3 EXPERIMENTAL DESCRIPTION

The experiments were carried out using a pulse transmission technique. Sending and receiving transducers were mounted on aluminum buffer caps at opposing ends of the cylindrical samples. The attenuating media consisted of glycerol saturated packs of either glass beads or quartz sand (Table 1). Glycerol was used as a saturant due to its relatively high P-wave velocity that resulted in a relatively large effective saturated grain pack velocity, preventing potentially contaminating head waves. The lengths of the packs were changed in order to provide measures of the evolution of the wave-packet with distance propagated. The Ottawa sand is a clean quartz sand. The glass beads are those normally employed in sand blasting operations and according to the manufacturer consist primarily of recycled soda-lime glass. Statistical image analysis from photomicrographs (Figure 3) of the sand grains and glass beads provided their physical mean and standard deviation of dimension, Table 1.

The saturated grain packs are prepared by pouring glycerol in an acrylic tube closed at the bottom with a relatively lossless aluminum buffer cap in which $Q \sim 120,000$ for ultrasonic frequencies. The sand or glass beads are then poured into the glycerol whilst the acrylic container is being oscillated at audible frequencies by an air driven cam. This shaking ensures the bead packs have minimal but most importantly, consistent porosity. For each length increment a known mass of the grains is added and the second aluminum buffer cap is placed on top. Excess glycerol flows past the buffer cap. The length of the grain pack is determined to ± 0.1 mm by a Vernier Caliper. The porosity, ϕ of the pack is simply determined via $\phi = 1 - M/\rho V$, where M is the total mass of grains added, ρ is the

known grain mass density, and V is the total volume of the cylindrical sample. The observed porosities of 36% and 38%, Table 2, are approximately equal to the 36% porosity expected for a random pack of spheres (Bourbie et al., 1981). For any given pack, errors in the sample measurement lead to errors in the individual porosity of less than 1% which is comparable to the observed range of porosities indicated by the first standard deviation of error in Table 2.

Piezoelectric ceramics (BaTiO_3 , 25.41 mm diameter, 1 MHz resonant frequency) were mounted to the ends of the aluminum buffer rods (45.00 mm diameter, 48.21 mm length). Such buffer cap lengths are required to ensure the piezoelectric ceramics are perpendicular to the tube axis. These ceramics are mechanically damped using an epoxy-metal powder mixture to produce a broad-bank input pulse.

A square wave input voltage (~200 Volts) excites the transmitting piezoelectric ceramic. The resulting pulse propagates through the aluminum buffer caps, the saturated grain pack, and the second aluminum buffer cap to be recorded by the piezoelectric receiver. Individual pulses are digitally recorded at a 1 GHz sampling rate and stacked over 50 acquisitions at each given pack length (from approximately 10 mm to 50 mm length). A windowing technique (Appendix A) was developed to isolate the first arriving wave-packet, as later arrivals and scattering of energy in the coda of the traces can influence the measures of V_p , V_g and V_x . This windowing method is based on the assumption that the amplitude envelope follows a Gaussian shape.

4.4 RESULTS

Both the directly observed traces and isolated traces for each of the three different grain packs are shown in Figure 5. The corresponding isolated pulses broaden noticeably with propagation length, indicative of dispersion. An advantage of the present procedure is that the several independent wave-velocity measurements obtained from each grain pack allow for robust uncertainty estimates. The acquisition of as many as eight different lengths corresponds to 28 redundant measurements of Δx and corresponding Δt for each of the packs; the slope of such a plot yields the wave-velocity.

These differential measurements have a number of advantages. For example, the requirements that the buffer cap delay times be known and amplitude corrections for reflection at the sample-buffer interface be accounted for are removed. Further, any systematic phase unwrapping, sample heterogeneity, length determination error, and electrical noise errors are reduced by the multiplicity of the measurements. One disadvantage of the present procedure is that the samples are not perfectly homogeneous with length as indicated by the 1-2% standard deviation in the porosity, Table 2. However, this minor sample heterogeneity is at worst comparable to that expected in measurements of real earth materials, which are anything but uniform.

Both group and phase delay times are found over the range of frequencies from 0 MHz to 0.8 MHz. These are calculated at each frequency in the digital Fourier transform for every combination of the traces acquired for a given sample. The redundancy of measurement enables statistical error estimation on the determination of $V_p(\omega)$ and $V_g(\omega)$. One such series of relative group time lags for the #7 glass bead pack at a

frequency of 0.38 MHz is shown in Figure 6. The 21 group delay times are plotted versus the relative length for the 7 grain pack lengths tested and the slope of a line fit to these data provides the group wave-velocity at this frequency. Least squares linear regression yields a group velocity of 2.30 km/s, the standard deviation in the linear slope suggests an uncertainty in this velocity measurement of ± 0.04 km/s. The wave-velocity estimates provided by the conventional travel time picking methods are determined using the same differential procedure, Table 2. Uncertainties are solely based on the first standard deviation of slope (Spiegel, 1961) that exist in the distance-time scatter plots.

The frequency dependent phase and group wave-velocities for each of the different packs are summarized in Figure 7a over the frequency range from 0 to 0.8 MHz. Fourier amplitude spectra indicate that the predominant signal energy lies between 0.2 – 0.6 MHz; consequently V_p and V_g are expected to be most valid in this band.

The various measures of velocity for each of the packs are compared in table 2. Phase and group velocities are provided at the peak amplitude, or predominant, frequencies of 0.33 MHz and 0.38 MHz for the sand and the glass bead packs, respectively. Phase velocity measurements are most uncertain because of phase skipping error in the unwrapping procedure. Any phase skip cumulatively influences calculation of all subsequent phase velocities at greater frequencies. In contrast, the group velocity is affected only at the frequency at which the phase skip error occurs and so is a more robust measurement.

To account for geometric effects on the propagating signal amplitude the same experiments were carried using the acoustic apparatus on a pure glycerol medium. The pulse shape remained stationary over a range of propagated distances with no detectable

change in either temporal or frequency domain character. That is, intrinsic attenuation within the fluid could not be detected with the present experimental configuration. However, an almost linear, yet weakly exponential amplitude decay with distance was observed, with a correlation coefficient of 0.98. Therefore, instead of mathematically determining the diffraction corrections (e.g. see Winkler and Plona, 1982) we used an empirical correction based on this exponential decay to modulate the traces, based on the sample length.

$$A = A_0 e^{-\alpha x} \tag{11}$$

The exponential decay factor α is 0.0067 +/- 0.006 of standard distribution and x is the distance measured in millimeters where A and A_0 are the observed and zero length first peak amplitudes in millivolts.

The frequency dependent attenuation for each pack is determined from equation (8) with up to 28 differential comparisons. At each frequency the resulting attenuation values, α , are widely distributed as observed by the large single standard deviation error bars, Figure 7b. This is common with attenuation measurements and uncertainties of 100% are not unusual (e.g. see White, 1992). This merely reflects uncertainties in the spectral decomposition and windowing of the signal. The quality factor Q is calculated using equation (9) for comparative purposes, Figure 7c. Such Q calculations are

consequently more uncertain due to propagation of errors from both the α and V_p measurements but only the central trend is shown.

4.5 DISCUSSION

The primary objective of this chapter is to find the most representative relationships between the fundamental material properties of group-and phase-velocity and those velocities determined by common travel-time picking methods. As this may depend on how the waves are attenuated, the character of the attenuation is first examined.

4.5.1 Character of the Attenuation

The obvious decay in amplitude and spreading in time of the first arriving pulses (Figure 5) indicate that these saturated glass bead packs successfully produced strongly attenuating media. This further supported by the high values of attenuation (~ 100 nepers/m) and corresponding low Q (~ 4) derived directly from the waveforms, Figure 7b and 7c.

It is not clear what the major source of the attenuation might be in these bead packs and it is likely that a number of mechanisms such as grain-grain sliding, scattering, mode-conversion, bead resonance, and differential fluid motion all contribute to some degree. A detailed discussion of the mechanisms is delayed for a later contribution.

A plot of attenuation versus frequency would have a constant slope with frequency in a constant Q medium; Wuenschel (1965) observed a nearly linear attenuation-frequency plot in polymethyl methacrylate over frequency band below 150 kHz as did

Sachse and Pao (1978) in 6061-T6 aluminum alloy. Such linearity contrasts with the results of Figure 7c that show that Q generally increases with frequency.

4.5.2 Wave-velocity Comparisons

Comparisons of the various measures of wave-velocity are made in Table 2. The group velocity is used as the reference as it is usually taken for granted that this is what wave-velocity measurements derived from travel-time picking determine. Further, it is more stable than the determination of the other intrinsic property of phase velocity that is subject to the previously mentioned unwrapping errors.

4.5.3 Group and Phase Velocities

There is no requirement that V_p and V_g should have the same magnitude, except in the absence of attenuation (and anisotropy). That they are not the same in such highly attenuating media is not surprising. The greatest discrepancy is observed for the #3 sand where at the dominant frequency the group-velocity is about 11% greater than the phase-velocity. In the other samples, the group-velocities are less than the phase velocity by about 3%. These discrepancies suggest that care should be taken when attempting, in lossy materials, to use an estimate of group-velocity to further gain an estimate of the phase-velocity.

These wave-velocities are also compared to value for the Woods formula of phase velocity in which the predominant wavelength is long compared to the suspension particle size (e.g. see Berryman, 1995),

$$V_{Wood} = \sqrt{\frac{\left(\frac{K_f}{\phi} + \frac{K_s}{(1-\phi)}\right)}{(\phi\rho_f + (1-\phi)\rho_s)}} \quad (12)$$

where ρ_f and ρ_s are the mass densities and K_f and K_s are the adiabatic bulk moduli of the fluid and solid portions, respectively. Equation (12) ignores any frame or skeleton compressibility; this is justified by the fact that the beak packs are at room pressure during the experiments and have not been in any way further compacted. The bulk modulus of the frame is expected to be very low even in relation to that for the fluid and as such is ignored, frame bulk moduli for such unconsolidated materials have been estimated to be near 0.1 GPa (e.g. Hamilton, 1972). The determined Woods velocities for the grain packs, Table 2, are derived from the constituent properties in Table 1. The calculated and measured values for the #3 quartz grain pack are in very good agreement while those for the glass beak packs are slightly less so. This general agreement may suggest that the observed velocities are close to the low frequency limit of this particular effective medium theory. This is expected as the wavelengths of the pulses (~6.5 mm) are larger than the bead diameters (Table 1) by a factor of more than 8, such that the packs should act as effective media to the passing waves (e.g. Yin et al, 1994). It is worth noting that all velocities for the quartz sand are lower than the corresponding measure in the glass bead packs. At first examination this appears unusual due to the higher elastic moduli of quartz (Table 1), and relatively low sand pack porosity. Such effects are more than offset by the relatively high quartz density as indicated from the Wood's formula

calculation of velocity in which the quartz sand pack is lower velocity than either bead pack, Table 2.

4.5.4 Conventional Time Picks

We compare the intrinsic group velocity properties to more common velocity analyses, Table 2. The wave-velocities that are determined from the two most commonly applied time picking criteria are V_x and V_m . Both of these are of nearly the same magnitude and are biased 2% to 3% greater than V_g at the predominant frequency. In contrast, the time lag derived from the peak of the amplitude envelope yields V_H velocities that also differ from V_g by 2% to 3% but is not consistently biased to values lower or greater than V_g .

Ignoring for the moment V_s , all of the simple time picking methods give velocities in relative agreement with the group velocity, in that most velocity measurements are within one standard deviation of V_g at the predominant frequency with a velocity discrepancy of less than 3%. As such, V_x , V_m , and V_H provide a reasonably good, but not exact, estimate of the group velocity at the predominant frequency in these bead packs. For the two glass bead packs, both V_x and V_m are in good agreement with V_p at the predominant frequency, but this may be coincidental.

4.5.5 Signal Velocity

The signal velocity we measured from the time lag of the first detectable onset of the pulse is always greater than V_g , i.e., the relative signal-time delays are smaller than the respective group delays. Theoretically, a small amplitude arrival with a discrete onset can occur well in advance of the main signal in attenuating media (Strick, 1970), but are

generally obscured by noise. In electromagnetic propagation investigations, such theoretically described *precursors* (e.g. Stratton, 1941) have been experimentally detected (e.g. Stenius and York, 1995). This suggests that the onset lag time may not give a valid estimate of the transmission time of the pulse at the predominant frequency in highly attenuating media. Indeed, our measured signal velocity is always greater than all the velocity measures, with discrepancies of up to 19%. As a caveat, Molyneux and Schmitt (in press) note that the discrepancy between signal velocity measurements and other common timing measurements is negligible when the frequency independent $Q > 30$.

The first arriving energy is arguably associated with the fastest phase speed components. It is generally considered that in normal acoustic propagation through rock, these fastest phases occur at the highest frequencies. Such high frequency signal is strongly attenuated and thus has minimal amplitude with respect to background noise and the first arrival is likely to be picked late with associated lower velocities. Therefore, in highly attenuating media the best physical interpretation of the signal-velocity is that it provides a lower bound to the value of phase speed at high frequency.

4.5.6 Consistency of Criteria

There is one additional observation worth noting from Table 2. Despite the time picking criteria used a plot of the relative time lags versus relative distances, as for example seen in Figure 6, are all of high quality with correlation coefficients near unity. This holds true even for the time lags given by picking the onset of the pulse used in determining V_s , despite the increased difficulties inherent in determining this time. This

observation suggests that each criterion is self-consistent. Similar linearity of result was found by Kuster and Toksöz (1974) in a series of pulse-propagation measurements on an attenuating suspension medium, where the relative distance measurements were plotted against the time to first extremum.

4.6 CONCLUSION

Ultrasonic wave pulses were propagated through attenuative media in order to obtain a series of propagating pulses that evolve with distance traveled. The frequency dependent group-and phase-velocities were extracted from these pulses using a Fourier transform method and then compared to those derived using more standard travel-time picking procedures.

The saturated quartz and glass bead packs used here were highly attenuating with a quality factor Q which increased with frequency from 2 to 6 over the useful bandwidth of 200 kHz to 500 kHz of the tests. The mechanisms of attenuation in such packs are not completely understood but probably include scattering, bead resonance, mode conversion, grain-grain sliding, and differential fluid motion.

Most of the common wave velocity determinations yield similar, but not exact, values for the compressional wave-velocity. Group- and phase-velocities are not generally the same and differ at the predominant frequency by up to 12%. Wave-velocities estimated from picking the time of the signal's first amplitude extremum, from cross-correlation procedure, and from the peak of the amplitude envelope generally agree well with the group wave-velocity at the predominant frequency to better than 3%. As

such, these simple measures appear to provide reasonable estimates of the group-velocity at the predominant frequency.

In contrast the wave-velocity V_s , determined from the picked time of the pulse's onset always varies substantially from all other speed measures with discrepancies of up to 19%. When forming a distance-time plot of the first detectable onset of energy, the greater propagated distances produce a more attenuated signal. This reduced signal-to-noise-ratio results in a bias to uncharacteristically late identifiable time picks with *lower* associated velocities. However, we observe that the signal velocity is *greater* than all the measured group-and phase-velocities of our band-limited pulse. Consequently, if the onset of energy is built up from the high phase velocity components (first arriving signals), the observed V_s is a fundamental lower bound to the fastest phase velocities.

The results of this study suggest that some care need be exercised in wave-velocity determinations that employ pulse transmission methods. The media used here are exceptional in that they are highly attenuating and the variations between group- and phase-velocities will be accentuated. However, such attenuating conditions may be obtained in a number of cases in laboratory experimentation and the spreading of the waveform can be important in determining the wave-velocity. Determining phase- and group-velocity frequency dispersion in such cases can aid in more detailed characterization of the material.

APPENDIX – Windowing the First Arrival

Determining group and phase wave-velocities ideally requires an isolated pulse uncontaminated by later events and scattered energy. Unfortunately, in the real data (e.g. Figure 5) the first arrivals are followed shortly by secondary events. These later events are often attenuated by modulating the signal with a smooth edged Hanning window. The appropriate shape, duration and position of such windows can be highly subjective. Here, a more objective method of producing the window from the trace itself is developed. A modulation window is derived directly from the signal amplitude. The derivation exploits the empirical observation that the Hilbert transform amplitude envelope (Taner et al., 1979) of the analytic signal centered on the first arriving wave packet is well described by a Gaussian function of the form,

$$G(t) = B e^{-\frac{(t_0 - t)^2}{2\sigma^2}} \quad (A1)$$

where B is the constant, t is time, t_0 is the peak time of the Gaussian curve and σ is the standard deviation. A 100 ns window about the amplitude maximum fit with a Gaussian yields a correlation coefficient of fit of more than 0.99 for the real data, validating this Gaussian approach.

In development of the window, the early portions of the first arriving pulse around the peak of the amplitude envelope and before visual onset of spurious coda are fit by least-squares regression with the linearized form of (A1)

$$\ln|H(y(t))| = \ln B - (t_0 - t)^2 / 2\sigma^2 \quad (A2)$$

to yield the best values of B , t_m , and σ . Here, $|H(y(t))|$ is the absolute Hilbert transform of the real data, $y(t)$. This 'ideal' Gaussian shape, $G(t)$, is then divided by the amplitude envelope data to create the windowing function (t) which is applied directly to $y(t)$ to isolate the arrival. This process is illustrated in Figure A1.

The approach is tested on two superposed Ricker wavelets each of 0.36 MHz predominant frequency with peaks separated by $3.3 \mu\text{s}$ (1.2 times the predominant period) as shown in Figure A2(i). The peaks of the amplitude envelope do not coincide with the position of the delta functions, which represent the times of the centers of each zero-phase wavelet. It is the spurious coda that interferes with the energy envelope to incorrectly shift its peak position. Successive determination and application of the modulation function, from $1/20^{\text{th}}$ to unity strength in a series of 20 iterations slowly erode the effects of the spurious coda. This successive waveform windowing causes the peak of the amplitude envelope to correctly converge about the first delta-function position and the resulting wavelet compares well to the ostensibly known wavelet, Figure A2(ii).

REFERENCES

- Aki, K. and Richards, P.G., 1980, Quantitative seismology, theory and practice, 1:W.H. Freeman Company.
- Barnes, A.E., 1993, Instantaneous spectral bandwidth and dominant frequency with applications to seismic reflection data: *Geophysics*, **58**, 419-428.
- Bass, J.D., 1995, Elasticity of minerals, glasses, and melts, in: T.J. Ahrens, Ed., Mineral Physics and Crystallography – *AGU: A Handbook of Physical Constants*, **2**, 45-63.

- Berryman, J.G., 1995, Mixture theories for rock properties, in: T.J. Ahrens, Ed., Rock Physics and Phase Relations – *AGU: A Handbook of Physical Constants*, 3, 205-228.
- Birch, F., 1960, The velocity of compressional waves in rocks to 10 kilobars, 1: *Journal of Geophysical Research*, 65, 1083-1102.
- Bourbie, T., Coussy, O. and Zinszner, B., 1987, Acoustics of Porous media: Gulf Publishing Company.
- Brillouin, L., 1960, Wave propagation and group velocity: Academic Press, New York.
- Brown, R.L. and Seifert, D. 1997, Velocity dispersion: A tool for characterizing reservoir rocks: *Geophysics*, 62, 477-486.
- Carmichael, R.S., 1982, Handbook of physical properties of rocks, Volume II: CRC Press Inc.
- Claerbout, J.F., 1992, Earth Sounding Analysis, Processing Versus Inversion: Blackwell Scientific Publications.
- Droin, P., Berger, G. and Laugier, P, 1998, Velocity dispersion of acoustic waves in cancerous bone: *IEEE Trans. Ultrasonics, Ferroelectrics and Frequency Control*. 45. 581-592.
- Futterman, W.I., 1962, Dispersive body waves, *Journal of Geophysical Research*, 67, 5279-5291.
- Gudmudsson, O., 1996, On the effect of diffraction on travel time measurements: *Geophysical Journal International*, 124, 304-314.
- Hamilton, E.L., 1972, Compressional wave attenuation in marine sediments: *Geophysics*, 37, 620-646.

- Hines, C.O., 1951, Wave packets, the Poynting vector, and energy flow: Part II – group propagation through dissipative isotropic media: *Journal of Geophysical Research*, **56**, 197-220.
- Jacobsen, R.S., 1987, An investigation into the fundamental relationships between attenuation, phase dispersion, and frequency using seismic refraction profiles over sedimentary structures: *Geophysics*, **52**, 72-87.
- Jones, T.D., 1986, Pore fluids and frequency-dependent wave propagation in rocks: *Geophysics*, **51**, 1939-1953.
- King, M.S., 1966, Wave velocities in rocks as a function of changes in overburden pressure and pore fluid saturation: *Geophysics*, **31**, 50-73.
- Kuster, G.T. and Toksoz, M.N., 1974, Velocity and attenuation of seismic waves in two-phase media, II: *Geophysics*, **39**, 607-618.
- Lay, T. and Wallace, T. 1995, Modern global seismology: Academic Press.
- Landau, L.D. and Lifshitz, E.M., 1958, Statistical Physics: Pergamon Press Ltd., Addison-Wesley Publishing Company Inc.
- Lu, W.Y., Maxfield, B.W. and Kuramoto, A., 1990, Ultrasonic velocity measurement by correlation method: SESA Spring Conference, 901-906.
- McDonal, F.J., Angona, F.A., Mills, R.L., Sengbush, R.L., van Nostrand, R.G. and White J.E., 1958, Attenuation of shear and compressional waves in Pierre Shale: *Geophysics*, **23**, 421-429.
- Merkulova, V.M., 1967, Accuracy of pulse methods for measuring attenuation and velocity of ultrasound: *Soviet Physics – Acoustics*, **12**, 411-414.

- Molyneux, J.B. and Schmitt, D.R., in press, First break timing: arrival onset times by direct correlation: *Geophysics*.
- O'Donnell, M., Jaynes, E.T. and Miller, J.G., 1981, Kramers-Kronig relationship between ultrasonic attenuation and phase velocity: *Journal of the Acoustical Society of America*, **69**, 696-701.
- Ragogzino, M., 1981, Analysis of the error in measurement of ultrasonic sound velocity in tissue due to waveform deformation by frequency-dependent attenuation: *Ultrasonics*, **19**, 135-138.
- Sachse, W. and Pao, Y-H, 1978, On the determination of phase and group velocities of dispersive waves in solids: *J. Appl. Phys.*, **49**, 4320-4327.
- Schmidt, T. and Muller, G., 1986, Seismic signal velocity in absorbing media: *Journal of Geophysics*, **60**, 199-203.
- Soga, N., 1968, The temperature and pressure derivatives of isotropic sound velocities of α -quartz: *Journal of Geophysical Research*, **73**, 837-829.
- Spiegel, M.R., 1961, Schaum's outline series: Theory and problems of statistics: McGraw-Hill.
- Stratton, J.A., 1941, Electromagnetic theory. McGraw-Hill.
- Stenius, P. and York, B., 1995, On the propagation of transients in waveguides: *IEEE Antenas and Propagation Magazine*, **37**, 39-44.
- Strick, E., 1970, A predicted pedestal effect for pulse propagation in constant-Q solids: *Geophysics*, **35**, 387-403.
- Taner, M.T., Koehler, F. and Sheriff, R.E., 1979, Complex seismic trace analysis: *Geophysics*, **44**, 1041-1063.

- Toksöz, M.N. and Johnston, D.H., 1981, Seismic wave attenuation, *Society of Exploration Geophysicists*,
- Yin, H., Mavko, G., Mukerji, T. and Nur, A., 1994, Scale-dependent dynamic wave propagation in heterogeneous media: I experiments: 64th Ann. Internat. Mtg., Soc. Expl. Geophys. Expanded Abstracts, 1147-1150.
- Young, H.W. Jr., 1962, Discussion of time delays in reference to electrical waves: IRE Transactions on Ultrasonics Engineering, 13-21.
- White, R.E., 1992, The accuracy of estimating Q from seismic data: *Geophysics*, **57**, 1508-1511.
- Winkler, K.W., 1983, Frequency dependant ultrasonic properties of high-porosity sandstones: *Journal of Geophysical Research*, **88**, 9493-9499.
- Winkler, K.W. and Plona, T.J., 1982, Technique for measuring ultrasonic velocity and attenuation spectra in rocks under pressure: *Journal of Geophysical Research*, **87**, 10,776-10,780.
- Wuenschel, P.C., 1965, Dispersive body waves – an experimental study: *Geophysics*, **30**, 539 – 551.
- Zamanek, J. Jr. and Rudnick, J., 1961, Attenuation and dispersion of elastic waves in a cylindrical bar: *Journal of the Acoustic Society of America*, **323**, 1283-1288.

Table 1: Physical properties of the porous media constituents

	#3 Ottawa Sand	#3 Glass Beads	#7 Glass Beads	Glycerol
Material	Quartz	Soda-lime glass	Soda-lime glass	C ₃ H ₈ O ₃
Mean Diameter (mm)	0.81 +/- 0.14	0.67 +/- 0.05	0.22 +/- 0.04	NA
Aspect Ratio	0.76 +/- 0.18	1	1	NA
Density (g/cm ³)	2.648 ¹	2.48 +/- 0.01 ²	2.47 +/- 0.01 ²	1.26 +/- 0.01 ²
Isentropic Bulk Modulus (GPa)	37.8 ¹	37.8 ³	37.8 ³	4.67 ³
Shear Modulus (GPa)	44.4 ¹	25.4 ⁴	25.4 ⁴	0
Shear Wave-Speed (km/s)	4.092 ⁶	~3.2 ⁵	~3.2 ⁵	0
Compressional Wave-Speed (km/s)	6.047 ⁶	~5.4 ⁵	~5.4 ⁵	1.926 +/- 0.001 ²

¹ Bass (1995)² Measured in this study³ Calculated: $K = \rho(V_P^2 - 4 V_S^2/3)$ ⁴ Calculated: $\mu = \rho V_S^2$ ⁵ Estimated from Glass 1 of Carmichael (1982)⁶ Soga (1968)

Table 2. Comparison of measured and estimated wave-speeds

	Porosity	Woods estimate	Group velocity	Phase velocity	First break velocity	Correlation velocity	First peak velocity	Envelope velocity	V_{gmax}	V_{pmax}
#3 Quartz	0.36±0.01	2.2	2.24±0.04 (0.998)	2.00±0.13 (0.975)	2.52±0.10 (0.997)	2.29±0.04 (0.998)	2.31±0.03 (1.000)	2.19±0.02 (1.000)	2.24±0.04 (360 kHz)	2.11±0.07 (740 kHz)
#3 Glass	0.38±0.02	2.3	2.42±0.02 (0.999)	2.48±0.06 (0.987)	2.58±0.03 (1.000)	2.46±0.02 (0.999)	2.46±0.01 (1.000)	2.39±0.02 (1.000)	2.43±0.02 (150 kHz)	2.49±0.08 (350 kHz)
#7 Glass	0.38±0.01	2.3	2.30±0.04 (0.999)	2.37±0.03 (0.999)	2.58±0.01 (1.000)	2.37±0.03 (0.999)	2.35±0.02 (1.000)	2.38±0.03 (1.000)	2.58±0.05 (800 kHz)	2.44±0.03 (100 kHz)

Note: Values in brackets generally refer to the linearity of the distance-time plot, which yield the speed measurement. In the case of V_{gmax} and V_{pmax} , the maximum observed group- and phase-speeds, the bracketed numbers refers to the frequency of the observed measurement. Error values are quoted to one standard deviation and the Woods effective media estimate [e.g., Berryman, 1995] is calculated from the physical properties of Table 1 parameters.

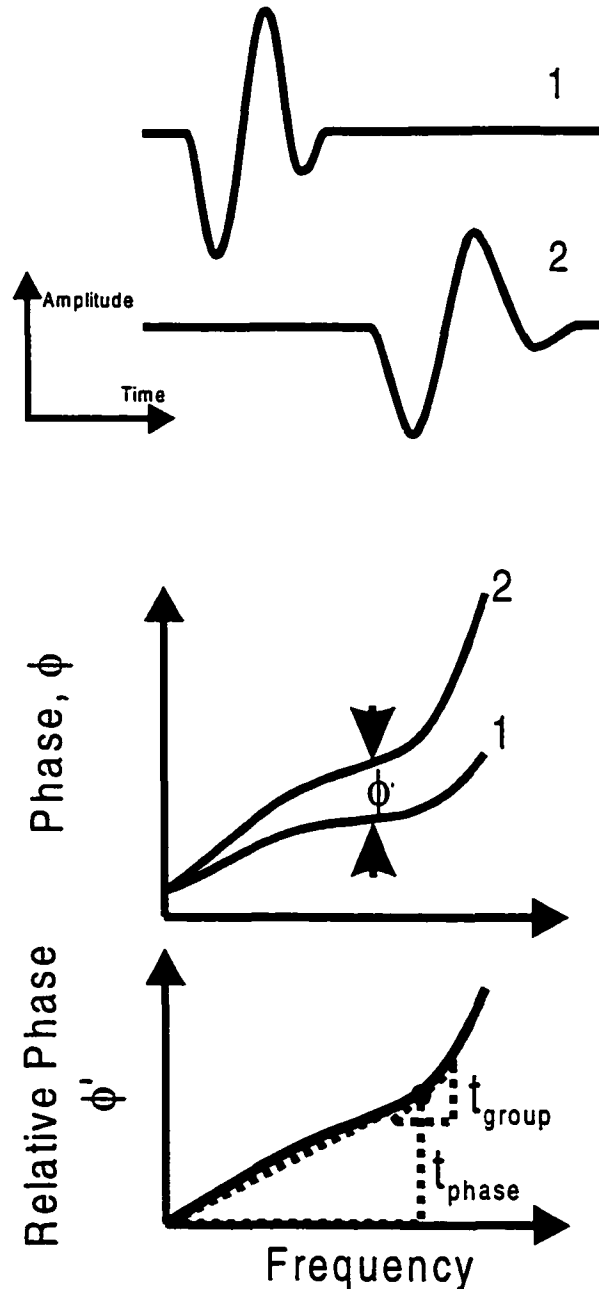


Figure 1 Illustration of Fourier method to calculate phase and group delay from a) 2 recorded traces through different lengths of the same attenuating medium and b) the respective phase (ϕ) spectra of both recorded wavelets and the relative phase (ϕ') spectrum from which relative group and phase delay is calculated.

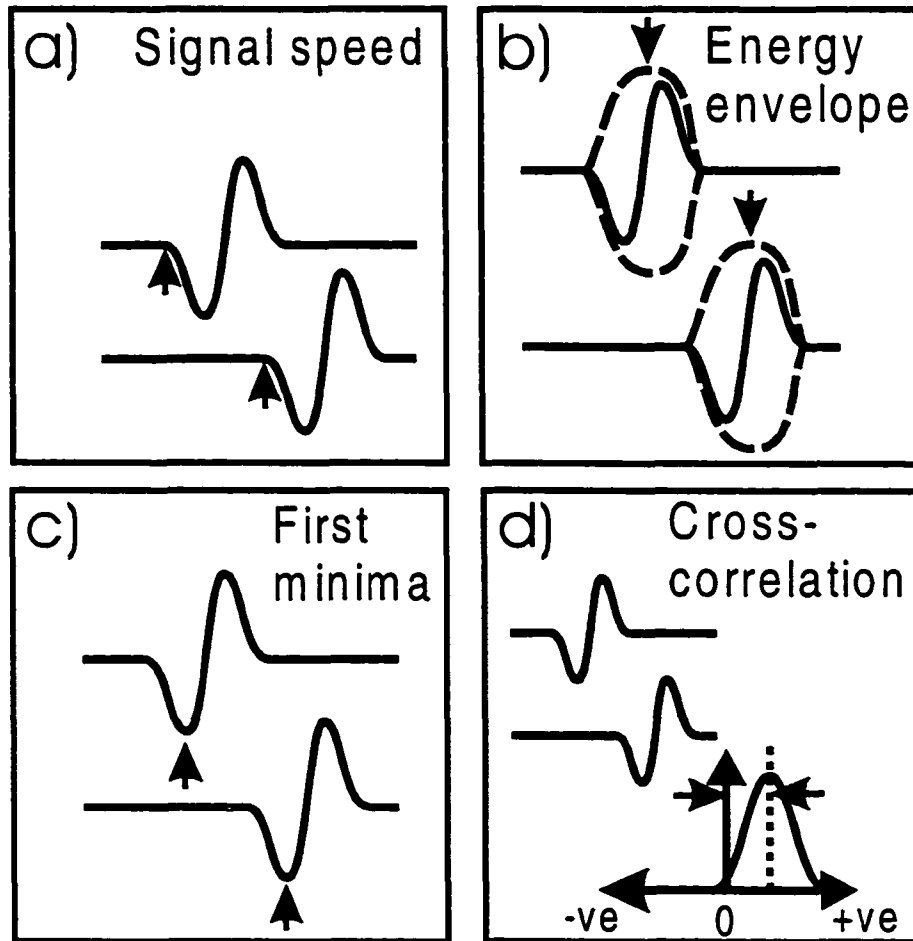


Figure 2 Illustration of the common time picking criteria employed.

- a) first detectable onset of the signal, V_s ,
- b) peak time of amplitude envelope calculated from the analytic signal, V_H ,
- c) time of the first amplitude extremum, V_m ,
- d) relative times provided by cross correlation of the signal with a reference, V_x .

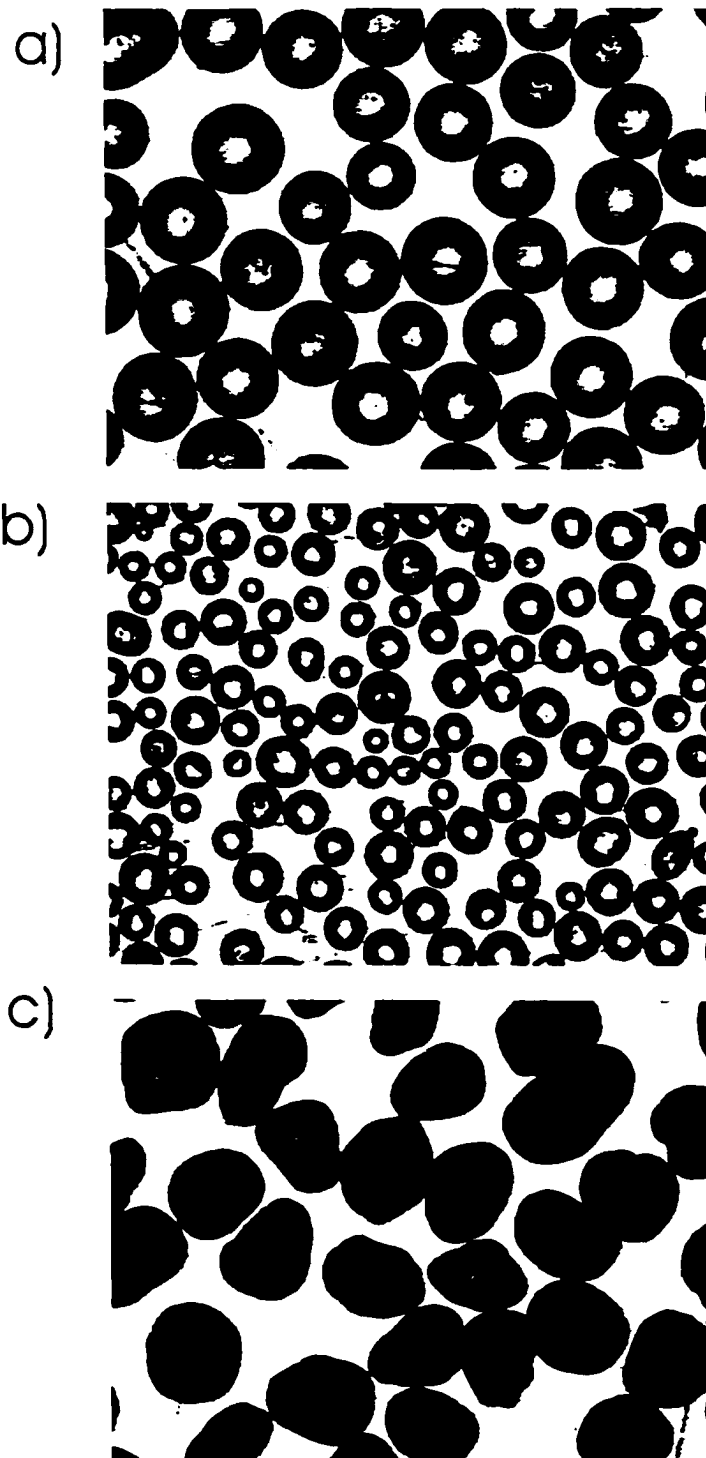


Figure 3

Photomicrographs of sand and glass pack constituents

a) #3 glass beads

b) #7 glass beads and

c) Ottawa quartz sand grains.

Each photomicrograph represents an area of 5.09 mm by 3.89 mm.

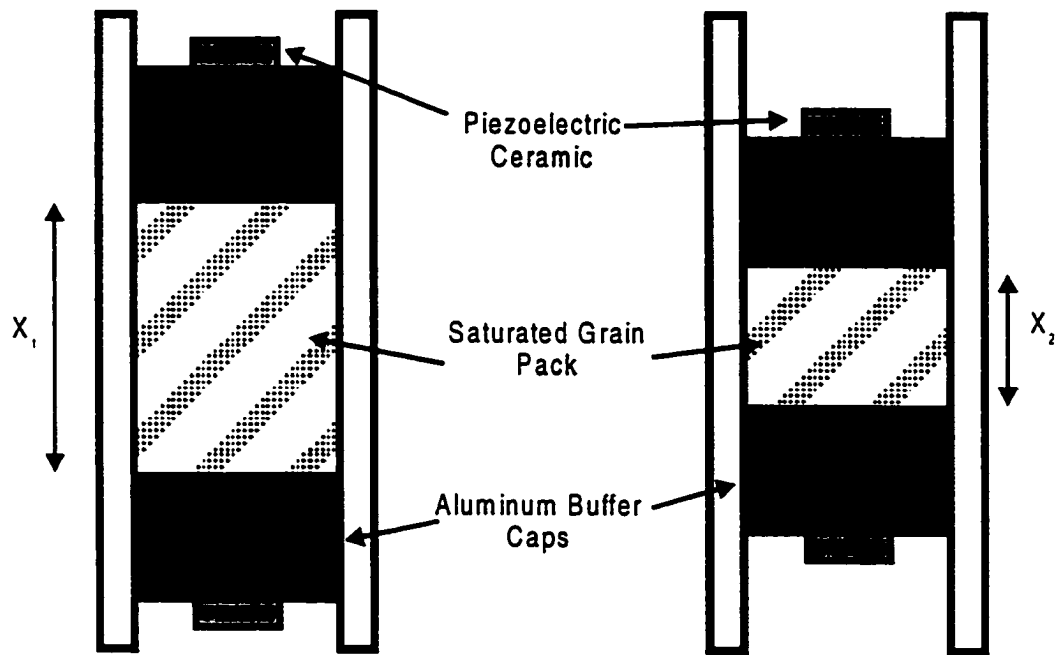


Figure 4 Experimental setup. Signal is recorded through several lengths of grain pack of which x_1 and x_2 are shown.

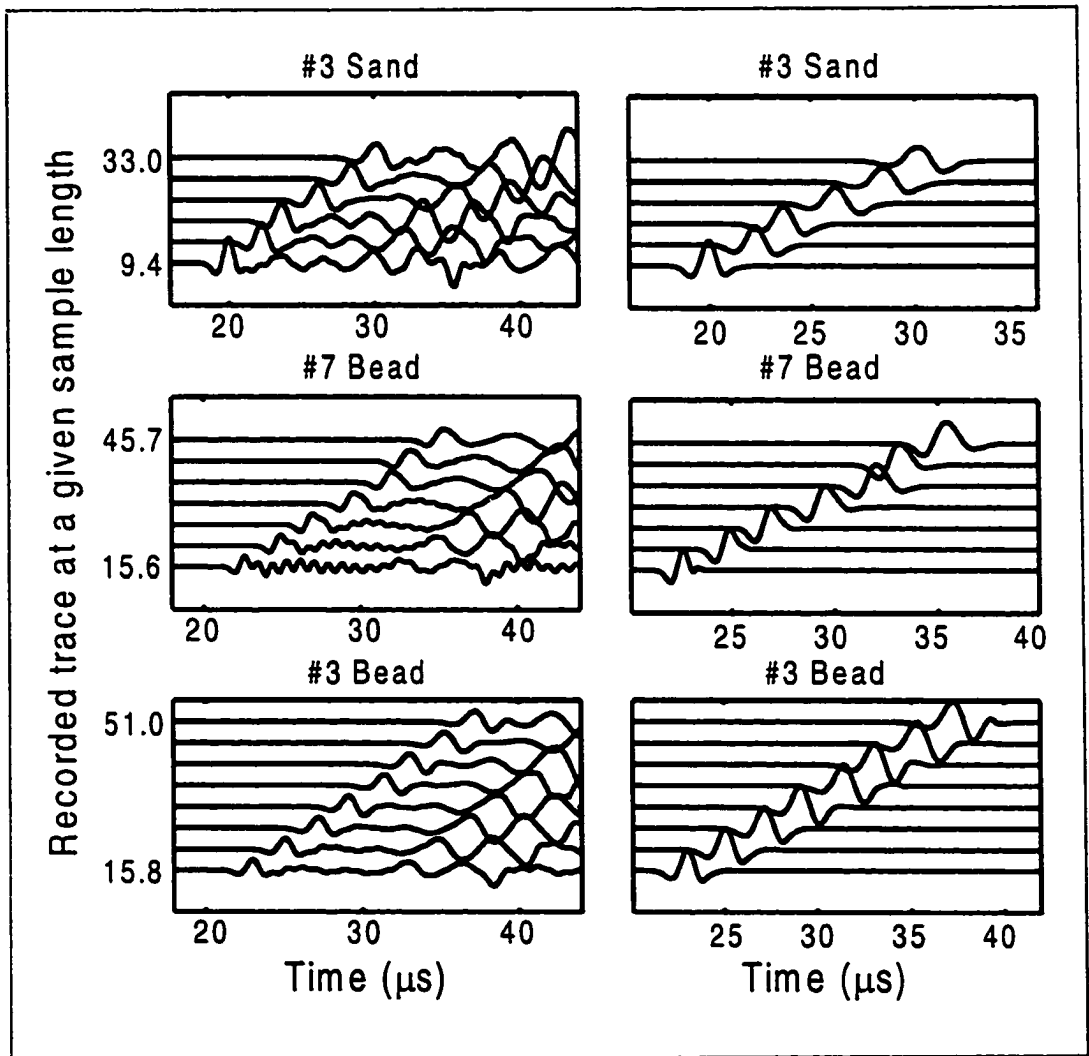


Figure 5 Directly observed (left hand side) and pulse-isolated traces (right hand side) for #3 sand, #7 glass beads, and #3 bead packs. Length of grain pack is indicated (mm).

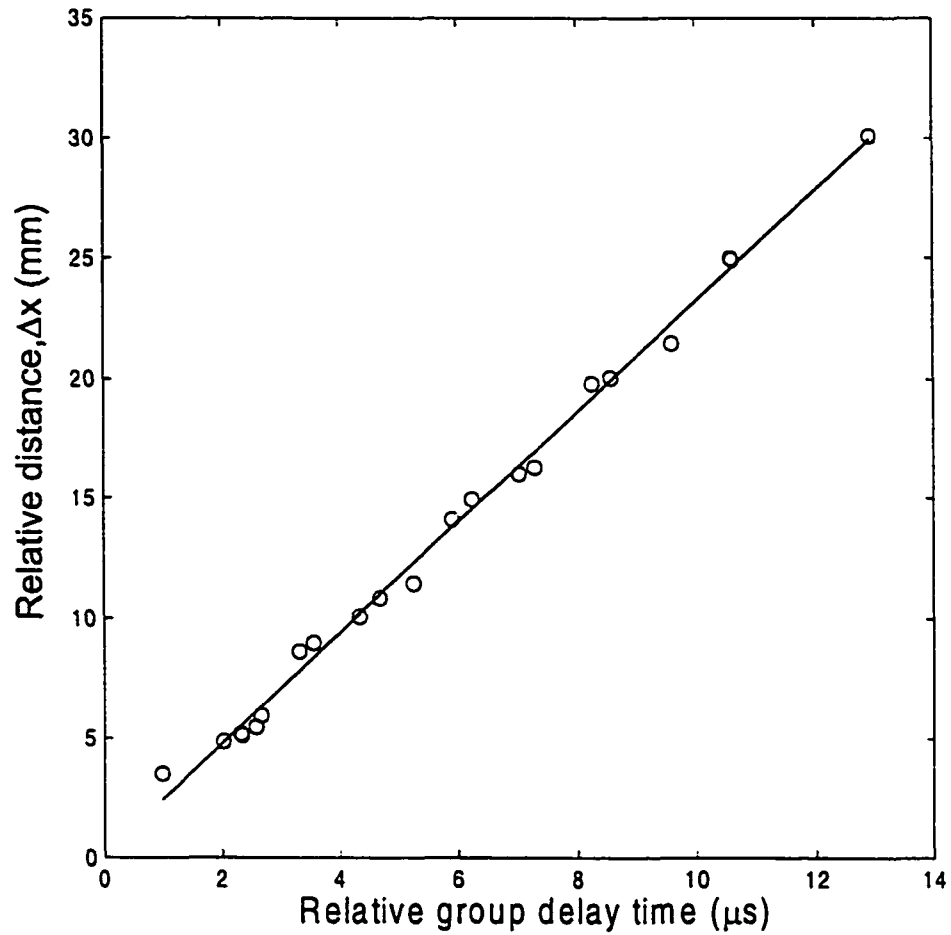


Figure 6 Relative distance ($x_2 - x_1$) versus relative group delay time ($t_2 - t_1$) for #7 glass beads @ 0.38 MHz. Line represents result of least squares linear regression the slope of which is the group-velocity.

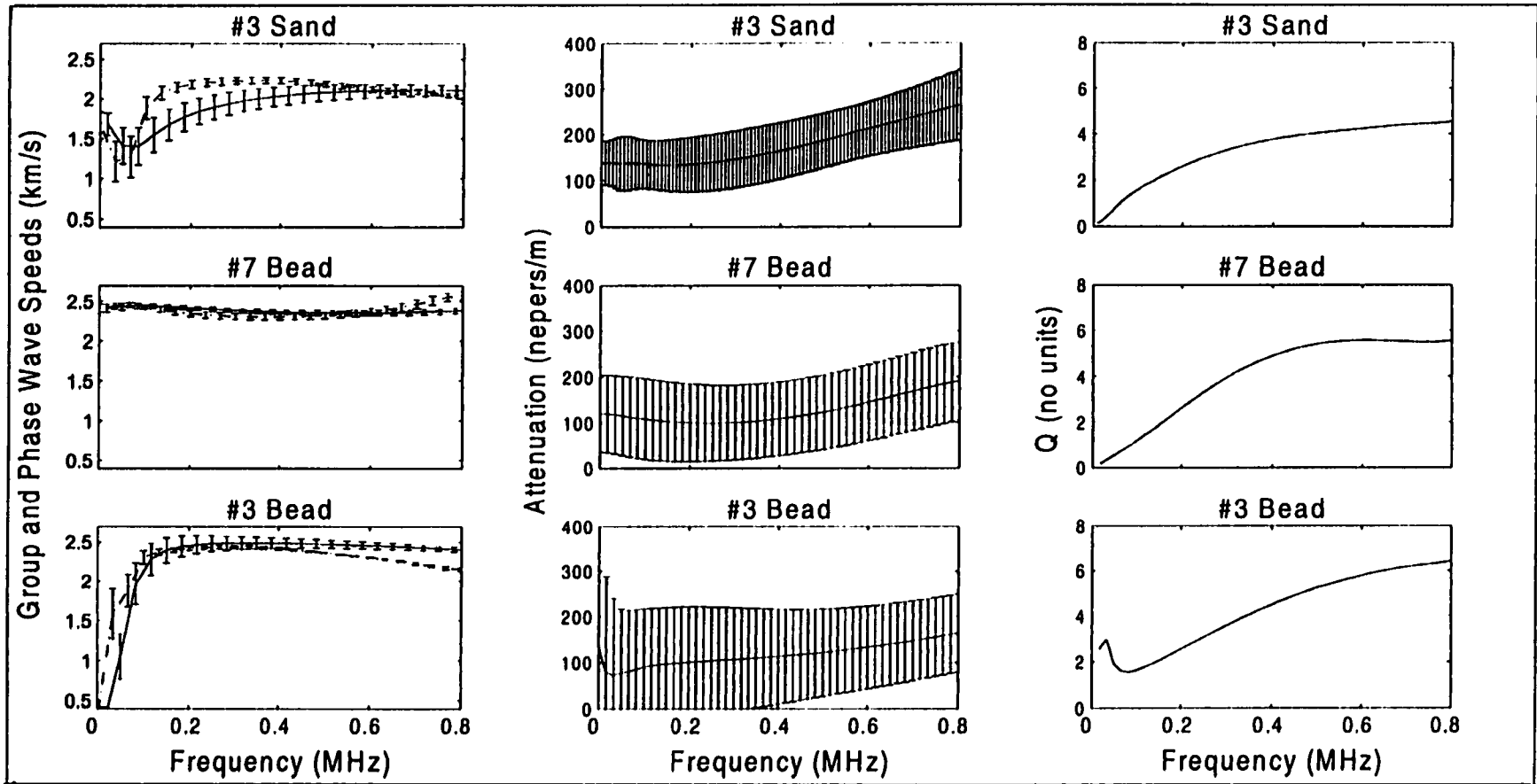


Figure 7 Attenuation, Q, group and phase velocity variation with frequency. Left, group (dashed line) and phase (solid line) wave velocities vs. frequency. Center, attenuation coefficient α . Right, quality factor Q with frequency. Error bars are 1 standard deviation of the distributed values.

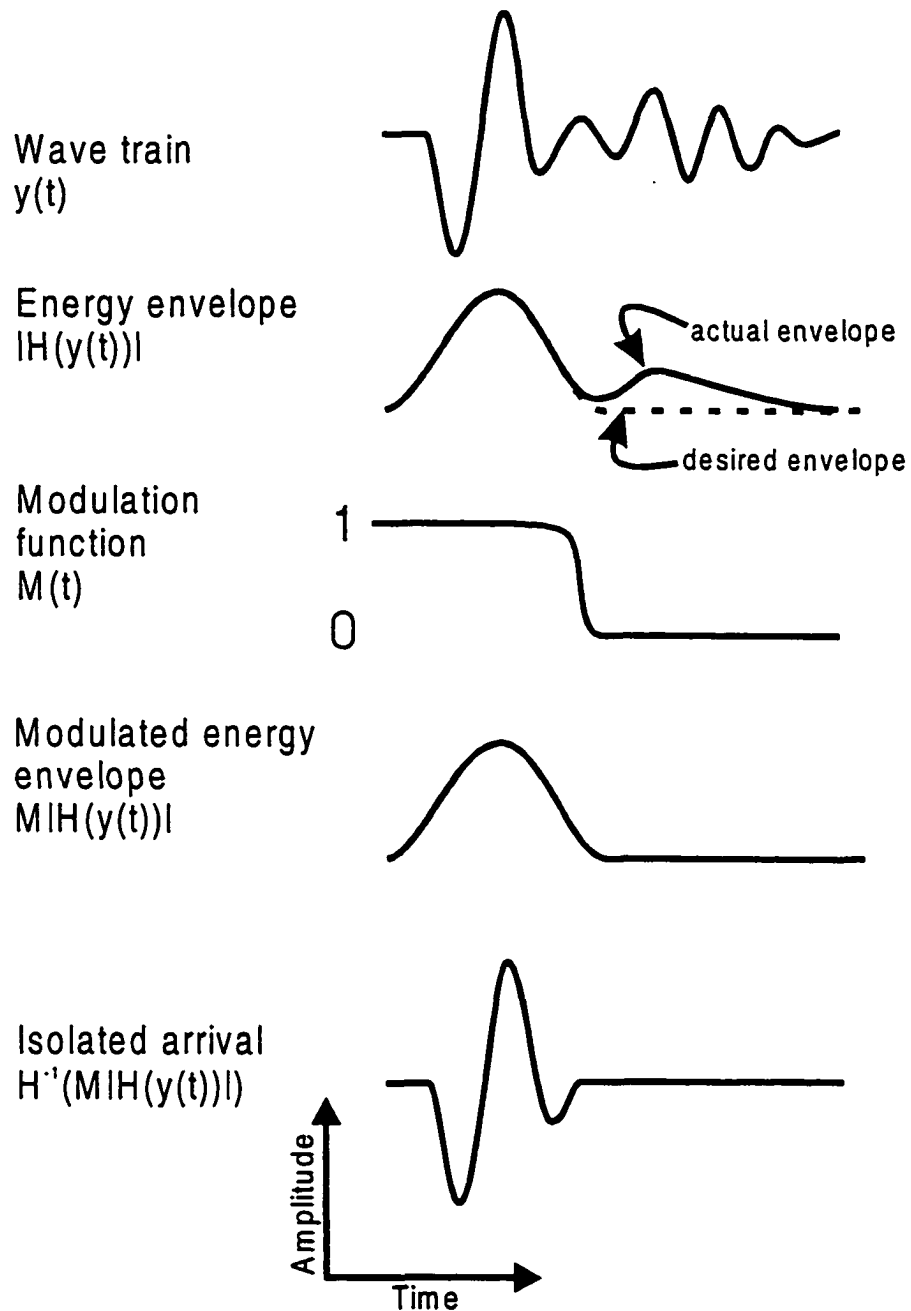


Figure 4.A1 Cartoon description describing the modulation of a primary arrival, $y(t)$, contaminated by secondary signal to an isolated primary arrival. The symbol H describes the Hilbert transform.

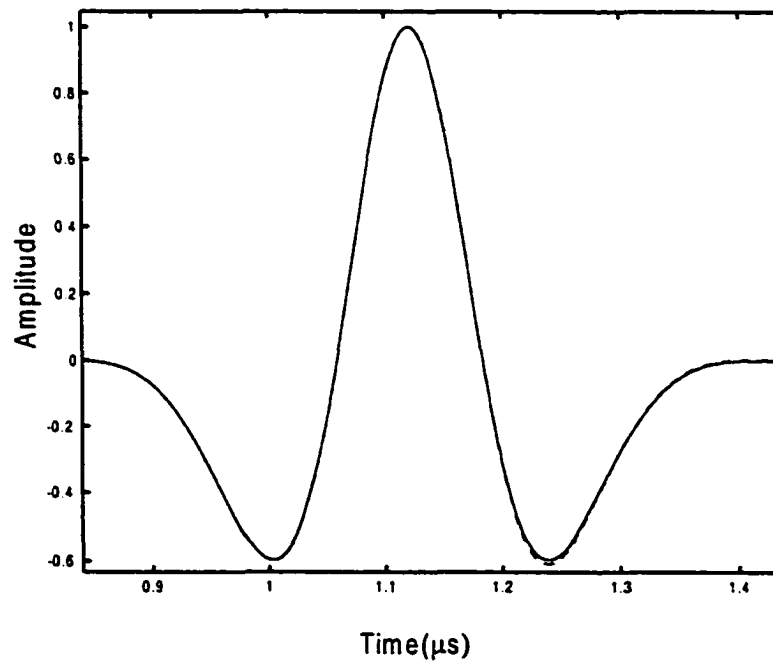
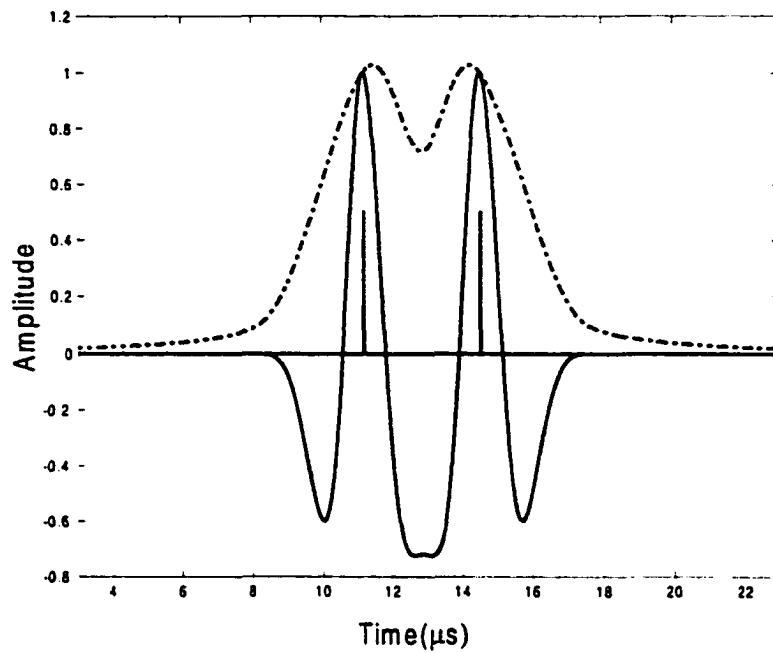


Figure A2. Two interfering Ricker wavelets. i) Two delta functions at approximately 11 and 15 μs are convolved with two zero phase Ricker wavelets. The Hilbert transform energy envelope is shown as dashed lines. ii) The isolated arrival from the data in i). Dashed lines indicate the isolated Ricker wavelets and the original Ricker wavelet is shown as a solid line.

CHAPTER 5

Scale Dependent Velocity, Attenuation, and Internal Resonance in Unconsolidated Glass Bead Media¹

5.1 Introduction

The earth is everywhere elastically heterogeneous at nearly any scale we chose to examine it. At the hand-sample scale, laboratory measurements of wave velocities and attenuation are strongly influenced by the cluster, crystal, and crack dimensions in the rock [e.g., Mukerji et al, 1995; Nishizawa et al, 1997]. In sedimentary formations, the spatial variations in properties due to layering (e.g., Backus, 1962) and saturation (Akbar et al, 1994) result in a heterogeneous structure. The metamorphic upper crust is particularly complex; and modeling of seismic wave propagation through such ill-defined structures remains problematic (e.g. Wu and Aki, 1985; Hurich, 1996). Teleseismic and local earthquake records contain manifold evidence for this heterogeneity (see review by Sato 1995). The coda that follow the directly arriving P and S waves from an earthquake and the elliptical polarization of vertically arriving shear waves are among the most compelling pieces of evidence. Deep within the earth, heterogeneity is also expected at transitions such as the core-mantle boundary where physical properties change rapidly and there exists the potential for limited mixing. This structural complexity may be indicated by ScS precursors (e.g. Vidale and Hedlin, 1998). Such heterogeneity can strongly influence seismic wave propagation but heterogeneity is usually ignored in the analysis and interpretation of seismic observations.

Seismic arrivals detected at the earth's surface consist of the interference of the direct, forward scattered, and rescattered waves and hence heterogeneity directly influences both travel-times and amplitudes [e.g. Gudmundsson, 1996; Roth et al, 1993] . The degree to which this scattering is influential depends on a characteristic dimension a of the geologic structure relative to the wavelength λ of the illuminating seismic waves.

This scattering affects what is observed at the earth's surface in two important and well-known ways. First, observed travel times are often declared when a characteristic of the recorded waveform attains some critical value such as the first amplitude peak. The waveform, however, is comprised of the interference of the initial forward propagating pulse with the slightly delayed scattered energy and as such influences the transit time determination and the consequent velocity determined using this transit time. Second, the amplitude of the arriving pulse is diminished due to the loss of energy portions scattered from the initial pulse. This loss of amplitude occurs in addition to any geometric wavefield spreading or intrinsic absorption and consequently is a component of any attenuation that might be measured.

¹ A version of this paper has been submitted for publication, Molyneux and Schmitt, in submission, JGR.

5.2 Background

5.2.1 A simple example of scale dependent dispersion: propagation through layered media

Scattering and wave propagation in the short ($\lambda \ll a$) and long ($\lambda \gg a$) wavelength regimes is relatively well understood. It is instructive to briefly review the simple case of waves propagating in a direction perpendicular to the layering in simple one-dimensional structures. Consider a structure consisting of layers of thicknesses h_i , elastic moduli M_i , mass density ρ_i , and interval velocities V_i (Backus, 1962; Marion et al., 1994, Melia and Carlson, 1984). If the layers are thick relative to the wavelength (or equivalently at high frequencies), the apparent velocity V_a is simply the ratio of the thickness of the structure to the sum of the transit-times through each of the individual layers. This is often referred to as the Wyllie time average equation:

$$V_a = \Sigma h_i / \Sigma (h_i / v_i). \quad (1)$$

In random 2-D and 3-D structures the apparent velocity will tend to be greater than that expected solely on the basis of composition due to fast pathing effects (Wielandt, 1987 Mukerji et al., 1995).

Conversely, when the wavelength is large relative to each of the individual layer thicknesses, then the low frequency limit or Backus [1962] harmonic average of the

elastic moduli is more appropriate $M_a = 1/\Sigma(c_i/M_i)$, with $c_i = h_i/\Sigma h_i$ being the volume fraction of each layer. The apparent velocity for this case is

$$V_a = \sqrt{M_a/\rho_{ave}} \quad (2)$$

where ρ_{ave} is the average density of the structure.

Wave propagation in the intermediate regime when $\lambda \approx a$ is less well characterized (Marion et al, 1994). Scattering attenuation is particularly severe and the wavefield is difficult to describe. Despite these problems, however, a better understanding of this regime is important because it is often likely that the dimensional scale of the geologic structure is comparable to the predominant wavelength of the propagating seismic waves. In such circumstances there exists substantial potential for errors in the interpretation of the seismic travel-time observations.

Numerous workers have noted that it is difficult to describe wave propagation through structures when the wavelengths are of similar dimensions to the illuminated structure. This regime lies between that of effective media theory ($\lambda \gg a$) and ray theory ($\lambda \ll a$) both of which are often relatively well understood. Modeling of such complex media still lies beyond our computational capacity and as such experimental tests provide useful insight into the behavior of such materials (e.g., Nishisawa et al, 1997). In this paper we describe the results of a series of experiments designed to examine the effects of relative scale on compressional wave propagation in saturated packs of unconsolidated glass

beads. Such a medium provides a highly attenuating material supposedly free of the additional wave modes existing in saturated porous structures with a frame modulus, and was intended to allow for study of the scattering behavior in isolation. Despite this initial motivation, additional effects due to an as yet not well understood resonance are found to accompany the scattering process. A few possible resonance mechanisms are investigated but further experiments are required. However, the present experimental results, although representing an extreme case, indicate this may be a previously unaccounted for attenuation which influences seismic body wave propagation.

5.2.2 Previous experiments of wave propagation through bead packs and unconsolidated materials

There have been numerous studies examining the propagation of elastic waves through media consisting of beads immersed in fluids and colloidal suspensions. The problem at first glance appears simple but in reality the propagation of waves in simple packs of saturated solid beads is complicated by numerous phenomena (e.g., Liu et al, 1990). Consequently, the study of such seemingly simple systems sheds considerable light on scattering processes.

A few of such studies worth mentioning follows. In the context of analogs to weakly consolidated rock, Paterson [1956], Wyllie et al, [1956, 1958], and Domenico [1977] measured ultrasonic longitudinal and shear velocities on glass beads and quartz grains to substantial confining pressures. However, once subject to confining pressure the overall

elastic properties of the bead pack differ significantly from the unconsolidated materials studied here. Hovem and Ingram [1980] and Hovem [1980] examined attenuation in glass bead and clay packs at frequencies below 300 kHz and found a small amount of velocity dispersion and frequency dependent attenuation. These trends were in agreement with theory and therefore suggestive of viscous attenuation. Molyneux and Schmitt [1999] and chapter 4 measured the group and phase velocities in highly attenuating bead packs and compared them to velocities determined by more conventional time picking methods.

Industrial and university research groups carried out a substantial amount of work on bead packs and colloidal suspensions in the 1970's. Kuster and Toksoz [1974a] developed a long-wavelength, low frequency approximation for the compressional velocity through a dilute suspension of solid spheres in fluid. In their theory, the detected wavefield includes the superposed components due to single scattering from each of the spheres. This theory predicted well the laboratory velocities observed in a variety of different suspensions in which fluid porosity exceeds 40% [Kuster and Toksoz, 1974b] and was also in close agreement to those velocities determined using the Reuss model [1929]. They suggested the slight discrepancies between their calculated and observed velocities were possibly due to either the fact that theory ignored multiple scattering or scale dependent effects. Mehta [1983] included the effects of multiple scattering effects and was able to match Kuster and Tokzöz's [1974b] experimental observations more accurately. Kuster and Toksöz [1974b] also contrasted their results with those provided by the Wyllie time average equation as the high frequency limit [Wyllie et al, 1956]).

Johnson and Plona [1982] examined the ultrasonic properties of both unconsolidated and weakly consolidated glass bead packs ($\phi = 0.38$) saturated with water. Using pulse transmission (~ 500 kHz) through the unconsolidated beads ($177 \mu\text{m} < a < 210 \mu\text{m}$) they detected a single longitudinal mode propagating at a velocity of 1.79 km/s. Upon lightly fusing the same bead pack, however, two longitudinal modes appeared with speeds of 2.81 km/s and 0.96 km/s. These two longitudinal modes are predicted to exist in saturated porous media in which the skeletal solid frame has nonzero bulk and shear moduli and both the solid and fluid components are connected networks [Biot, 1956a, b, de la Cruz, and Spanos, 1985]. In this case the faster is associated with the solid frame and is manifest when the fluid and solid particles oscillate together in phase. The slower travels more in the fluid and depends on differential particle displacement between the solid and fluid. As the bulk and shear moduli of the frame of the unconsolidated packs essentially vanish the slow wave ceases to exist [see also Geertsma and Smit, 1961; Sen and Johnson, 1983]. Once the beads are fused, the moduli are no longer trivial and the dual mode propagation is possible. Johnson and Plona [1982] concluded that the character of the solid-solid contacts and hence the elastic frame moduli were important factors controlling the acoustical properties of the medium.

Schwartz and Plona [1984] measured phase velocities and attenuation of broadband (300 kHz - 2 MHz) pulses transmitted through water-saturated packs of acrylic ($a \sim 0.275$ mm) and glass beads ($a \sim 0.545$ mm) at the typical random packing porosity of $\phi = 0.38$ [Bourbie et al, 1987]. In these experiments the phase velocities and inverse attenuation both decrease with increasing frequency. Attenuation in the larger glass beads varied

simply with the fourth power of frequency, predicted by Rayleigh [1929] and seen in other scattering experiments [e.g., Mason and McSkimmin, 1947]. Attenuation in the smaller acrylic beads deviated from this trend being dominated by viscous processes at lower frequencies.

Kinra and Anand [1982] determined the compressional and shear wave velocities in composites of various sizes ($1 \text{ mm} < a < 3 \text{ mm}$) and volume fractions (5% - 45%) of glass beads in an epoxy matrix. They sent relatively long tone-burst signals that are comprised mostly of a single frequency component through the samples. At long wavelengths ($\lambda > 1.15a$) the transmitted waveforms displayed little evidence of dispersion and both the observed compressional and shear velocities were in good agreement with those expected theoretically. They did not obtain any velocity measurements over the intermediate range ($0.77a < \lambda < 1.15a$) due to substantial waveform distortion which made unambiguous determination of the pulse transit-time problematic. At even shorter wavelengths the observed velocities substantially exceeded the long-wavelength predictions.

In a series of similar experiments, Yin et al [1994] measured both compressional and shear-wave velocities using 2.25 MHz pulses through glass bead, epoxy mixtures. The samples were composed of beads with dimensions from 5 mm to 0.05 mm diameter; all samples had nearly identical overall composition, density, and static elastic properties. They observed little dispersion for wavelength to bead size ratios greater than 3 but below this value the P and S wave velocities increased by 22% and 15%, respectively,

towards the high frequency values. Fourier transforms of the observed waveforms changed little while in the long-wavelength limit but shifted to lower frequencies once the short-wavelength regime was entered.

Brillouin scattering has been used effectively in studying the acoustic characteristics of colloids consisting of very small (370 nm and 680 nm) acrylic beads suspended in an organic liquid with the same mass density [Liu et al, 1990]. An advantage of Brillouin scattering measurements is that the k - ω dispersion relationship, and hence the corresponding phase velocities, is measured directly without the added complications inherent to processing and interpreting acoustic waveforms in ultrasonic pulse transmission experiments. At low frequencies and for concentrations less than 20% only a single propagation mode is observed, the velocity of this mode is intermediate to the intrinsic velocities of the acrylic and the liquid and increases with the bead concentration. However, at greater concentrations and higher frequencies ($\sim \omega > \pi V_l/a$, where V_l is the compressional wave speed in the liquid) two distinct wave modes exist. The first also propagates at a velocity between those of the liquid and the acrylic and increases with solid concentration. Further, this faster wave does not exist at the frequencies at which an isolated sphere within the fluid would resonate. The velocity of the second mode is less than that for the liquid and, conversely, decreases with concentration.

Liu et al's [1990] observation of the second mode was unexpected as the colloidal suspension has no connected solid frame to support such a mode as suggested by earlier work at lower frequencies [Sen and Johnson, 1983; Schwartz and Plona, 1984].

Extensive theoretical and numerical modeling of the colloid suggests the faster wave [Jing et al, 1991, 1992] is transmitted through both the fluid and the solid. This intuitively explains the increase in its velocity with solid concentration. In contrast, the slower wave is the coupling between adjacent beads of the Stoneley modes propagating at the solid-liquid interface of the beads. The velocity of this mode decreases with concentration because of the longer fluid-solid interface path lengths.

Page et al [1996] investigated the coherent ballistic propagation of compressional waves through thin (2 mm to 5 mm) packs of water saturated glass beads ($a = 0.25$ mm and 0.5 mm). They found that although the ballistic pulse remains coherent with that incident on the sample, it is still strongly influenced by scattering resonances, which produce substantial dispersion and significantly slow the phase and group velocities.

Most recently, Cowan et al [1998] describe a novel series of ultrasonic pulse experiments (~1 MHz to 4 MHz) on the propagation of the forward scattered, or ballistic, pulse through random suspensions of glass beads ($a \sim 0.438$ mm) in a water/glycerol mixture. They detected ultrasonic transmissions through a fluidized bed of the mixture whose solid to fluid volume ratio was varied between 0.21 and 0.61. For many of the Fourier components of the pulse when $\lambda \sim a$, strong scattering results. The degree of scattering depended on the volume fraction; a specific manifestation of this scattering is that phase and group velocities dispersion increased with the volume fraction of solid. They successfully modeled the observed dispersion curves and on this basis inferred that the

velocities were slowed by both trapping of energy within the beads (resonant scattering) and by the tortuosity of the fluid pathway.

The experiments described here are similar in configuration to those of Kinra and Anand [1982] and Yin et al., [1994] with the important difference that the beads reside within a fluid matrix. The variation in elastic properties between the glycerol and the glass beads is more extreme with greater effects of scattering expected. Further, the unconsolidated bead packs are highly compressible and the influence of the frame moduli on propagation and wave velocity may essentially be ignored.

To our knowledge, this work is the only one of its kind to examine the most complicated acoustic propagation of a broad band pulse through a highly attenuating medium in the intermediate frequency regime ($ka \sim 1$). The medium is a random packing of glass beads saturated in a fluid of vastly different acoustic properties. The medium further has a very low frame strength. The signal is expected to be complicated by multiple scattering. Such an extreme was used primarily for its dramatic dispersion [Molyneux and Schmitt, 1999], but additional unexpected resonance effects were displayed and are the focus of this work.

5.3 Experiments

5.3.1 Sample Preparation

The samples consisted of packs of commercially available glass beads saturated with glycerol, the constituent elastic properties are given in Table 1. The velocity measured for the glycerol is in very good agreement with published values. The glass beads are formed from a common soda-lime glass as confirmed by microprobe examinations (Na_2O - 12.1wt%, Al_2O_3 - 4.6 wt%, MgO - 1.6, wt%, SiO_2 - 71.8wt%, K_2O - 0.9wt%, ZnO - 1.3wt%, CaO - 6.9wt%). The P and S velocities given in Table 1 are from the literature [Carmichael, 1982] for glass of a similar composition. Attempts were made to measure both velocities on larger samples prepared by melting of the beads into 2.54 diameter cylinders. However, each cylinder tested contained bubbles and the observed P and S velocities, while close to those in Table 1, were up to 4.5% lower. Consequently, the published values are presented in the following calculations; this discrepancy does not in any significant way alter the final conclusions. Each pack was composed of monodisperse spherical beads ranging in diameter d from 220 μm to 6 mm as determined from image analysis of the smaller beads and vernier caliper measurements on the larger (Table 2). Although Table 2 describes that many bead sizes do not match an integer millimeter diameter description, for ease of use we will refer to the integer specifications hereafter. The packs were unconsolidated and as such have essentially no frame modulus [Johnson and Plona, 1982; Murphy et al., 1993].

A number of packs of increasing length were prepared for each set of bead sizes. The beads were dropped into the glycerol filled sample tube that was bottom-stoppered with an aluminum buffer rod (45.00 mm diameter, 48.21 mm length). At the same time the sample was vigorously shaken using an air driven vibrator operating at audible frequencies; as such the beads touch but are not fused either chemically or by pressure. A predetermined weighed amount of glass bead was placed and finally covered with the second top aluminum buffer rod while shaking continued (Figure 1). This procedure produced a series of relatively uniform packs with lengths from 10 mm to 50 mm as measured by a vernier caliper to ± 0.1 mm. The porosity of each pack was determined from the known radius of the tube, the pack length, and the volume of glass bead calculated using the measured mass and density. Mean and standard variation of porosity for each bead size pack is given in Table 2. Both porosity and porosity error increased by a small amount with grain size due to geometric packing constraints, Figure 2 [Yin et al., 1994].

5.3.2 Pulse Transmission Measurements

Ultrasonic pulses were created and received by transducers made from 2.54 cm disks of piezo-electric ceramic (BaTiO_3 , 1 MHz resonant frequency) polarized to expand parallel to the disk's axis. The ceramics were glued directly to the outside ends of the aluminum buffer rods (Figure 3) with a conducting epoxy and mechanically damped with a urethane-metal powder mixture. The transducers were activated by a 10 ns rise time, 200 V pulse. The transmitted signals were recorded unamplified by 12 bit digital oscilloscope

at 1 ns/sample. Random noise was reduced by stacking 50 individual pulses for each sample. The final waveforms were recorded on a computer for further analysis.

The resulting 10 μ s duration pulse (Figure 4a) has a noticeable bandwidth from 0.25 MHz to 1.5 MHz (Figure 5b) with a strong ringing peak at 1.13 MHz. The pulse character displays this oscillation as recorded through pure glycerol. Note that the pure glycerol waveforms in Figure 4a show multiple reflections within the aluminum buffer rods. Each trace is individually scaled by a constant value for visual purposes. Amplitude information is displayed in Table 3, Figure 7.

5.4 Results

The complete set of recorded waveforms plotted with sample length is given in Figure 4. As noted in earlier studies [Kinra and Anand, 1982; Yin et al, 1994] determination of transit times and hence velocities is problematic in such scattering media. Here, transit times are declared at the first detectable onset of the wave energy and what is referred to as the signal velocity (Table 2) is then determined by linear regression between the observed times and lengths for a given bead pack [Molyneux and Schmitt, 1999]. Velocity is quoted with one standard deviation of distribution in Table 2.

The waveforms display periodicities, which are extracted using the fast Fourier transform to provide amplitude spectra (Figure 5). In order to study the first arriving energy with omission of the multiple end cap reflections, the initial sections of the signal

were windowed by a Hanning-tapered boxcar commencing at the onset of the signal and of $9 \pm 3 \mu\text{s}$ duration. For each of the bead packs, the number at the side of each trace in Figure 5 represents the individual pack length L . The actual amplitudes appear as dark scale bars in the figure. Although signal velocity is prone to overestimate physical properties of group and phase velocity [Molyneux and Schmitt, 1999] it is a robust measurement in erratic and noisy signal.

It is worth noting that the shape of the amplitude spectra of the pulses transmitted through pure glycerol do not visibly change with increasing length (Figure 5). The apparent frequency independent amplitude decay in this case is primarily due to geometric effects. An empirical length dependent amplitude correction was derived from the pure glycerol waveforms and applied to the bead pack traces.

Many of the amplitude spectra for the glass bead packs are bimodal (Table 3). One peak below 0.4 MHz appears in all the bead packs and is referred to as f_L . A second spectral peak appears only for the packs with beads of diameters greater than 2 mm and is designated f_H . The frequencies and amplitudes of these peaks are plotted versus pack length in Figures 6 and 7, respectively. It is noted that in most cases the frequency of the peak amplitude decays with distance – as expected for an attenuating media. However, it is useful to calculate a characteristic frequency associated with the propagation through packs of different bead diameter. To compare frequencies with bead size, the linear extrapolation of peak frequency at zero pack length was used (Figure 6). Note, the f_H and f_L values are quoted with one standard deviation of error (Table 3).

In Figure 7, the log amplitudes decay linearly with distance with correlation coefficients generally in excess of 0.8; the slope of the lines fit to these data was used to find an apparent attenuation α for each of the peaks under the assumption the amplitude decline could be described by an exponential decay proportional to the $\exp(-\alpha L)$. Apparent Q values are also calculated, using the formula,

$$Q = \pi f / V \alpha \quad (3)$$

where V is measured signal velocity and the frequency is the peak frequency, f_H or f_L .

In much of the acoustics literature, resonant scattering results are scaled with respect to a normalized frequency which is the product of the wavenumber in the fluid $k_f = 2\pi/\lambda = 2\pi f/V(f)$ and the radius a of the object under study, this normalized frequency will be referred to hereafter as $k_f a$. The values are provided for both peaks in Table 3.

5.5 Discussion

The character of the waveforms and their relative strength differs dramatically depending on the bead dimensions.

5.5.1 Bead Size Dependent Waveform Attributes

5.1.1.1 Low Frequency Regime: $k\alpha < 1$.

A distinct pulse is seen to propagate through the 0.22 mm and 0.67 mm bead packs (Figure 4) for which the normalized frequency is substantially less than 1 (Table 3). At short sample lengths the waveforms still display the predominant 1.13 MHz transducer resonance but this component is rapidly attenuated despite its initial strength (Figure 5). The signal strengths are less than that through pure glycerol by a factor of 20. The attenuation of these bead packs have been previously examined [Molyneux and Schmitt, 1999] and are consistent with propagation through a material with a low and relatively uniform quality factor $Q \sim 3$ over the bandwidth of the signal. The apparent attenuation of the predominant spectral peak for both packs is very similar (Table 3). Further, a plot of peak natural log amplitude spectrum vs. length of sample results in the same intercept at zero length for the two bead packs, Figure 7, Table 3 indicating similar length-dependent attenuation mechanisms.

As distinct pulses are seen to propagate for these two bead packs, a second measure of the velocity determined by picking the transit times of the first amplitude extremum [see Molyneux and Schmitt, 1999] is also provided (Table 2). These first peak velocities are in close agreement with the Wood's formula prediction (Figure 8) and suggest that the two packs are reasonably well represented by a simple mixture theory and may be considered as an effective media over the transducer bandwidth. It is noted that such velocity models do not include signal attenuation. De la Cruz and Spanos (1985) offer a

more complete physical theory accounting for both velocity and attenuation properties of waveform propagation under certain scale constraints.

5.5.1.2 Intermediate Frequency Regime: $k_0 a \sim 1$.

The 2.0 mm bead pack falls within this regime. No distinct pulse is observed (Figure 4d) and the strength of the signals is diminished by approximately a factor of 5 from the smaller bead packs. Indeed, this intermediate frequency peak when extrapolated to zero length has an amplitude less than that observed in the low frequency case, Figure 7, Table 3. This implies a secondary attenuation regime, partitioning energy from the main signal. The low frequency spectral peak, $f_L \sim 0.33$ MHz, decays with $Q \sim 4$.

The signal velocity for this pack is statistically larger than that for the low frequency regime (Figure 8).

Combining the evidence of a different zero length amplitude, different Q , and different signal velocity from the small bead diameter samples, it is thought that the 2.0 mm bead pack indicates the onset of an additional attenuation mechanism.

5.5.1.3 High Frequency Regime: $k_1 a$ bigger or equal to 1.

The most interesting variety of waveform characters is seen for packs with bead diameters of 3 mm and greater. They all share the same attribute in that no distinct pulse is seen. A ringing is easily seen in the time amplitude traces (Figures 4e-h) and displayed as narrow peak in the amplitude spectra in addition to the low frequency peak (Figures 5e-h). This high frequency signal component decays with a $Q \sim 6$. Again, the low frequency component displays a significantly diminished zero length amplitude component with respect to the low frequency regime, Figure 7, Table 3. It is suggested that the attenuation associated with the high frequency peak is partitioning energy from the low frequency peak, reducing its zero-length amplitude.

The signal velocity increases dramatically with bead size (Figure 8). However, the uncertainties in the determinations are substantially greater (as much as 9% for the largest bead size), this may be caused by error in picking of transit times due to the weaker signal.

5.6 Velocity modeling

5.6.1 Simple mixture theories

A characteristic measure of the expected velocity for the packs is given by Wood's formula [Wood, 1941] presumably exact for a suspension [Sen and Johnson, 1983] which can be rearranged to the form [after Berge et al, 1999]

$$V_{Wood} = \left[\rho \left(\phi / \rho_f V_{fluid}^2 + (1 - \phi) / \rho_s V_{solid}^2 \right) \right]^{-1/2} \quad (4)$$

where the bulk density is

$$\rho = (1 - \phi) \rho_s + \phi \rho_f \quad (5)$$

For the present experiments with a solid within a fluid matrix with velocities V_{solid} and V_{fluid} respectively. Equation (4) is identical to the formulations of Reuss [1929] and Kuster and Toksoz [1974a,b].

Alternatively, another characteristic measure is that given by Wyllie et al's [1958] time average equation used for models with porosity, ϕ .

$$V_{Wyllie} = \left[\frac{\phi}{V_{fluid}} + \frac{(1 - \phi)}{V_{solid}} \right]^{-1} \quad (6)$$

It is noted that equation (6) is theoretically only correct for high frequency signal propagating through layered media, as noted in the introduction. In practice it yields velocities in excess of those calculated from Reuss [1929]. However, the Wyllie model is often applied for particulate media and so is included in this section for completeness.

In contrast to Reuss like models, the compressional wave velocity calculated using Voigt's [1910] estimate:

$$V = \left[\frac{\phi \rho_{fluid} V_{fluid}^2 + (1 - \phi) \rho_{solid} V_{solid}^2}{\rho} \right]^{1/2} \quad (7)$$

is generally considered to be the upper bound to the velocity. The Voigt prediction does exceed the observed velocities but care must be taken in generalizing this observation, as the theory was not intended to describe behavior in the high frequency regime ($\lambda < a$).

The formulations above were generally developed under the low frequency - long wavelength assumption. Some are even further restrictive and were intended for dilute concentrations of scatterers within a matrix. Thus, their inability to describe the apparent velocities of the packs with the larger beads should not be surprising and two high frequency predictions were instead employed. The first is the well known Wyllie time-average Equation (6) which yields velocities near 3200 m/s for the bead packs. This value exceeds those observed in the low frequency regime (small beads) and is less than those at high frequencies (large beads). Equation (6) may be simply derived by assuming that an elastic wave propagates through layers of each of the constituent materials with thicknesses in proportion to the relative volume. Equation (6) predicts well the overall velocities for layers much thicker than the wavelengths of the propagating elastic wave energy. The frequencies must be sufficiently great that 2-D ray approximations may be employed and in such a case the transit time through each layer is easily determined. However, this simple layered geometry does not describe the 3-dimensional character of

the bead pack and the preference of the high frequency components to seek the minimum travel time path as discussed by Weilandt [1987] and others.

5.6.2 Velocity Modeling Incorporating Frame Strength

As mentioned previously, the Wood's formula for a suspension predicts well the velocity for the smallest bead pack suggesting that the 0.22 mm bead pack may be considered as an effective medium for purposes of this study. Wood's formula is no longer correct for bead sizes in excess of 2 mm. The velocity for the saturated packs were also estimated using Gassmann's low frequency formulae [Gassmann, 1951] for the bulk modulus,

$$K = K' + \frac{(1 - K' / K_{solid})^2}{(1 - \phi) / K_{solid} + \phi / K_{fluid} - K' / K_{solid}^2} \quad (8)$$

where K' , K_{fluid} and K_{solid} is the frame, fluid and solid bulk modulus respectively. K' is expected to be small for unconsolidated materials, and Gassmann's Equation (8) gives Wood's result (Equation (4)) in the limit of vanishing K' . Neither the frame bulk nor shear moduli were measured for these packs but the empirical relations developed by Murphy et al., [1993] for unconsolidated sands provided useful, porosity dependent, upper bound values that were used in calculating the Gassmann estimate. As expected, this and Wood's estimate are close and only appear adequate for the smallest bead sizes.

Berryman [1980a,b] provides a self-consistent variation of Kuster and Toksoz's [1974a,b] method which under the assumption of vanishing shear modulus for the composite provides a porosity dependent velocity:

$$V = \sqrt{\left(\frac{K_{solid} K_{fluid}}{\phi K_{solid} + (1-\phi) K_{fluid}} \right) / \rho} \quad (9)$$

with values only slightly less than those given by Wood's Equation (4).

5.6.3 Empirical base velocity modeling

Determining the transit time of elastic waves through such complex structures is not straightforward and may have to be carried out numerically in a case by case basis. Roth et al., [1993] developed an empirical relationship for the velocity shift δv as a percentage of the mean velocity of the medium $V_o = \phi V_{fluid} + (1-\phi) V_{solid}$ from a series of numerical models of wave propagation through a heterogeneous earth

$$\frac{\delta V}{V_o} = 0.2 \varepsilon^{1.3} \quad (10)$$

where the standard deviation in terms of percentage is

$$\varepsilon = 100\% * \frac{\sqrt{\phi(V_f - V_o)^2 + (1-\phi)(V_s - V_o)^2}}{V_o} \quad (11)$$

This empirical formula gives expected values for the apparent velocity of the overall medium, which are greater than that for pure glass (Figure 8). This situation is not physically possible and simply highlights the difficulties encountered in attempting to estimate the velocity of a composite with a complex 3-dimensional structure insonified with elastic wave energy with wavelengths close to the typical internal structural scale.

The observations here are more extreme but similar to the earlier experimental results described by Kinra and Anand [1982] and Yin et al., [1994] on fully solid glass bead-epoxy mixtures. As noted by these authors, once the bead sizes, or equivalently the frequencies, are sufficiently large the wave propagation undergoes a transition from the effective medium limit to the ray limit. The velocity determined by measuring the timing of the signal peak with increasing bead pack length is a good measure of the group velocity near the predominant frequency [Molyneux and Schmitt, 1999] and for the 0.22 mm diameter beads is described well by the effective medium theories. The velocities increase from this point with even a slight dispersion possible for the 0.67 mm bead diameters. The relative magnitude of the true dispersion is even greater than suggested here because the porosity generally increases with bead diameter from pack to pack (Figure 2); the variation in porosity is responsible for the theoretically predicted decline in velocity with bead diameter. With the visible onset of the ringing signal for bead diameters above 2.0 mm, a consistent first peak measurements becomes problematic.

The high frequency components of a wave propagating through such a complex 3-dimensional composite medium will seek the minimum ray travel-time [Mukerji et al.,

1995; Wielandt, 1987; Muller et al., 1993] with this effect called variously 'fast pathing', the 'Wielandt effect', or the 'velocity shift'. The fact that the uncertainty in the determination of the velocity also substantially increases with bead size (Figure 8) provides further support for this interpretation as the transit time through a given pack, and hence the apparent velocity, would be expected to fluctuate with changes in the random packing of the material. The apparent velocity of such a medium cannot be described by any long-wavelength effective medium approach.

5.6.4 Comparison of Experiment to Theory

The observed signal and peak amplitude velocities depend strongly on the bead size with an apparent velocity dispersion of 81% from the smallest to the greatest bead size. Velocity increases monotonically across the series of measurements. These observations are summarized in Figure 8 and contrasted with a wide variety of different theoretical predictions. None of the mixture theories describe the observed dispersion.

5.6.5 Internal Resonances

The fast pathing effects above were generally expected as they had been previously observed by other workers in similar experiments. However, the amplitude spectra of the transmitted signals for the high frequency bead packs (Figure 5) shows some unexpected spectral peaks; a bimodal frequency spectrum from a monofrequency input source. The higher frequency spectral peaks appear to result from the same scale-dependent

resonance because they plot linearly with respect to the reciprocal bead diameter (Figure 9), and they all share nearly the same value $k_f a \sim 5$ of the normalized frequency (Table 3). Further, for bead sizes 2mm and larger the low frequency peak in the amplitude spectrum has an extrapolated zero length amplitude which is far less than the similar zero-length amplitudes of the 0.22 and 0.67 mm diameter bead packs. This indicates that an additional mechanism is being invoked to partition energy away from the low frequency signal. The high frequency spectral peaks for the bead sizes ≥ 2 mm have a consistent apparent $Q \sim 6$. Such constant apparent attenuation with bead size suggests an acoustic mode distinct from the low frequency signal. Also, the decay in amplitude with distance is more severe for the high frequency spectral peak than it is for the low frequency peak (Figure 7). This is consistent with the high frequency resonant phenomena radiating with substantial amplitude decay due to spherical geometric spreading than the more plane wave main signal. This resonant energy partitions energy away from the relatively low frequency carrier signal. To our knowledge, such a strong internal resonance has not been previously observed in the context of wave propagation through a nondilute medium of scatterers. However, it is suggested that only due to the severe attenuation of the main signal does the resonant signal have relatively large amplitude and become visible within the recorded signal.

The back-scattering of compressional waves from an elastic object isolated within a fluid medium has long been studied both theoretically and experimentally for obvious applications in naval warfare. Early experimental work [Faran, 1951] highlighted the complex frequency and azimuthal dependence of the backscattered energy for even

simple cylindrical shapes. In particular, he noted the 'ringing' of the observed waveforms when the frequency of the signal input to the cylinders matched the normal modes. Since this time, the study and interpretation of such scattered waveforms has culminated in the 'Resonant Scattering Theory' for acoustic waves. This theory is well described in a number of monographs and reviews [e.g., Gaunard, 1989; Numrich and Überall, 1992; Überall, 1992]. In short, this resonant scattering theory is similar to the normal mode theory which has been used in the resonant sphere method of determining material elastic properties [e.g., Schreiber et al., 1973] and in describing wave propagation in the earth but further complicated by the additional modes introduced by the coupling between the object and its surrounding fluid. The types of modes available for an isolated, uniform, isotropic sphere surrounded by fluid depend on the relative frequency of the insonifying waves. The modes available include:

- a) The normal poloidal (breathing modes) and toroidal (torsional) modes [e.g., Sato and Usami, 1962; Shui et al, 1988; Hosseini-Hashemi and Anderson, 1988]
- b) 'whispering gallery' modes at higher frequencies which can be considered as multiply reflected rays within the sphere [e.g., de Billy and Quentin, 1992]
- c) 'creeping' or 'Franz' waves which are the diffraction of the waves around the body at the speed of the surrounding fluid [e.g. Veksler and Izbicki, 1996], and
- d) Stoneley-Scholte waves which are an interfacial wave circumnavigating the body [e.g., Überall et al., 1977; Überall et al., 1979].

The frequencies expected for some of these modes will be calculated here and compared to the observed f_H .

The solutions of the poloidal (or spheroidal) (S) and toroidal (or torsional) (T) normal modes of an isotropic elastic sphere are well known and are already provided numerically; only the relevant aspects of the calculations for the frequencies need be given here. The normalized toroidal frequencies ka are identical for any sphere independent of elastic properties. In contrast, the poloidal displacements are more complex and depend on Poisson's ratio ν . The values of some of the lower order frequencies calculated by Sato and Usami [1962] as reproduced in Schreiber et al., [1973] are given in Table 4; those for the poloidal mode were interpolated based on Poisson's ratio for the glass. The ratios π/ka and π/ha are the ratio of the oscillation period to the transit time of a shear and a compressional wave, respectively, over a distance equal to the sphere's diameter. In short, after Schreiber et al. [1973] (see their equation 5.12) the frequency of any given toroidal mode may be written in the form:

$$f = \frac{V_s(ka)}{\pi d} \quad (12)$$

with a similar formula for the poloidal modes. These frequencies are calculated as a function of the bead diameter for a number of different modes for ready comparison with the observed f_H resonances (Figure 10a, b). Neither toroidal nor poloidal modes can explain the observed resonant frequencies, save for the $1T_2$ mode all the expected frequencies exceed those observed. It is worth noting that the fluid surrounding the beads will not substantially alter these oscillation frequencies [Faran, 1951] and cannot explain

the discrepancy, this suggests that the observed resonance is not due to normal modes of the beads themselves.

In resonant scattering theory, other available modes for the isolated sphere are those due to circumferential Franz and the Stonely-Scholte waves propagating at the interface between the solid and the liquid. A resonant condition exists when the circumnavigating waves constructively interfere. This is complicated somewhat on a sphere because of the existence of the caustic points at the poles where the waves undergo a $\pi/2$ phase shift [Überall et al., 1979; Numrich and Überall, 1992] conceptually identical to the interference of shear and Rayleigh waves in describing the higher order normal modes of the earth [see Garland, 1979]. As such, at the resonant frequency the wavelength is:

$$\lambda = \frac{\pi d}{n + 1/2}, n = 0, 1, 2, \dots \quad (13)$$

such that the resonant frequency is:

$$f = V_{surf} \frac{(n + 1/2)}{\pi d}, n = 0, 1, 2, \dots \quad (14)$$

where V_{surf} is the phase velocity of the interfacial wave. For a flat interface between the glass and the glycerol with the physical properties as described in Table 1, the Stoneley wave velocity is calculated to be $V_{surf} = 1914.5$ m/s [see Ewing et al., 1957, pg 112] which is 99.4% the glycerol velocity. The frequencies calculated using this velocity in

Equation (14) are plotted as functions of bead diameter (Figure 10c). Again, none of these circumferential modes yield frequencies that can explain the observed f_H suggesting that these circumferential modes, prevalent for an isolated sphere, cannot explain the internal resonances observed.

The above discussion has focussed primarily on the beads as the principal structural unit within the composite. However, the packs are also saturated with glycerol and the space between the beads may be equally as valid an elementary building block. Visualizing what the shape of such a fundamental unit might be, especially within the ostensibly random packing of the beads, is difficult. Despite this, the porosities of the bead smaller bead packs (~ 0.38) are not that different from that expected for an ordered packing of monodisperse diameter beads in either a face-centered-cubic or a hexagonal-close-packed arrangement for which $\phi = 0.36$. When considering the shape of the facets for such porosity one theme which must be repeated often is that of the concave triangular shape produced between three adjacent beads (Figure 11) with a perimeter of $\pi d/2$. The dimensions of a typical pore could be described in terms of units of this facet perimeter and it is interesting to note that if this perimeter is substituted for the bead circumference πd in Equation (14) there is good agreement between the observed and calculated frequencies for $n = 2$ for the three larger bead diameters (Figure 10d).

This correspondence suggests that the pore geometry and not the beads directly, may play an important role in this particular resonance. That the frequency for the smallest bead does not fall on the trend (Figure 9) is not unexpected as a substantial dispersion of

the Stoneley mode occurs [e.g., Überall et al., 1979] with an increased phase velocity V_{surf} at diminished $k_f a$. The higher V_{surf} also results in a greater resonant frequency by Equation (14).

5.7 Conclusion

The observed signal of a pulsed propagation through a glycerol saturated glass bead pack results in a bimodal frequency spectra for normalized frequencies, ka_f , greater than one. When ka_f is less than one, only one peak is observed in the frequency spectra and the signal velocity is at an asymptote value of 2.6 km/s. With increased normalised frequency the velocity increases, ultimately reaching an experimental 81% velocity dispersion in a similar manner to that described in experiments on solid epoxy-glass bead composites [Yin et al 1994] but far more extreme. The observed velocities all lie below those calculated according to Voigt's mixture model but are in poor agreement with an oft-employed time-average formulation that is often taken to representing the high frequency limit. The largest bead size packs have the greatest normalized frequency, but the high velocity asymptote associated with the ray theory limit may not be reached [Marion et al, 1994].

Resonant effects are most evident in signals propagated through bead packs larger than 2mm diameter. In such bead packs a second high frequency peak is present in the received frequency spectrum which has a constant normalized frequency with bead size: a property suggesting resonance. Further, the zero length amplitude extrapolation of the

low frequency peak is substantially reduced with the onset of an additional high frequency spectral peak. This is consistent with the high frequency resonance phenomena partitioning energy from the main signal. It is suggested that such resonance effects are not normally detected as the reemitted resonant energy is swamped by the main propagating signal. Only if the main signal is subject to substantial attenuation, such as with a fluid-bead pack media, is the reemitted resonant energy ($Q \sim 6$) comparable to the main signal. Several possibilities exist for the small levels of resonant energy in the recorded signal:

1. Energy partition from the main signal is inefficient
2. The resonant energy is radiated radially in all directions from each incident glass bead, yet only a small solid angle is recorded at the receiver.
3. The resonant energy is radiated over a long period of time with respect to the incident pulse, which is not accounted for in our short temporal windowing spectral analyses.

Indeed, such resonances may be thought to solely exist in the intermediate frequency regime, $ka \sim 1$. However, effective media properties displayed by the bead pack samples with diameters less than 2mm have a zero length extrapolation of the amplitude spectrum which is smaller than that in the predominately unattenuative glycerol sample, Table 3. Arguably, resonances not strong enough to be recorded in the received signal could be partitioning energy away from the main signal, causing the amplitude discrepancy.

Our findings suggest the resonance is not due to normal mode oscillations of the beads themselves nor to Stoneley waves circumnavigating the beads at the glycerol-glass

interface as is suggested by resonant scattering theories. However, the resonance may be related to Stoneley wave propagation at the fluid-solid interface of the pore space between the beads.

Resonant scattering theory was developed primarily in order that one may discern something of the elastic properties and shape of an isolated solid object submersed in a fluid. The amplitude of an elastic wave scattered from such an object depends strongly on azimuth and frequency. The normalized amplitude spectrum from such objects, referred to in the acoustics literature as a form function [e.g. see Numrich and Überall, 1982], can be extremely complex, and this complexity does not cease with increasing frequency. Extending this to the present situation suggests that further resonances should be observed in the bead packs at both higher and lower frequencies than discovered here. Another aspect of resonant scattering theory is that a forward propagating pulse will be robbed of energy at the resonant frequencies of the object: such phenomena may have a part in explaining why frequencies in excess of 100 Hz are so difficult to propagate to and from the surface.

The present experiments were not designed to examine this resonance in detail and its source can only be suggested. New experiments over a greater range of frequencies with different types of beads and saturating fluids are required. Whether lightly fusing the beads will significantly impact the scattering for the larger bead sizes is also important [Johnson and Plona, 1982].

The resonant energy loss from the main signal represents a new and fundamental attenuation mechanism that inspires several questions. How efficient is this energy loss mechanism in natural media with random particle shape and distribution? Does resonance from grain size to boulders contribute to the white noise observed in elastic wave solid earth observations? The implications of our findings have impact on attenuation modeling in all scales of geophysics: from centimeter ultrasonic investigations to low frequency teleseismic probing.

References

- Akbar, N., G. Mavko, A. Nur, and J. Dvorkin, Seismic signatures of reservoir transport properties and pore fluid distribution, *Geophysics*, 59, 1222-1236, 1994.
- Backus, G. E., Long-wave anisotropy produced by horizontal layering, *Journal of Geophysical Research*, 67, 4427-4440, 1962.
- Berge, L.I., K.A. Jacobsen, and A. Solstad, Measured acoustic wave velocities of R11 (CCl₃F) hydrate samples with and without sand as a function of hydrate concentration, *J. Geophys. Res.*, 104, 15415-15424, 1999.
- Berryman, J.G., Long-wavelength propagation in elastic media I. Spherical inclusions, *J. Acoust. Soc. Am.*, 68, 1809-1819, 1980a.

Berryman, J.G., Long-wavelength propagation in elastic media II. Elipsoidal inclusions. J. Acoust. Soc. Am., 68, 1820-1831, 1980b.

de Billy, M., and G. Quentin, Scattering by cylindrical targets using very short ultrasonic pulses and Fourier analysis, in H. Überall, ed., Acoustic Resoance Scattering, Gordon and Breach, Philadelphia, 105-121, 1992.

de la Cruz, V., and T. J. T. Spanos, Seismic Wave Propagation in a Porous Medium. Geophysics, 50(10), 1556-1565, 1985.

Biot, M.A., Theory of propagation of elastic waves in a fluid-saturated porous solid. I. Low-frequency range, J. Acoust. Soc. Amer.. 28. 168-178, 1956a.

Biot, M.A., Theory of propagation of elastic waves in a fluid-saturated porous solid. II. Higher frequency range, J. Acoust. Soc. Amer., 28, 179-191, 1956b.

Bourbie, T., Coussy, O., and Zinszner, B., *Acoustics of porous media*, Gulf Publishing company, 1987.

Cowan, M.L., K.Beaty, J.H. Page, Z. Liu, and P. Sheng, Group velocity of acoustic waves in strongly scattering media: Dependence on the volume fraction of scatterers, Phys. Rev. E., 58, 6626-6636, 1998.

Carmichael, R. S., 1982, Handbook of physical properties of rocks, volume II. CRC Press Inc.

Domenico, S. N., Elastic properties of unconsolidated porous sand reservoirs*. Geophysics, 42, no. 07, 1339-1368, 1977. (* Discussion in GEO-44-04-0830-0833 with reply by author)

Ewing, W.M., W.S. Jardetzky, and F. Press, Elastic Waves in Layered Media, McGraw-Hill, pp. 380, 1957.

Faran, J.J., Sound scattering by solid cylinders and spheres, J. Acoust. Soc. Amer., 23, 405-418, 1951.

Garland, G.D., Introduction to Geophysics (Mantle, Core, and Crust), W.B. Saunders. Philadelphia, pp. 494, 1979.

Gassmann, F., Uber die Elastizitat poroser Medien, Vier. d. Naturforsch. Ges. Zurich, 96, 1-22, 1951.

Gaunard, G.C., Elastic and acoustic resonance wave scattering, Appl. Mech. Rev., 42, 143-192, 1989.

Geertsma, J. and Smit, D. C., Some aspects of elastic wave propagation in fluid-saturated porous solids. *Geophysics*, 26, no. 02, 169-181, 1961.

Gudmundsson, O., On the effect of diffraction on travel time measurements. *Geophys. J. Int.*, 124, 304-314, 1996

Hosseini-Hashemi, S., and Anderson, J.S., Orthogonality and normalization of torsional modes of vibration of solid elastic spheres. *J. Sound and Vibration*, 121, 511-524, 1988.

Hovem, J.M., Viscous attenuation of sound in suspensions and high-porosity marine sediments, *J. Acoust. Soc. Am.*, 67, 1559-1563, 1980.

Hovem, J.M., and G.D. Ingram, Viscous attenuation of sound in saturated sand. *J. Acoust. Soc. Amer.*, 66, 1807-1812, 1980.

Hurich, C.A., Statistical description of seismic reflection wavefields: A step toward quantitative interpretation of deep seismic reflection profiles, *Geophys. J. Int.*, v. 125, 719-728, 1996.

Jing, X., P. Sheng, and M. Zhou, Theory of acoustic excitations in colloidal suspensions. *Phys. Rev. Lett.*, 66, 1240-1246, 1991.

Jing, X., P. Sheng, and M. Zhou, Acoustic and electromagnetic quasimodes in dispersed random media, *Phys. Rev. A*, 46, 6513-6534, 1992.

Kinra, V.K., and A. Anand, Wave propagation in a random particulate composite at long and short wavelengths, *Int. J. Solids Structures*, 18, 367-380, 1982.

Kuster, G.T., and M.N. Toksöz, Velocity and attenuation of seismic waves in two-phase media: Part I. Theoretical formulation, *Geophysics*, 39, 587-606, 1974a.

Kuster, G.T., and M.N. Toksöz, Velocity and attenuation of seismic waves in two-phase media: Part II. Experimental results, *Geophysics*, 39, 607-618, 1974b.

Liu, J., L. Ye, D.A. Weitz, and P. Sheng, Novel acoustic excitations in suspensions of hard-sphere colloids, *Phys. Rev. Lett.*, 65, 2602-2605, 1990.

Mason, W. P., and McSkimin, H. J., Attenuation and scattering of high frequency sound waves in metals and glasses, *Journal of the Acoustical Society of America*, 93, 464-473, 1947.

Marion, D., Mukerji, T., and Mavko, G., 1994, Scale effects on velocity dispersion: From ray to effective medium theories in stratified media: *Geophysics*, 59, 1613-1619.

Mehta, C.H., Scattering theory of wave propagation in a two-phase medium. *Geophysics*, 48, 1359-1370, 1983.

Melia, P. J. and Carlson, R. L., An experimental test of P-wave anisotropy in stratified media: *Geophysics*, 49, no. 04, 374-378, 1984.

Molyneux, J. B., and Schmitt, D. R., Compressional wave speeds in attenuating media: a laboratory physical model study. Submitted to *Geophysics*.

Murphy, W.F., A. Reischer, and K. Hsu, Modulus decomposition of compressional and shear velocities in sand bodies, *Geophysics*, 58, 227-239, 1993.

Mukerji, T., G. Mavko, D. Mujica, and N. Lucet, Scale-dependent seismic velocity in heterogeneous media, *Geophysics*, 60, 1222-1233, 1995.

Müller, G., M. Roth, and M. Korn, Seismic-wave traveltimes in random media, *Geophys. J. Int.*, 110, 29-41, 1992.

Nishizawa, O., Satoh, T., Lei, X., and Kuwahara, Y., Laboratory studies of seismic wave propagation in inhomogeneous media using a laser Doppler vibrometer. *Bulletin Seis. Soc. Am.*, 87, 809-823, 1997.

Numrich, S.K., and H. Überall, Scattering of sound pulses and the ringing of target resonances, *Phys. Acoustics*, 21, 235-318, 1992.

Page, J.H., P. Sheng, H.P. Schriemer, I. Jones, X. Jing, and D. A. Weitz, Group velocity in strongly scattering media, *Science*, 271, 634-637, 1996.

Paterson, Norman R., Seismic wave propagation in porous granular media. *Geophysics*, 21, no. 03, 691-714, 1956.

Rayleigh, Theory of sound. The Macmillan Company, 1929.

Reuss, A., Berechnung der Fließgränze von Meschkristallen auf Grund der Plastizitätsbedingung für Einkristalle Agnew, *Math u. Mech.*, 9, 49, 1929.

Roth, M., G. Müller, and R. Snieder, Velocity shift in random media, *Geophys. J. Int.*, 115, 552-563, 1993.

Sato, Y. and T. Usami, Basic study of the oscillation of a homogeneous elastic sphere, Part I: Frequency of oscillation, *Geophys. Mag.*, 31, 15-24, 1962.

Sato, H., Formulation of the multiple non-isotropic scattering processes in 3-D space on the basis of energy transport theory, *Geophys. J. Int.*, 121, 523-531, 1995.

Schreiber, E., O.L. Anderson, and N. Soga, Elastic constants and their measurement, McGraw-Hill, New York, pp. 196, 1973.

Schwartz, L., and T.J. Plona, Ultrasonic propagation in close-packed disordered suspensions, *J. Appl. Phys.*, 55, 3971-3977, 1984.

Sen, P.N., and D. L. Johnson, Topological limitations of effective-medium approximation in fluid-solid systems having two longitudinal-acoustic modes, *Phys. Rev. B.*, 27, 3133-3137, 1983.

Shui, Y., D. Royer, E. Dieulesaint, and Z. Sun, Resonance of surface waves on spheres, *IEEE Ultrasonics Symposium*, 3430-3446, 1988.

Überall, H., L.R. Dragonette, and L. Flax, Relation between creeping waves and normal modes of vibration of a curved body, *J. Acoustic. Soc. Am.*, 61, 711-715, 1977.

Überall, H., J. George, A.R. Farhan, G. Mezzorani, A. Nagl, K.A. Sage, and J.D. Murphy, Dynamics of acoustic resonance scattering from spherical targets: Application to gas bubbles in fluids, *J. Acoustic. Soc. Am.*, 66, 1161-1172, 1979.

Überall, H., ed. *Acoustic Resonance Scattering*, Gordon and Breach, Philadelphia, pp. 341, 1992.

Usami, T. and Y. Sato, Torsional oscillation of a homogeneous elastic spheroid, *Bull. Seis. Soc. Am.* 52, 469-479, 1962.

Veksler, N.D., and J.-L. Izbicki, Modal resonances of the Franz waves, *Acustica*, 82, 18-26, 1996.

Vidale, J.E., and M.A.H. Hedlin, Evidence for partial melt at the core-mantle boundary north Tonga, *Nature*, 391, 682-685, 1998.

Voigt, W, *Lehrbuch der Kristallphysik*, Teubner, Leipzig, 1910.

Wielandt, E., On the validity of the ray approximation for interpreting delay times, in G. Nolet, ed., *Seismic Tomography*, D. Reidel Publ. Co., Dordrecht, 1987.

Wood, A.B., *A Textbook of Sound*, MacMillan, Indianapolis, Indiana, 1941.

Wu R. S., and Aki, K., Elastic wave scattering by a random media and the small scale inhomogeneities in the lithosphere. *J. Geophys. Res.*, 90, 10261-10273, 1985

Wyllie, M.R.J., A.R. Gregory, and G.H.F. Gardner, Elastic wave velocities in heterogeneous and porous media, *Geophysics*, 21, 41-70, 1956.

Wyllie, M.R.J., A.R. Gregory, and G.H.F. Gardner, An experimental investigation of factors affecting elastic wave velocities in porous media, *Geophysics*, 23, 459-493, 1958.

Yin, H., G. Mavko, T. Mukerji, and A. Nur, Scale-dependent dynamic wave propagation in heterogenous media: I. Experiments, 64th Annual Internat. Mtg., Soc. Expl. Geophys., Expanded Abstracts, 1147-1150, 1994.

Table 1. Constituent Physical Properties

	Glass Beads	Glycerol
Material	Soda-Lime Glass	C ₃ H ₈ O ₃
Density		
(kg/m ³)	2480 +/- 10 ¹	1260 +/- 10 ¹
Bulk Modulus		
K	37.8	4.67
(GPa)		
Shear Modulus		-
μ	25.4	
(GPa)		
Compressional Wave		
V _p	~5400 ²	1926 +/- 10 ¹
(m/s)		
Shear Wave		-
V _s	~3200 ²	
(m/s)		
Poisson's Ratio		-
ν	0.225	

¹ Molyneux and Schmitt, 1999

² Estimated from Glass I of Carmichael, 1982

Table 2. Summary of Observations for the Bead Packs

Sample	Bead Diameter d (mm)	Porosity ϕ (%)	Signal Velocity V (m/s)	First Peak Velocity (m/s) ¹	Wood's Formula V _{Wood} (m/s)	Wyllie Estimate V _{Wyllie} (m/s)
220 μm ¹	0.22 +/- 0.04	37.8 +/- 1.0	2570 +/- 10	2350 +/- 20	2350	3200
670 μm ¹	0.67 +/- 0.05	37.7 +/- 0.9	2580 +/- 30	2460 +/- 10	2350	3200
2 mm	1.93 +/- 0.07	37.5 +/- 0.4	2730 +/- 30	-	2350	3200
3 mm	2.99 +/- 0.08	38.6 +/- 1.1	2890 +/- 100	-	2340	3180
4 mm	3.99 +/- 0.06	39.7 +/- 0.7	3000 +/- 100	-	2310	3160
5 mm	4.89 +/- 0.09	41.3 +/- 1.7	3600 +/- 160	-	2300	3090
6 mm	5.90 +/- 0.08	46.8 +/- 2.7	4260 +/- 370	-	2200	2930
Glycerol	-	100.0	1926 +/- 3	-	-	-

¹. As measured in Molyneux and Schmitt, [1999].

Table 3. Frequency and apparent attenuation of spectral peaks

Sample	Pulse f_L (MHz)	Normalized f_L (ka) ¹	Log _e (A(f_L)) extrapolated to zero length	α_L (neper/m)	Q_L	Resonance f_{11} (MHz)	Normalized f_{11} (ka) ¹	Log _e (A(f_{11})) extrapolated to zero length	α_{11} (neper/m)	Q_{11}
0.22mm	0.36 +/- 0.01	0.13 +/- 0.03	8.98 +/- 0.63	153 +/- 18	2.9	-	-	-	-	-
0.67mm	0.30 +/- 0.01	0.32 +/- 0.04	9.01 +/- 0.58	152 +/- 21	2.4	-	-	-	-	-
2 mm	0.33 +/- 0.01	1.04 +/- 0.07	6.18 +/- 0.70	87 +/- 21	4.4	-	-	-	-	-
3 mm	0.28 +/- 0.01	1.37 +/- 0.09	4.00 +/- 0.34	74 +/- 11	4.1	1.17 +/- 0.01	5.71 +/- 0.20	6.45 +/- 0.31	203 +/- 10	6.3
4 mm	0.23 +/- 0.01	1.50 +/- 0.09	1.24 +/- 0.07	20 +/- 2	12.0	0.78 +/- 0.02	5.08 +/- 0.21	4.41 +/- 0.17	120 +/- 5	6.8
5 mm	-	-	-	-	-	0.63 +/- 0.02	5.03 +/- 0.25	4.07 +/- 0.10	92 +/- 3	6.0
6 mm	-	-	-	-	-	0.51 +/- 0.03	4.90 +/- 0.36	3.83 +/- 0.21	58 +/- 10	6.5
glycerol	1.13 +/- 0.00	-	-	-	-	-	-	10.17 +/- 0.06	-	-

1. $ka = 2\pi f/V_f$ and a = bead radius.

Table 4. Normalized Frequencies of the Toroidal and Poloidal Normal Modes for an Isotropic Sphere with Poisson's ratio = 0.225

Toroidal Mode	ka	Poloidal Mode	ha
${}_1T_2$	2.5011	${}_1S_0$	4.2530
${}_1T_3$	3.8647	${}_1S_2$	2.6370
${}_2T_1$	5.7635	${}_1S_3$	3.9067
${}_2T_2$	7.1360	${}_1S_4$	4.9928
${}_2T_3$	8.4449	${}_1S_5$	6.0100
${}_3T_1$	9.0950	${}_2S_1$	3.3781
${}_3T_2$	10.5149	${}_2S_2$	4.8037
${}_3T_3$	11.8817	${}_2S_3$	6.3870
		${}_3S_1$	6.6287

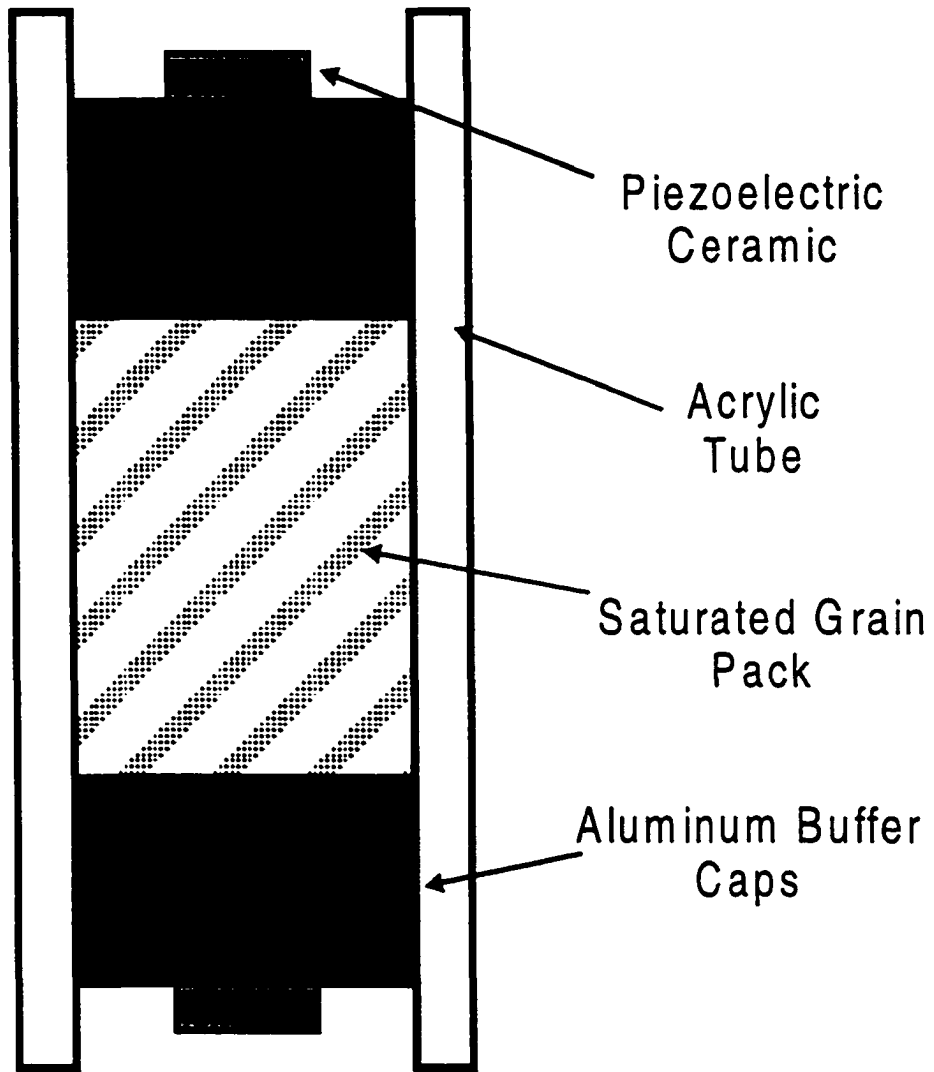


Figure 1. Sample configuration

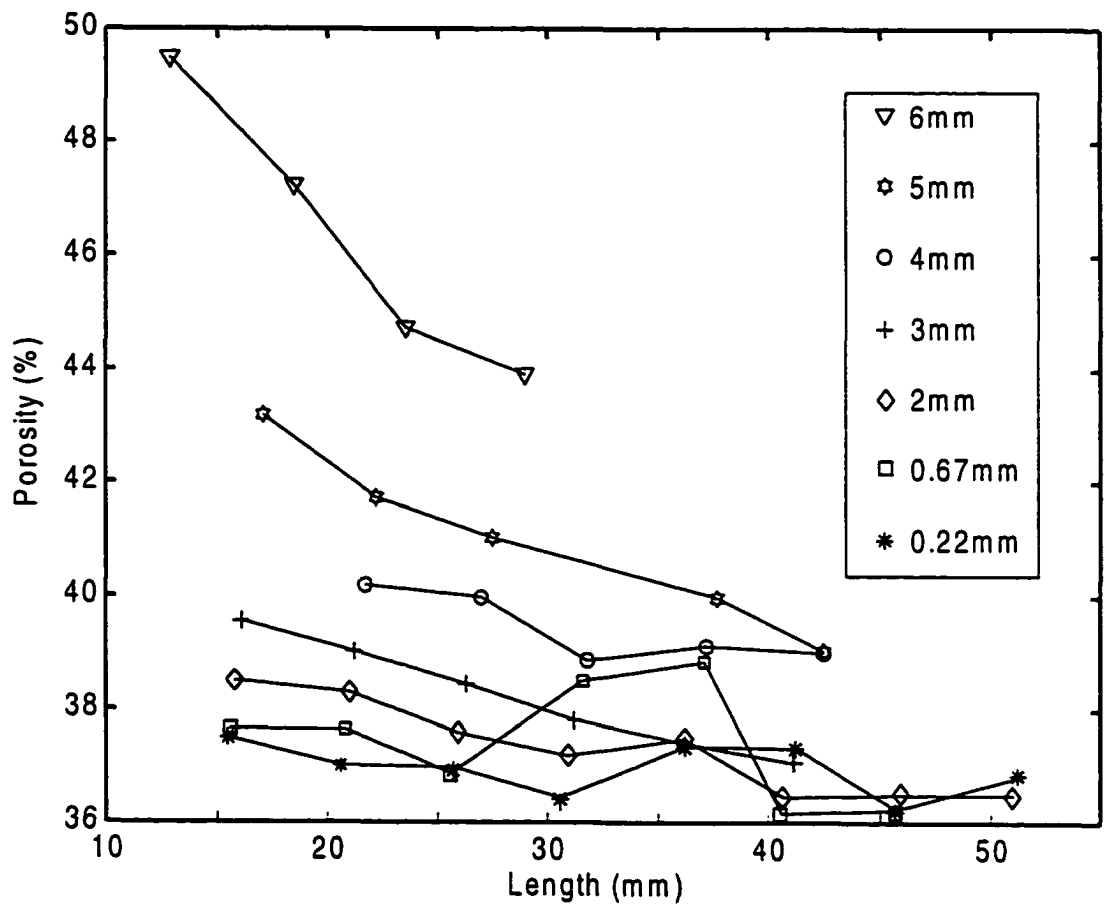


Figure 2. Sample porosity versus bead pack length

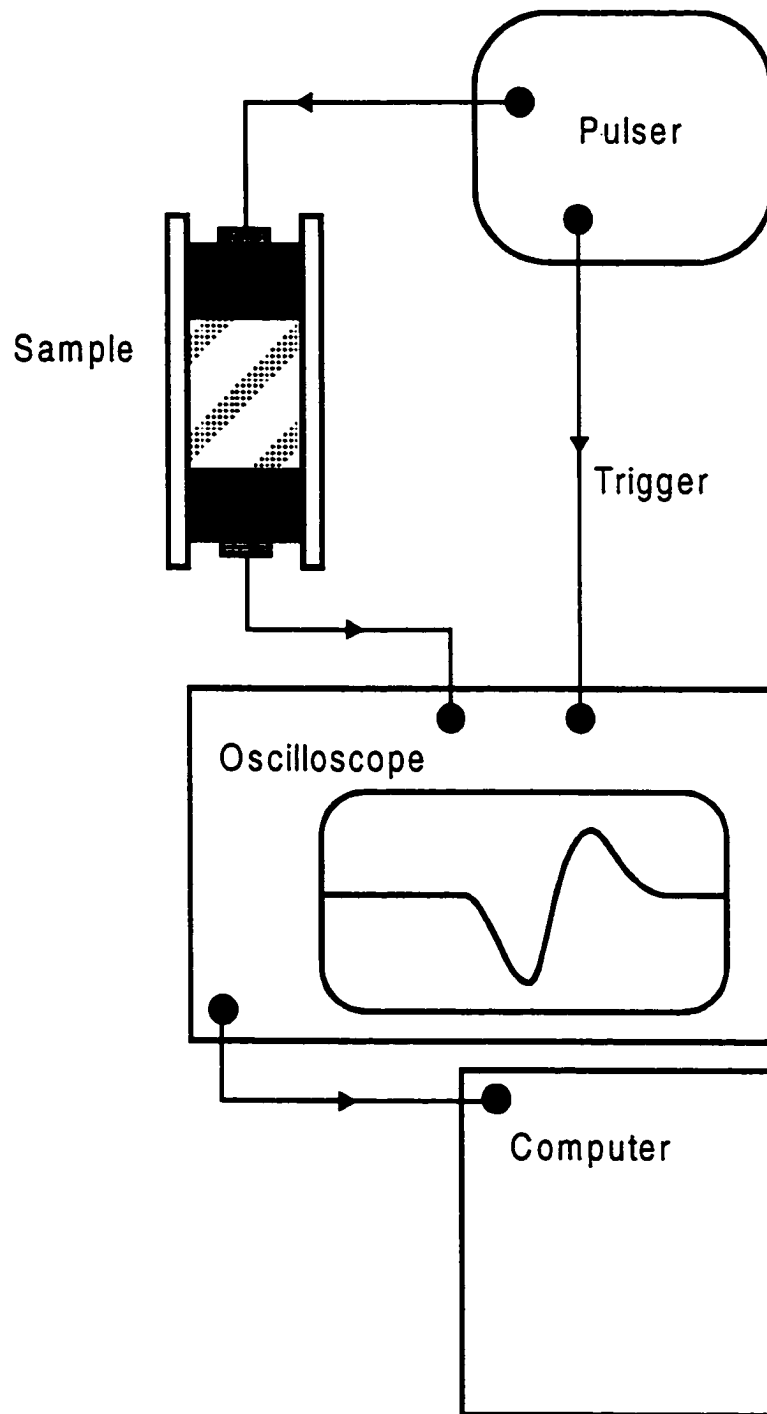


Figure 3. Experimental Configuration

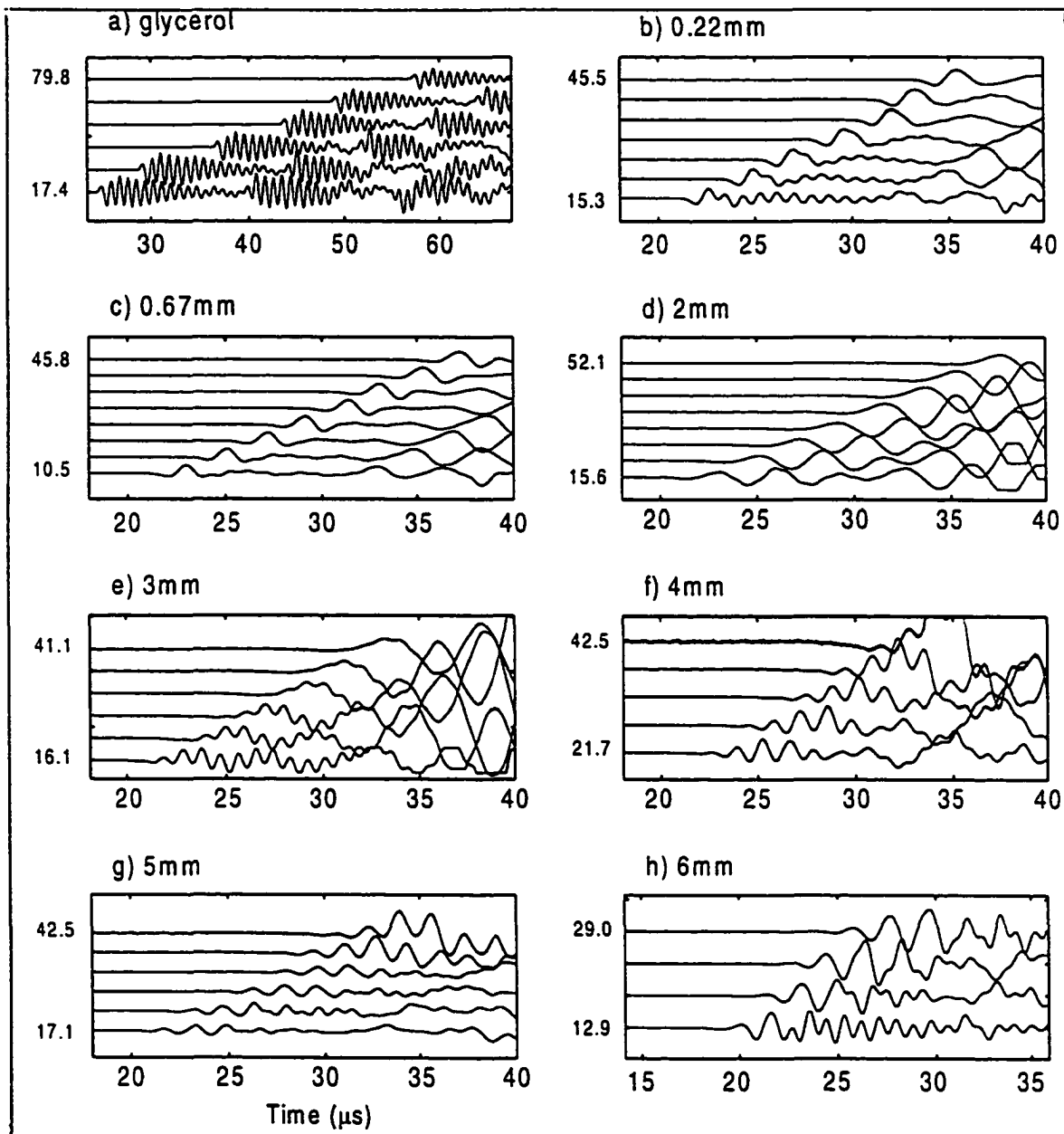


Figure 4. Transmitted pulse normalized amplitude versus time for differing pack lengths of a) pure glycerol and glycerol saturated packs of glass beads with diameters of b) 0.22 mm, c) 0.67 mm, d) 2 mm, e) 3 mm, f) 4 mm, g) 5 mm, and h) 6 mm. Note, maximum and minimum sample lengths are indicated.

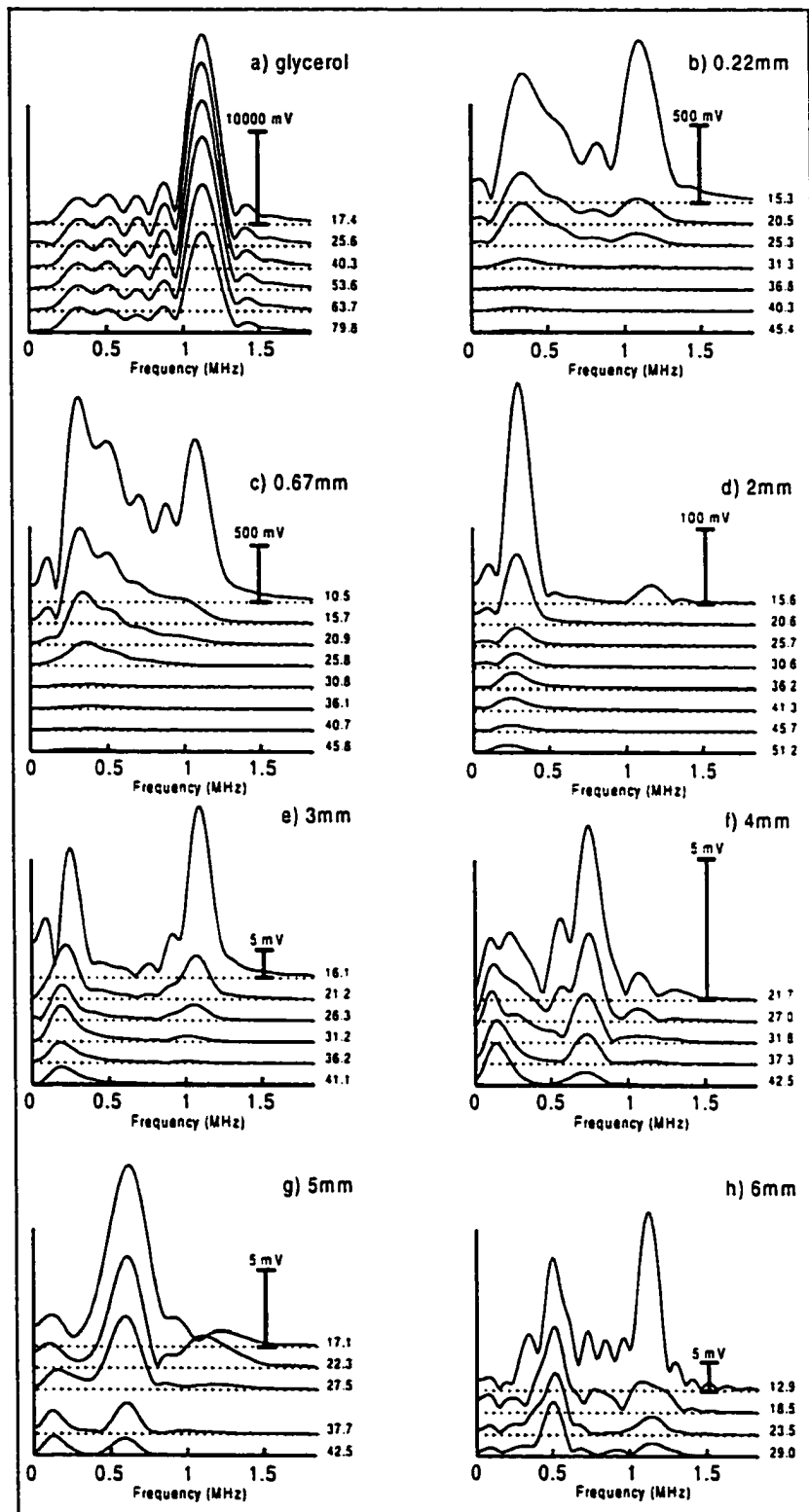


Figure 5. Amplitude spectra of the observed traces of Figure 4 for the differing lengths of a) pure glycerol and glycerol saturated packs of glass beads with diameters of b) 0.22 mm, c) 0.67 mm, d) 2 mm, e) 3 mm, f) 4 mm, g) 5 mm, and h) 6 mm. Amplitude spectra derived from a Tapered window of the first arriving signal. Dark error bars show true amplitudes for each pack. Note, sample pack-lengths (mm) are indicated.

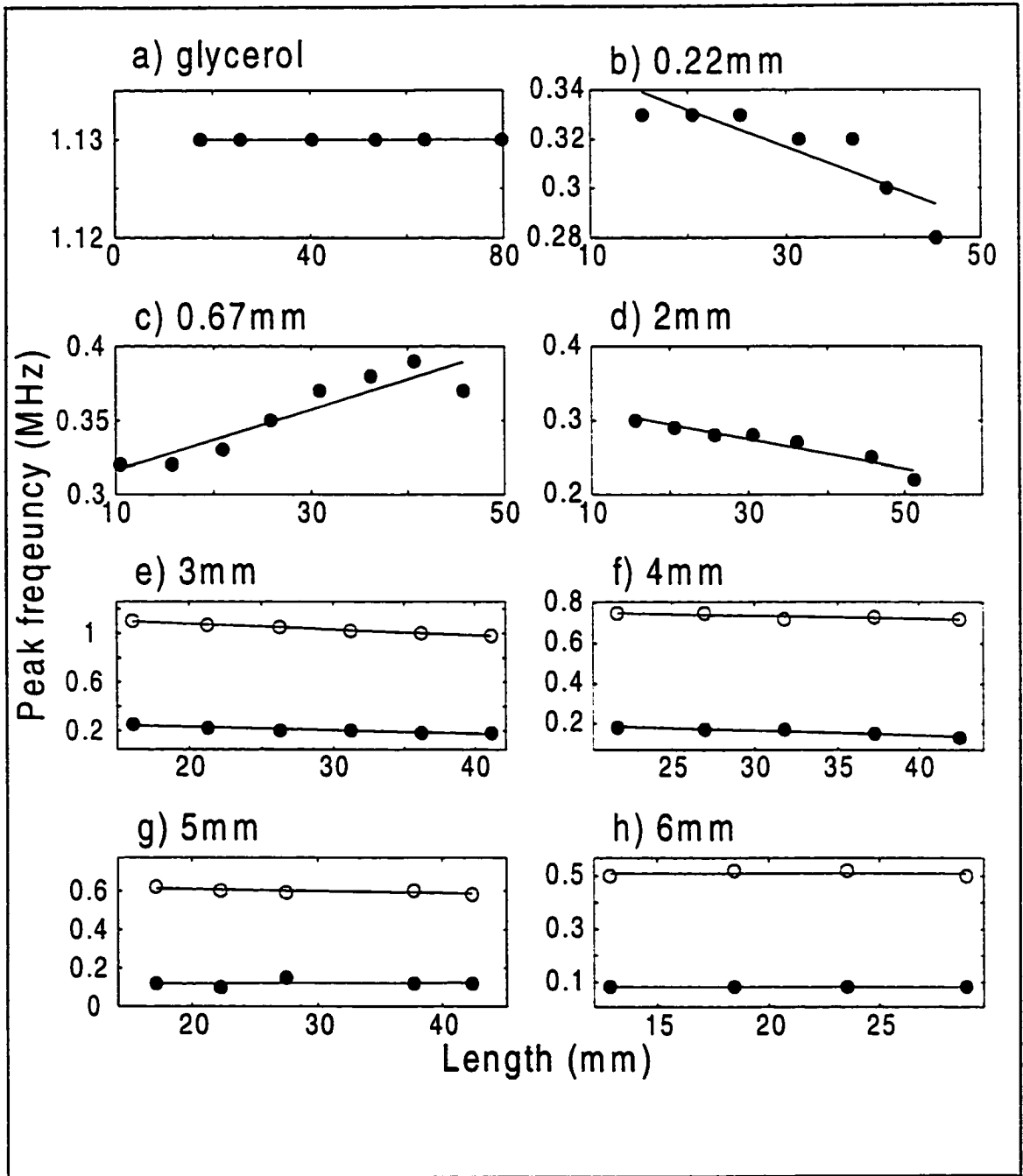


Figure 6. Peak spectral frequencies observed from Figure 5 versus pack length for the differing lengths of a) pure glycerol and glycerol saturated packs of glass beads with diameters of b) 0.22 mm, c) 0.67 mm, d) 2 mm, e) 3 mm, f) 4 mm, g) 5 mm, and h) 6 mm. Open circles represent the second high frequency peak observed for bead sizes greater than 2 mm

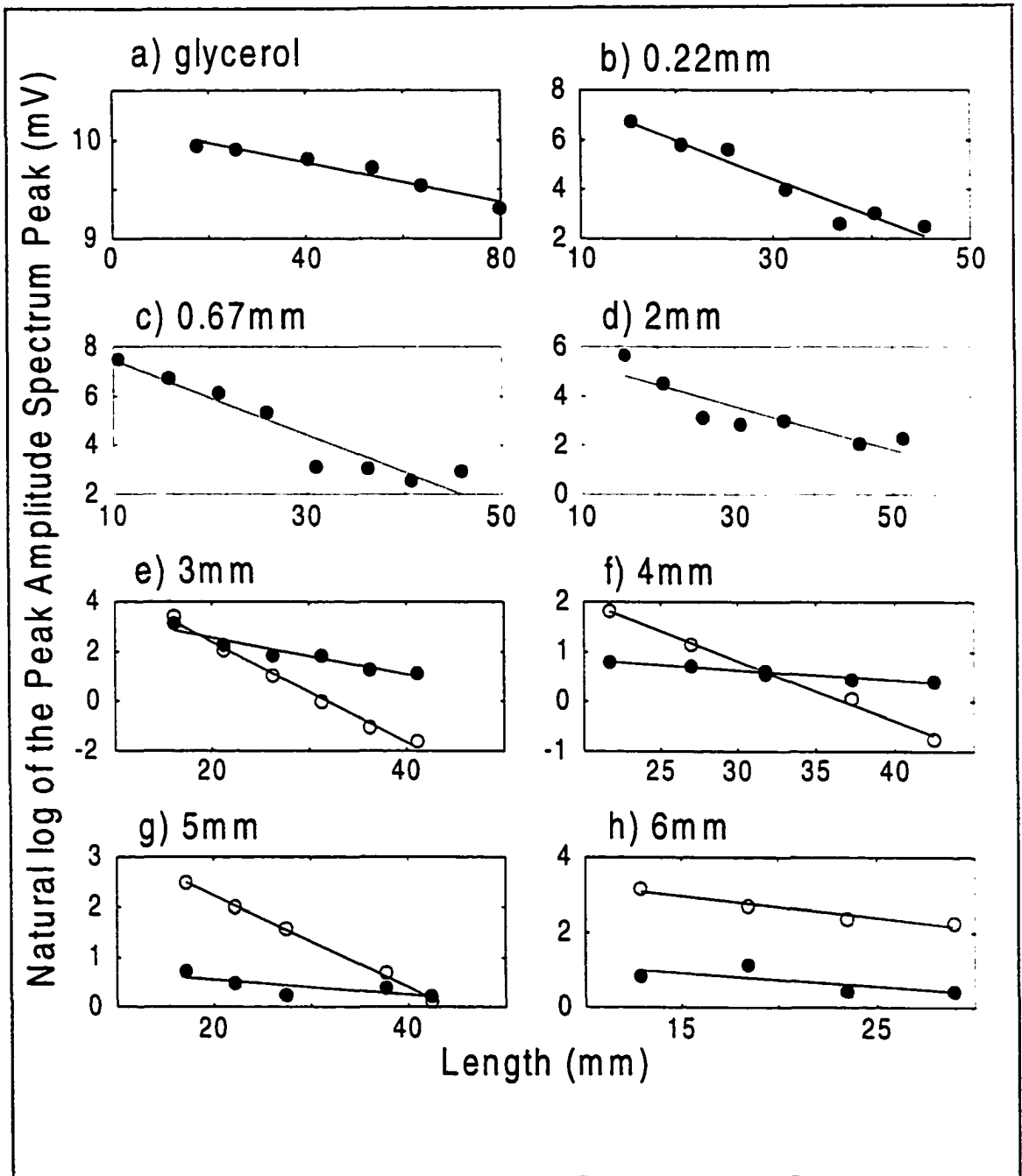


Figure 7. Natural log of the observed amplitude of the spectral peaks versus pack length for the differing lengths of a) pure glycerol and glycerol saturated packs of glass beads with diameters of b) 0.22 mm, c) 0.67 mm, d) 2 mm, e) 3 mm, f) 4 mm, g) 5 mm, and h) 6 mm. Open circles represent the second high frequency peak observed for bead sizes greater than 2 mm.

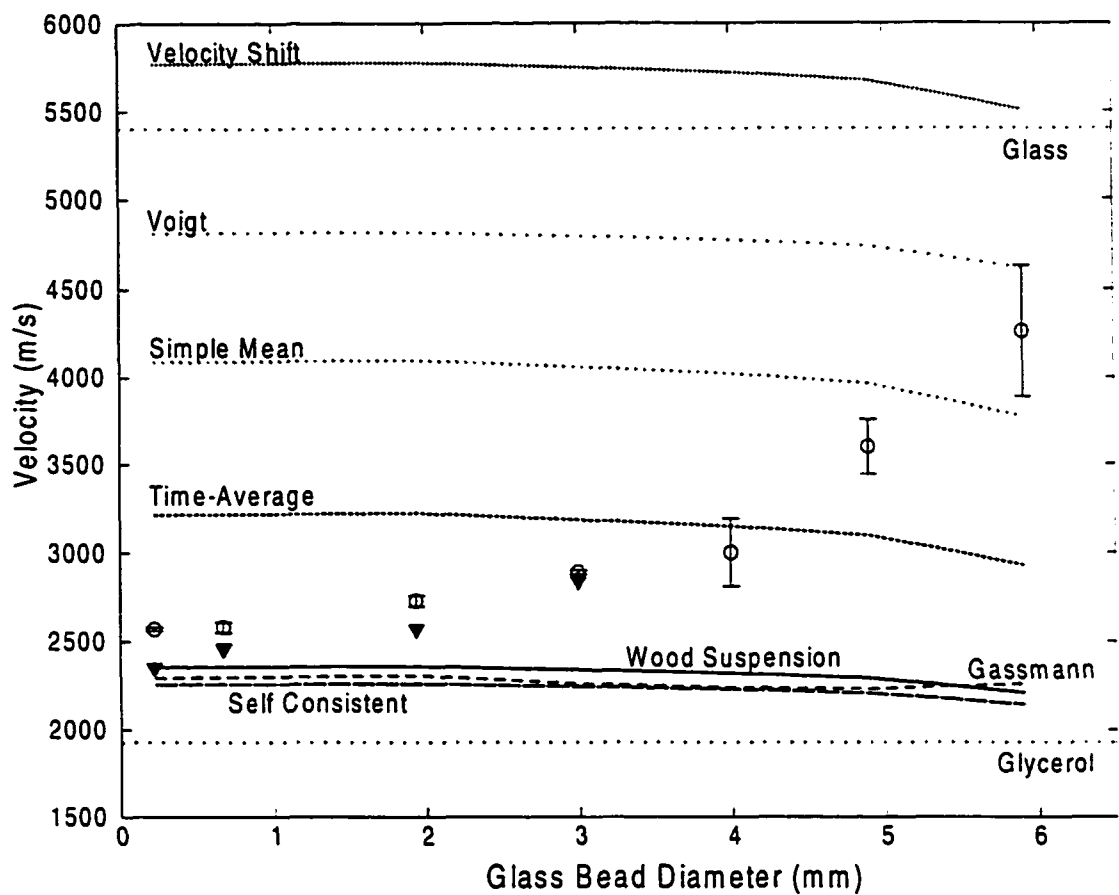


Figure 8. Velocities determined by the pulse onset (signal velocity - open circles) and pulse amplitude peak (peak velocity - inverted solid triangle) versus diameter of glass beads. The observed values are compared with the theoretical predictions for the velocity shift [Roth et al., 1993], the simple mean, the Voigt mixture bound [Voigt, 1910], the time average equation [Wyllie et al., 1956], the self consistent method [Berryman, 1980a,b], the Gassmann formula [Gassmann, 1951], and the Wood suspension formula [Wood, 1941] which in the present case is identical to the Reuss bound [Reuss, 1929] and the Kuster-Toksoz estimate [Kuster and Toksoz, 1974a,b]. The true pack porosities are used in each of the sets of calculations.

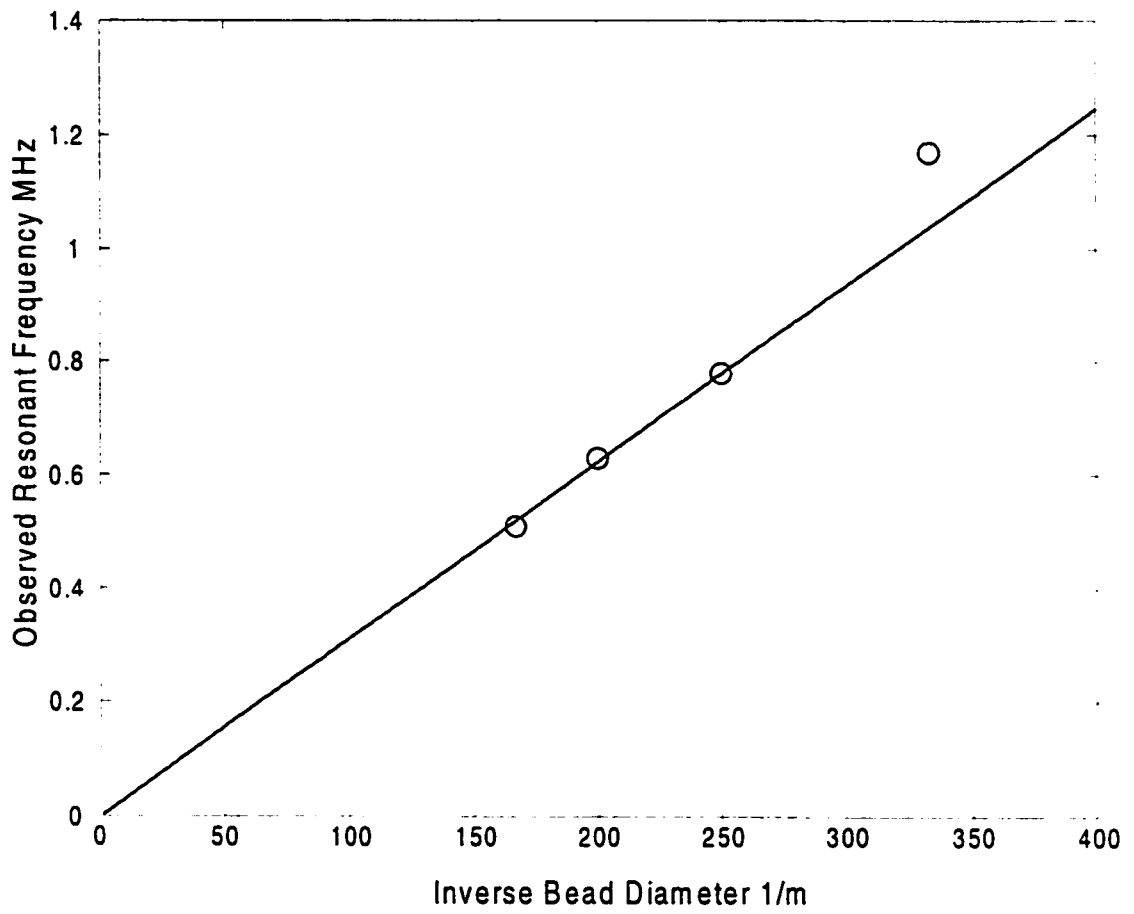


Figure 9. Peak frequencies versus reciprocal bead diameter observed for the 3 mm to 6 mm diameter bead packs.

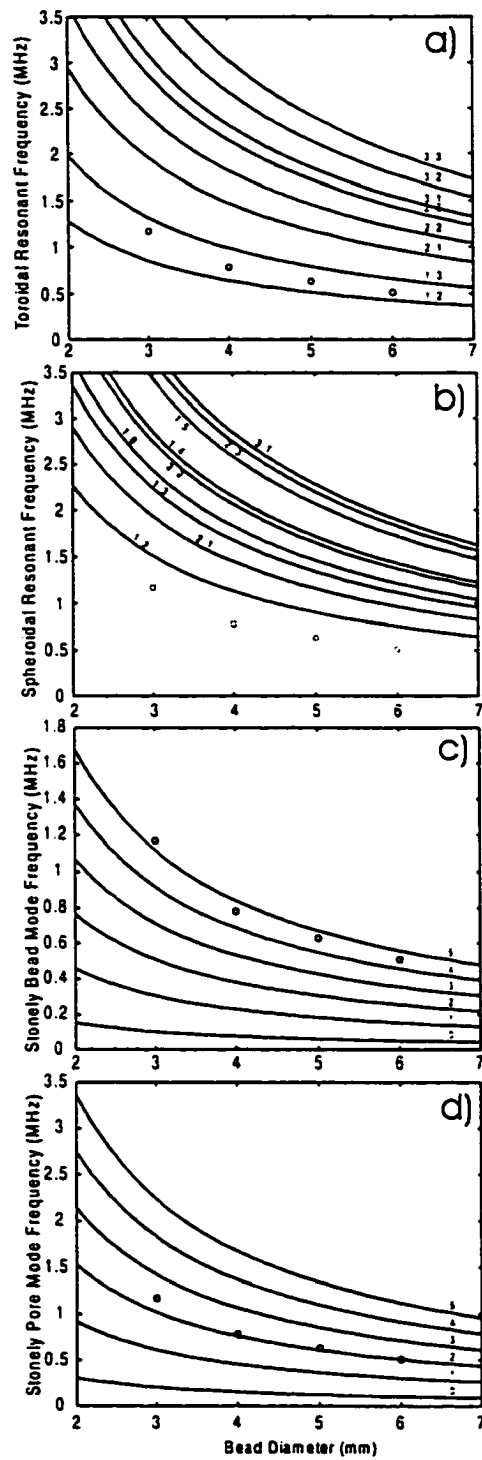


Figure 10. Expected modal frequencies versus glass bead diameter for a) toroidal oscillations, b) poloidal oscillations, c) interfacial Stoneley wave circumnavigation, and d) interfacial Stoneley wave circumnavigation of a pore facet. Numbers on the curves refer to the order of the mode.

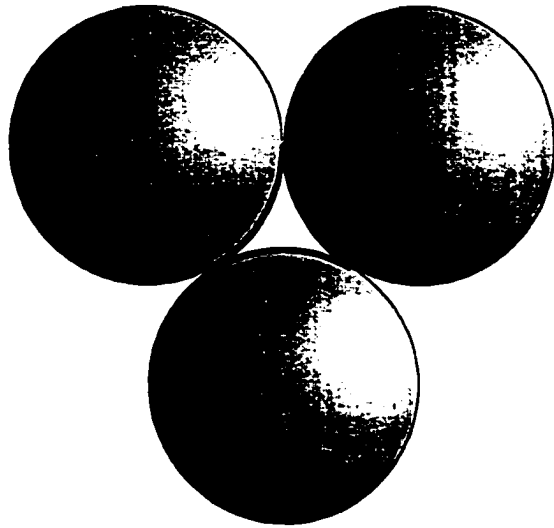


Figure 11. Concave triangular pore facet shape.

CHAPTER 6

Conclusion

In rock samples, the characteristics of a propagating ultrasonic pulse depend on the sample length, the saturation, and the pressure dependent attenuation, compressibility, and rigidity. This waveform non-stationarity complicates determination of meaningful travel times. As a result, substantially different values of interval velocity can be obtained depending on the time picking criteria employed. This problem is particularly severe in high frequency laboratory time-of-flight measurements on intrinsically porous or microcracked rock at low confining pressure.

In Chapter 3, a semi-automated method was developed to determine this onset time in high fidelity pulse waveforms acquired during pressure-dependent core measurements. Such a tool proves useful when performing extensive suites of velocity measurements in the lab. The greatest value of the Pearson's correlation co-efficient between segments of observed waveforms near the pulse onset and at an appropriate reference serves as the time determination criteria.

Tests of the method on artificial data suggest the signal velocity may be determined to better than 0.3%. A series of ultrasonic (MHz) velocity measurements in microcracked rock to confining pressures of 300 Mpa (~45,000 Psi) was also carried out to test the method. At the lowest confining pressure where attenuation is greatest ($Q \sim 6$), the signal onset time differs from those more conventionally derived by more than 4%. This large discrepancy illustrates that care should be exercised when determining velocity in such attenuating materials. Conversely, the consistency of waveform attributes, such as

the difference in the onset to the first peak time or the apparent quality factor, is useful when estimating intrinsic material velocities in low porosity, micro-cracked carbonate and metamorphic rocks at high confining pressures. Where the quality factor, Q , is constant with elevated hydrostatic confining pressure it is assumed that most microcracks have closed. These microcracks no longer significantly influence the propagating signal by scattering ($Q > 40$) yielding intrinsic rock properties as all the different velocity measures yield the same value; the waveform is stationary.

In Chapter 4, it is noted that pulse transmission ultrasonic experiments are often used to determine material velocities in rock. Such mechanical wave-speeds are often determined by 'picking' the transit-time of a certain feature of the propagating pulse, such as the first amplitude maximum. However, attenuation and dispersion conspire to change the shape of a propagating wave making determination of a physically meaningful speed problematic from a recorded signal. As a consequence, the speeds so determined are not necessarily representative of the material's intrinsic wave phase- and group-speeds. These more fundamental measures of speed are found experimentally in a highly attenuating media consisting of glycerol-saturated, unconsolidated, random packs of glass beads and quartz sand. The quality factor Q varies between 2 and 6 over the useful frequency band in these experiments from ~200 to 600 kHz; Q is not constant over this range in these materials. The fundamental speeds are compared to more common and simple speed estimates derived from picking of a single transit time. In general, the simpler methods estimate the group-speed at the predominant frequency to better than 3%, but are in poor agreement with the phase-speed. Wave speeds determined from the time at which the pulse is first detected (here referred to as the signal speed) differ from

the predominant group-speed by up to 13%. At best, this onset wave-speed provides a lower bound for the high frequency limit of the phase velocity in a material in which wave-speed increases with frequency. Each method of time picking, however, is self-consistent as indicated by the high quality of the linear regression between the observed arrival times and the propagation distance.

In chapter 5, wave propagation through fluid saturated, random packs of unconsolidated glass beads is investigated. In this section the influence of the scale of the structure (i.e., the beads and their fluid interstitial pore space) on the wave propagation is of most interest. In particular cases in which the glass beads have comparable size to the dominant wavelength of the compressional wave are the least well understood. The glass bead-glycerol media are difficult to formally describe. The low fluid porosity (~40%) means the beads are in close proximity with the presence of multiple scattering. The fluid-solid mixture provides for potential fluid-solid coupling effects. When the dominant wavelength (low-frequency regime) is greater than the bead size in the grain packs, attenuation and propagation velocity are consistent ($Q \sim 3$, and signal velocity = 2.6 km/s respectively). These velocities are close to those predicted from mixture theory using simple mixture theories such as Wood's formula. A simple Zener type attenuation model describes the decay of the waveforms in this case. In contrast, when the dominant wavelength is comparable to the bead size the received amplitude spectra of the signal displays two peaks. This behaviour was unexpected. The frequency of the higher frequency peak depends inversely on bead diameter; this character strongly indicates some kind of resonance. As the λ/d ratio increases, where λ is the dominant wavelength and d the characteristic particle size, the individual resonances gain in relative importance

within the amplitude spectrum. The low frequency peak, which is possibly related to the propagation of the ballistic pulse through the medium decreases in strength relative to the resonant peak. However, the high frequency signal component decays more rapidly with sample length. This may be a consequence of the fact that the scattered energy radiates in all directions whereas the ballistic pulse propagates in a single direction from the sender to the receiver. The source of the resonant peak is unknown. This partition of the input signal into resonance type phenomena constitutes a new and fundamental attenuation mechanism that to our knowledge is not documented in the literature. The resonant frequencies observed do not agree with the free spheroidal and toroidal modes for a sphere. A fluid borne mode (Stonely wave) circumnavigating the beads compares poorly. However, it is interesting to note that if it is assumed the pore space, and not the beads, is the crucial structural unit, then the value of the fluid borne interface wave of order $n = 2$ matches the observed frequencies well. The present study was not designed to study these unexpected resonances, however, and this good match may simply be coincidental. Further experiments are needed to address this issue.

With the increasing importance of advanced seismic inversion techniques, more definitive characterizations of reservoir rocks is required. Information on in-situ velocity is primarily derived from shot gathers, sonic logs, and VSP's. However, laboratory analysis still provides the only direct measure of rock velocity although its extent is severely limited in terms of the volume of material that may be studied. Further, laboratory tests on core are able to delineate more sophisticated phenomena such as velocity anisotropy. Unfortunately, both sonic-log and laboratory determined velocities usually exceed the corresponding in situ seismic velocity. This dispersion is due to both

the attenuative character of the rock and to the dimensions of the geologic structure relative to the wavelength of the sound energy used. Knowledge of such effects can prevent inappropriate laboratory measures of seismic velocities, as described below.

The decline in the apparent velocity with wavelength to particle size ratio (λ/d) is well documented in the literature [e.g. Marion et al., 1994, Kinra and Anand, 1982, Yin et al., 1994]. I have extended such observations to fluid saturated porous media. Our laboratory results (Figure 8, Chapter 5) show that when (λ/d) is greater than 2 that the physics associated with ultrasonic wave propagation is equivalent to that defining the seismic wave propagation when $\lambda \gg d$, the effective media limit. It is seen that by ignoring such scale effects, laboratory velocity measurements in which $\lambda \sim d$, may be twice as large as the equivalent seismic velocity, where $\lambda \gg d$, (at least in the highly heterogeneous medium studied here).

Additionally, seismic waves propagate in an effective half-space, whereas in laboratory experiments the propagating waveform is subject to the boundary conditions of the core plug. If the propagating wavelength is comparable to the dimensions of the plug (diameter l , and length x), low velocity surface waves and bar modes may be generated in preference to body waves (Silaeva and Shanmina, 1958). Defining appropriate limits of λ/l and λ/d allows for consistent P-wave propagation.

Finally, as seen in chapters 3 and 4, in attenuating medium ($Q < 40$) the related dispersion causes difficulties in defining the propagation velocity. For example, I demonstrate that the velocity determined from the first break (first detectable onset of the waveform) can be 13% different from the group or first peak velocities. Therefore, it is inaccurate and inconsistent to use a velocity based on a *first break* measurement if this

information is to be included in the processing of a seismic image where, for example, isochrons will be picked from the *signal peak* of a reflector.

In summary, to ensure that laboratory velocities have bearing on equivalent seismic propagation velocities the dominant propagating wavelength should be more than twice that of the characteristic size of the particle inclusions yet smaller than the dimensions of the rock core. Also, the signal velocity is not an indicative rock property measurement in highly attenuating media ($Q < 40$).

Finally, the resonances in the glass bead medium documented in chapter 5 need further investigation because this may be important to how we describe attenuation in the earth. The present results indicate the low frequency propagation (i.e., long wavelength) is when $\lambda \approx a$, and the second high frequency peak scales with bead diameter and is consistent with resonance of individual beads. However, the current experiments were not designed to examine these unexpected resonances and cannot delineate precisely what the resonance is. The results do suggest that they are not due to free resonances of the beads themselves. This suggests a fluid borne mode may be the cause of the resonance. A mono-frequency input source that slowly swept through a range of frequencies may aid such delineation. Further the directionality of the energy re-emitted by the resonance is of interest, and this could be monitored with a series of spatially arranged receivers surrounding the bead pack. Another interesting question relates to how the resonance might be modified by including spheres of differing sizes within the pack or by including spheres of differing composition and shape. All such experiments might illuminate the presently poorly recognized role resonance may have on the propagation of compressional waves through complex materials.

The as yet unquantified resonances within the bead pack raise a number of issues related to wave propagation through a heterogeneous earth. First, might such resonances be important for the overall wave propagation and how might they influence the observed velocities and attenuations? Second, where in the earth might such resonances exist? A simple one-dimensional example may be the “multiple” reverberations produced by low impedance coal beds in sedimentary formations. Might such effects be important in regions of high contrast such as the core-mantle boundary where there exists the potential for mixing of high temperature metallic fluids and silicates? Are such mechanisms even more pervasive: present with irregular sized inclusions throughout the earth from sand grains to large boulders and from the core of the earth itself? Might such phenomena contribute to the white noise present in all solid-earth elastic wave investigations?

References

Kinra, V.K., and A. Anand, Wave propagation in a random particulate composite at long and short wavelengths, *Int. J. Solids Structures*, 18, 367-380, 1982.

Marion, D., Mukerji, T., and Mavko, G., 1994, Scale effects on velocity dispersion: From ray to effective medium theories in stratified media: *Geophysics*, 59, 1613-1619.

Yin, H., G. Mavko, T. Mukerji, and A. Nur, Scale-dependent dynamic wave propagation in heterogenous media: I. Experiments, 64th Annual Internat. Mtg., Soc. Expl. Geophys., Expanded Abstracts, 1147-1150, 1994.